MECHANISITIC STUDIES OF CHEMICAL BIOLOGY PROBES REGULATING MTOR PATHWAY

By

Ruojing Li

A dissertation submitted to Johns Hopkins University in conformity with the requirements for the degree of Doctor of Philosophy

Baltimore, Maryland

November 2016

Abstract

Mechanistic target of rapamycin (mTOR) plays an essential role in sensing a myriad of environmental cues including nutrients and growth factor stimulation to regulate cell growth and proliferation. mTOR independently associates with different proteins to form two distinct complexes, mTORC1 and mTORC2. The previous antiangiogenesis study of antifungal drug itraconazole in endothelial cells showed that inducing lysosomal lipid accumulation inhibits mTORC1 signaling. On the other hand, lysosomal lipid accumulation blocks lysosomal calcium release. However, the mechanism by which lysosomal calcium regulates mTORC1 has remained undefined. In this work, we used pharmacological and genetic methods to illustrate that proper lysosomal calcium release through the calcium channel TRPML1 (transient receptor potential cation channel, mucolipin 1) is required for mTORC1 activation by inducing association of calmodulin (CaM) with mTOR. Moreover, we showed CaM is capable of stimulating the kinase activity of mTORC1 in a calcium-dependent manner *in vitro*.

Bearing the strategy of inhibiting mTOR by inducing lysosomal cholesterol accumulation in endothelial cells, we sought to identify novel mTOR inhibitors by drug repurposing that potentially can be used in anti-angiogenesis and anti-cancer treatment. First, we further characterized the divergence of antiangiogenesis activity and hepatotoxicity of different stereoisomers of itraconazole by assessing *in vitro* antiangiogenic activity of itraconazole and each stereoisomer using human umbilical vein endothelial cells (HUVEC), as well as determining their hepatotoxicity using primary human hepatocytes *in vitro* and a mouse model *in vivo*. Of the four stereoisomers

contained in commercial itraconazole, we found that IT-C showed more potent antiangiogenic/antitumor activity with lower hepatotoxicity compared with itraconazole and other stereoisomers. Therefore, these results suggest that IT-C may be superior to the racemic mixture of itraconazole as an anticancer drug candidate due to its lower hepatotoxicity and improved antiangiogenic activity. In addition to itraconazole, we also identified that selective estrogen receptor modulators (SERM), such as tamoxifen, inhibit angiogenesis and produce anti-breast cancer effect through blockade of cholesterol trafficking as well as inhibiting mTOR rather than estrogen receptor antagonism. Together, these results unraveled a previously unrecognized mechanism of angiogenesis inhibition by inducing lysosomal cholesterol accumulation, implicating cholesterol trafficking and mTOR inhibition as an attractive therapeutic target for cancer treatment.

Thesis advisor: Dr. Jun O. Liu

Thesis committee: Dr. Solomon H. Snyder, Dr. Philip Cole, Dr. Duojia Pan

Acknowledgement

There are many people who have helped me along the way up to this point in my career. The first two people who have truly influenced my path are my parents. Both of my parents are scientists, especially my mother is a doctor who worked in Centers for Disease Control and Prevention (CDC) as a microbiologist in Beijing, China. They were not only educating me as parents educating their kids, but also led me to get onto the road of science. I visited my mother's lab when I was in elementary school, and it was my very first time seeing what a lab was like. I could still remember how fascinated I felt when I watched my mother and her coworkers working in the lab across the glass windows. From that time, I have been very interested in life science. I have to say my parents are the greatest influence in my decision to pursue science as a career.

The next person helped me go through an important transition point was Professor Wan-Liang Lu of Peking University School of Pharmaceutical Sciences, where I earned my B.S. and M.S. degrees. I would like to say Prof. Lu was the first person that gave me the systematic scientific training, and helped me go through many difficulties at the beginning of being a scientist. I joined Prof. Lu's lab as a volunteer undergraduate student when I was in my 2nd year of the college, and got great opportunities to be involved in many senior graduate students' projects. That was my first time to get exposure to academic research with its culture of pre-doctoral and post-doctoral trainees, weekly lab meetings, and open scientific discourse. During that four-year's training (undergraduate's and master's), I learned variety of techniques, scientific ideas, and more importantly, critical thinking. I was able to publish my own first-author paper and several

co-author papers in top pharmaceutical journals at the end of my Master's training, which I definitely couldn't achieve without Prof. Lu's help.

At Johns Hopkins I was very fortunate to join the lab of Professor Jun Liu, the most recent of my influential mentors along the path of my training. During the last five years, Dr. Liu's office door was always widely opened, and all lab members could just knock and walk in whenever they needed to talk about projects. This is a great mentoring quality that the trainees can always get discussions and suggestions as soon as they need with their advisor, and this spurred on new and exciting directions and ideas in the lab. Another greatest quality of Dr. Liu that I really appreciate is that he is always financially generous and supports us to study what we feel interesting and are willing to pursue. I couldn't recall any instance that I had to stop the experiments because of financial issues. He always encouraged me to come up my own ideas and plans, and after discussing with him, he gave me enough space so that I could pursue them with a great passion. Dr. Liu's enthusiasm for science is also very impressive. Everytime when I or other lab members got good results, he was always very excited and almost jumped up. Working with such a mentor, I have been truly influenced and always passionate about my projects. Dr. Liu is definitely one of the most intelligent but also diligent persons I have ever met. I can recall so many times that when I discussed my project with him or in seminars, his broad as well as deep knowledge in biology always amazed me. It definitely shows how tremendous amount of papers he has read and how great his memory is. I was always inspired by his great ideas when had a discussion with him.

I also thank the members of the Liu lab for their scientific discourse, technical assistance, and camaraderie over the years. In particular I want to thank Dr. Joong Sup

Shim, a previous senior post-doc in the lab, for his great help when I just joined the lab. We collaborated for a couple of years and published several co-first author papers. Many of the work in this thesis could not have been done without his help. I also want to thank Drs. Yongjun Dang and Feiran Zhang, who are previous post-doc and student in the lab, for teaching me many important techniques that were very useful through my whole PhD training. Drs. Sarah Head, Sam Hong, Brandon McClary and Zufeng Guo are the people I spent the longest time together in this lab during the last five years. I want to say it is my great pleasure to have them not only as coworkers, but also as friends. And I also want to thank Felix Yu, who used to sit next to me, for discussing experiments with me.

I am also indebted to Dr. Jin Zhang, who used to be a professor at Johns Hopkins Pharmacology and currently is professor at UCSD Pharmacology, as well as Dr. Robert Siliciano at Johns Hopkins Pharmacology. Without their generously financial support, as an international student, I couldn't have the opportunity to be accepted by Johns Hopkins Pharmacology PhD program to pursue my scientific training. I am likewise grateful to the members of my thesis committee, Drs. Solomon Snyder, Philip Cole and Duojia Pan for their input and guidance. They both not only provided outstanding support scientifically, but also treated me with a level of respect beyond what I expected as a graduate student.

In the end, it has been a great fun to spend my five years at Johns Hopkins.

Table of Contents

List of tables

List of Figures

Chapter 1: Introduction

1.1 mTOR structure

Target of rapamycin (TOR), discovered from yeast mutants that resistant to the inhibitory effect of rapamycin (*1, 2*), is highly conserved in all eukaryotes including plants, worms, flies, and mammals. The mammalian TOR (mTOR, also known as mechanistic target of rapamycin) in humans is encoded by the *MTOR* gene (*3, 4*). mTOR independently associates with regulatory-associated protein of mammalian target of rapamycin (raptor) or rapamycin-insensitive companion of mTOR (rictor) to form two distinct complexes, mTORC1 and mTORC2, respectively. The two complexes share several common subunits, including the catalytic mTOR subunit, mammalian lethal with sec-13 protein 8 (mLST8), DEP domain containing mTOR-interacting protein (DEPTOR), and the Tti1/Tel2 complex (*5*). Among the remaining components, raptor and proline-rich Akt substrate 40 kDa (PRAS40) are specific to mTORC1, whereas rictor, mammalian stress-activated map kinase-interacting protein 1 (mSin1) protein observed with rictor 1 and 2 (protor1/2) are unique to mTORC2 (*5*).

Cryo-electron microscopy (cryo-EM) studies have shown that mTOR forms an obligate dimer with an overall rhomboid shape and a central cavity at a relatively low resolution (26 Å) (*6*). Subsequently, another study crystalized N-terminally truncated human mTOR and mLST8, which is a subunit shared by both mTORC1 and mTORC2, to disclose a more detailed structure of mTORC1 and its inhibition by rapamycin-FKBP12 complex at a higher resolution (3.2 Å) (*7*). However, information of the arrangement of

the subunits within the complex was missing because mTOR was truncated and only mLST8 was presented, while raptor, the key subunit of mTORC1 was no included. A more resent study successfully obtained a high-resolution cryo-EM of mTOR complex 1 including purified raptor and mLST8 from insect cells (*8*). The N-terminus of mTOR contains two α-helical solenoids. The larger section is a highly curved super-helix, while the smaller region adopts a relatively linear arrangement. Both sections are exposed to the environment, indicating a potential role in binding mTOR associated proteins. In addition, the larger and smaller regions of HEAT domains pack against one another, and the first HEAT repeat of the larger region interlocks with the adjacent mTOR FAT domain, through which the two mTOR subunits forms a dimer independent of Raptor (*8*), which makes mTORC1 a dimeric architecture and presented in a hollow lozenge shape, in which raptor and mLST8 form peripheral parts of the complex, respectively. Interestingly, mTOR kinase domain was not affected by the dimerization, indicating that the regulation of the kinase activity was mainly achieved by controlling the access of substrates.

1.2 Regulation of mTOR signaling pathway

mTORC1 and mTORC2 differ in their sensitivity to rapamycin, upstream signals and downstream outputs (*5*). The mTORC1 complex integrates different extracellular and intracellular signal inputs, such as growth factors, amino acids, stress and energy status, to regulate cellular processes such as protein and lipid synthesis and autophagy, by phosphorylating and activating p70 S6 kinase (p70S6K) (*9, 10*) and eukaryotic translation initiation factor 4E-binding protein 1 (4E-BP1) (*11, 12*). In contrast, mTORC2 is involved in Akt phosphorylation and regulation of the cellular cytoskeleton (*13*). mTOR

directly binds to GTP-bound Rheb and is subsequently activated on the surface of the lysosome. Therefore, the activation of mTORC1 required the translocation of mTORC1 onto lysosomes, where it encounters Rheb. This translocation is controlled by the Rag GTPase and the Ragulator complex in response to amino acids (*14-16*). Rag is a heterodimeric GTPase consisting of RagA or B in complex with RagC or D. Amino acids stimulate guanine nucleotide exchange in Rag. However, it is still controversial whether Rag delivers mTORC1 onto lysosomal surface or Rag is fixed on lysosomes, from where it recruits mTORC1 to lysosomal surface (*16-19*). However, amino acid-mediated mTOR translocation was no longer observed when Rag or Raptor expression was genetically knocked-down by RNA interference. The exact mechanism that how Rag translocate mTORC1 onto lysosomal is still remained determined.

Another requirement to activate mTORC1 is that Rheb (Ras-homolog enriched in brain) needs to be activated by binding to GTP in response to growth factors. Rheb is a farnesylated GTPase that is anchored to the surface of the lysosome (*16, 20*). Rheb directly binds (*21*) and activates mTOR in vitro and in vivo (*22*). Rheb knockdown abolishes S6K1 and 4EBP1 phosphorylation (*23*), whereas, overexpression of Rheb stimulates S6K1 and 4EBP1 phosphorylation (*24, 25*). Tuberous sclerosis complex (TSC), a GAP of Rheb localized on lysosomes, negatively regulates Rheb. It is also known that TSC is inhibited by activation of Akt in response to growth factors (*26*).

The regulation of mTORC1 by TSC-Rheb and amino acids-Rag are distinct. Amino acid starvation still induces dephosphorylation of S6K1, S6 and 4EBP1 in TSC2-/- MEFs, suggesting TSC1/2 is not required for amino acid-mediated mTORC1 regulation (*27, 28*). On the other hand, mTORC1 locked on lysosome still needs growth

factors and Rheb to be activated, although it is not dependent on amino acids and Rag (*19*). This indicates that activation of mTORC1 needs the availability of both amino acids and growth factor, to make sure mTORC1 is translocated onto lysosome, where it encounters and binds to Rheb, which is activated by growth factors. Rheb also interacts with Raptor and mLST8, however, the interaction was not affected by amino acids (*29*). In addition, the modulation of the interaction between mTOR and raptor was also evaluated. The recovery of Raptor co-immunoprecipitated with mTOR was negatively regulated by amino acids stimulation in HEK293T cells. However, mTOR kinase activity was inversely correlated with the strength of Raptor binding to mTOR in vitro (*30*). On the other hand, insulin stimulation did not affect mTOR-Raptor interaction although it increased S6K1 phosphorylation.

Two independent groups have reported that Vps34 plays a key role in mTORC1 regulation by amino acids (*31, 32*). Vps34 (vacuolar protein sorting 34) belongs to Class III PI3K. It forms an active complex with another protein kinase Vps15 (*33*) and generates PtdIns(3)P (*34-36*). hVps34 activity was increased and decreased by amino acid stimulation and deprivation, respectively, in accordance with S6K phosphorylation (*31*). In addition, knockdown of hVps34 or overexpression of GFP-FYVE expression vector, which sequesters PtdIns(3)P therefore acts as a dominant negative to Vps34 signaling, also inhibited S6K phosphorylation. The mechanism of how hVps34 regulates mTORC1 has not been clearly known. It has been reported that addition of amino acid evoked a rapid increase in intracellular Ca2+ concentration and S6K phosphorylation. Furthermore, hVps34 activity and PtdIns(3)P production were inhibited by pre-incubation with Ca2+ chelator, BAPTA-AM. These results suggest that Vps34 and mTOR is

downstream of Ca2+. In addition, they reported that calmodulin (CaM) interacts with mTOR in a Ca2+ and hVps34-dependent manner. These evidences suggested a model that amino acid increases Ca2+ influx, which increases the interaction of Ca2+/CaM with the hVps34-mTOR and consequently activates mTORC1.

In addition to the lysosome, the subunits of mTORC1 were also detected to in the nucleus (*37-42*), mitochondria (*43-45*), stress granules (*46-48*), cytoplasm (*49-51*) and at the plasma membrane (*52*) under different conditions. However, whether the subunits can form intact mTORC1 (*53*), and some of the mechanism and regulation are not fully understood.

Activated mTORC1 phosphorylates several downstream effectors, including S6K1 and 4EBP1, via an interaction between raptor and a TOR signalling (TOS) motif in S6K and 4EBP (*54-56*). The serine/threonine kinase p70S6K1 is one of the most well-known downstream targets of mTORC1. The phosphorylation of S6K1 at Thr389 by mTORC1 is required for its activation. The phosphorylated S6K by activated mTORC1 phosphorylates S6 (40S ribosomal protein S6), enhancing the translation of mRNA (*57*). 4EBP1 is another well-characterize mTORC1 target. 4EBP1 inhibits the initiation of protein translation by binding and inactivating eIF4E (eukaryotic translation initiation factor 4E) (*58*). mTORC1 phosphorylates 4EBP1 to promote the dissociation of eIF4E from 4EBP1 (*59*). Free eIF4E can form the multisubunit eIF4F complex, enabling cap-dependent protein translation, and inducing increased translation of mRNAs (*57*). Multiple studies suggest a negative feedback loop from the mTOR-S6K1 pathway to the upstream IRS pathway (*60, 61*).

Although mTORC1 activity is prone to multiple positive and negative regulations driven by extracellular growth factors and stress stimuli, mTORC2 regulation mechanisms remain largely unknown. In mammalian cells, mTORC2 phosphorylates Akt upon growth factor stimulation such as insulin, indicating that mTORC2 is regulated by the PI3K pathway (*62, 63*). However, the mechanism by which insulin or other growth factors activate mTORC2 is unclear. A recent study indicated that TSC1/TSC2 complex may play a key role in the regulation of mTORC2 by growth factor. In contrast to the negative regulation of mTORC1, TSC1/TSC2 complex positively regulate mTORC2 in a GAP-independent manner (*64*). The GTPase Rheb, which is a downstream of TSC1/TSC2 and activates mTORC1, does not appear to regulate mTORC2.

1.3 mTOR in human cancer

Since mTOR plays the key role in cell growth and metabolism, it is not surprised that an abnormal mTOR pathway activity may exist in pathological states, including cancer. In a number of *in vitro* cell-lines and *in vivo* mice xenograft models, abnormal mTOR pathway activation through oncogene stimulation or loss of tumour suppressors contributes to tumour growth, angiogenesis and metastasis (*57*). Mutations in mTOR gene that confer constitutive activation of mTOR signaling under nutrient starvation conditions have been identified in a few human cancers (*65*). PI3K/AKT, the upstream signaling of mTORC1, is deregulated through a variety of mechanisms, including overexpression or activation of growth factor receptors, for examples, human epidermal growth factor receptor 2 (HER-2) and insulin-like growth factor receptor (IGFR), mutations in PI3K and mutations/amplifications of AKT (*66-68*). PTEN, the negative

regulator of PI3K signalling, was also reported to be decreased or lost its expression in many cancers (*69, 70*). mTOR downstream effectors S6K1, 4EBP1 and eIF4E are implicated in protein translation, and their overexpression has been linked to poor cancer prognosis (*71-74*).

Thus, the activation of mTOR has been reported to be lost control in many cancer types. Deregulation of multiple elements of the mTOR pathway has been discovered in cancer, such as breast, ovarian, renal, colon and head and neck cancers. Taken together, these data emphasizes the importance of mTOR signalling in cancer and reinforce the importance of considering mTOR targeting in cancer therapy.

1.4 Strategy that small molecules inhibit mTOR

mTOR inhibitors can be classified into two groups: rapamycin and rapamycin analogues that allosterically inhibit mTORC1 and the small molecules that inhibit mTOR kinase activity.

Originally, rapamycin (rapamune, sirolimus) was used an immunosuppressive drug for prevention of renal allograft rejection (*75*). Subsequent studies demonstrated that rapamycin can also slow or arrest growth of different cancer cell lines (*76-82*). Furthermore, rapamycin also inhibits cell proliferation, survival and angiogenesis (*83, 84*). Several rapamycin analogues have been developed with better pharmacokinetic c and solubility characteristics. Similarly to rapamycin, these analogues can form a complex with FKBP12 and further bind to mTOR and inhibit mTORC1 signaling pathway (*85, 86*). Currently, rapamycin and its analogues temsirolimus, everolimus and deforolimus are in clinical trials, and some of them showed encouraging results in a

subset of cancers (*87-90*). However, due to weak inhibition to phosphorylation of 4EBP1 and failure inhibition of mTORC2, the antiproliferative effects of the analogues are variable in cancer cells in some tumour types. In addition, the specific inhibition of mTORC1 also raised an issue that the upstream receptor tyrosine kinase signaling and Akt might be up-regulated, leading to the drug resistance (*91*). Thus, the combination therapy that targets both mTOR and Akt may improve anti-cancer effect.

Another class of mTOR inhibitors binds to the ATP-binding site of mTOR and inhibit both mTORC1 and mTORC2 potently, and they showed better anti-cancer effects in preclinical studies compared with that of rapamycin analogues (*92, 93*). PP242 and Torin1, selective ATP-competitive mTOR inhibitors, have been reported to display more potent effects to inhibit protein synthesis, cell growth and proliferation (*92, 93*). These compounds need to be further evaluated in the cancer treatment to determined how they will be affected by up-regulated PI3K signaling.

Currently, several dual PI3K-mTOR inhibitors are under development (*94-96*). This class of compounds is undergoing clinical trials for cancer treatment, and was reported to prevent the activity of PI3K-mTOR axis biomarkers more effectively than rapamycin, by inhibiting both mTORC1 and mTORC2.

So far in most tumor types, mTOR inhibitors are predominantly stabilizing the disease rather than leading to tumor regression. Thus, combination therapies are usually necessary with the aim to induce a cytotoxic rather than a cytostatic response, and subsequent tumour regression. Multiple studies have evaluated mTOR inhibitors used in combination therapies with conventional chemotherapy agents, such as carboplatin,

cisplatin, vinorelbine, doxorubicin, paclitaxel, and camptothecin, and showed synergistic or additive effects (*77, 97-99*).

On the other hand, temsirolimus or everolimus has also been tested in combination with bevacizumab, sorafenib or sunitinib in clinical trials, given mTOR inhibitors downregulate HIF and VEGF.

Recently, another class of compounds that indirectly inhibit mTOR in endothelial cells has been reported (*100*), and itraconazole was one of them. This class of compounds induces lysosomal cholesterol accumulation, which mimics Niemann-Pick C phenotype, and subsequently inhibits mTOR activity in human umbilical vein endothelial cells (HUVEC) and produces anti-angiogenesis effects. Interestingly, the inhibition of mTOR by this class of compounds was reversed by increasing cytosolic calcium concentration. The essential role of cholesterol homeostasis in the activity of the mTOR pathway in endothelial cells suggests that the intracellular cholesterol trafficking pathway, including NPC1 and NPC2, may serve as a promising target for developing inhibitors of angiogenesis. However, the mechanism that how NPC phenotype leads to mTOR inhibition remains unknown. Several studies have reported that in NPC cells, the homeostasis of lysosomal calcium is disrupted (*101*), and lysosomal calcium release through TRPML1 is blocked (*102*). This raised a question that whether mTOR is regulated by Ca^{2+}.

The goal of this thesis work has been to discover the mechanism of connection between NPC phenotype and mTOR inhibition, with the aim of understanding the novel regulator of mTOR signaling pathway, and therefore identify alternative strategy to inhibit mTOR activity. To accomplish this, I used pharmacological or genetic methods to

study the role of lysosomal calcium and calmodulin in mTORC1 activation in the cells, and evaluated the effect of Ca^{2+}/CaM in regulating mTOR kinase activity *in vitro* as well (Chapter 2). In addition, following this strategy that inhibiting mTOR by inducing NPC phenotype, I studied different stereoisomers of itraconazole in mTOR inhibition in endothelial cells as well as hepatotoxicity (Chapter 3). Furthermore, this strategy also prompted us to identify a class of selective estrogen receptor modulators that inhibit mTOR signaling through blockade of cholesterol trafficking, and produces anti-angiogenesis effect in breast cancers rather than estrogenreceptor antagonism (Chapter 4). The relevance of these studies and future directions will be discussed in each chapter.

1.5 References

1. J. Heitman, N. R. Movva, M. N. Hall, Targets for cell cycle arrest by the immunosuppressant rapamycin in yeast. *Science* **253**, 905-909 (1991)
2. J. Kunz, R. Henriquez, U. Schneider, M. Deuter-Reinhard, N. R. Movva, M. N. Hall, Target of rapamycin in yeast, TOR2, is an essential phosphatidylinositol kinase homolog required for G1 progression. *Cell* **73**, 585-596 (1993)
3. E. J. Brown, M. W. Albers, T. B. Shin, K. Ichikawa, C. T. Keith, W. S. Lane, S. L. Schreiber, A mammalian protein targeted by G1-arresting rapamycin-receptor complex. *Nature* **369**, 756-758 (1994)
4. P. A. Moore, C. A. Rosen, K. C. Carter, Assignment of the human FKBP12-rapamycin-associated protein (FRAP) gene to chromosome 1p36 by fluorescence in situ hybridization. *Genomics* **33**, 331-332 (1996)
5. M. Laplante, D. M. Sabatini, mTOR signaling in growth control and disease. *Cell* **149**, 274-293 (2012)
6. C. K. Yip, K. Murata, T. Walz, D. M. Sabatini, S. A. Kang, Structure of the human mTOR complex I and its implications for rapamycin inhibition. *Mol Cell* **38**, 768-774 (2010)
7. H. Yang, D. G. Rudge, J. D. Koos, B. Vaidialingam, H. J. Yang, N. P. Pavletich, mTOR kinase structure, mechanism and regulation. *Nature* **497**, 217-223 (2013)
8. C. H. Aylett, E. Sauer, S. Imseng, D. Boehringer, M. N. Hall, N. Ban, T. Maier, Architecture of human mTOR complex 1. *Science* **351**, 48-52 (2016)

9. J. Chung, C. J. Kuo, G. R. Crabtree, J. Blenis, Rapamycin-FKBP specifically blocks growth-dependent activation of and signaling by the 70 kd S6 protein kinases. *Cell* **69**, 1227-1236 (1992)

10. D. J. Price, J. R. Grove, V. Calvo, J. Avruch, B. E. Bierer, Rapamycin-induced inhibition of the 70-kilodalton S6 protein kinase. *Science* **257**, 973-977 (1992)

11. T. A. Lin, X. Kong, A. R. Saltiel, P. J. Blackshear, J. C. Lawrence, Jr., Control of PHAS-I by insulin in 3T3-L1 adipocytes. Synthesis, degradation, and phosphorylation by a rapamycin-sensitive and mitogen-activated protein kinase-independent pathway. *The Journal of biological chemistry* **270**, 18531-18538 (1995)

12. S. R. von Manteuffel, A. C. Gingras, X. F. Ming, N. Sonenberg, G. Thomas, 4E-BP1 phosphorylation is mediated by the FRAP-p70s6k pathway and is independent of mitogen-activated protein kinase. *Proceedings of the National Academy of Sciences of the United States of America* **93**, 4076-4080 (1996)

13. P. T. Bhaskar, N. Hay, The two TORCs and Akt. *Developmental cell* **12**, 487-502 (2007)

14. J. L. Jewell, R. C. Russell, K. L. Guan, Amino acid signalling upstream of mTOR. *Nature reviews. Molecular cell biology* **14**, 133-139 (2013)

15. E. Kim, P. Goraksha-Hicks, L. Li, T. P. Neufeld, K. L. Guan, Regulation of TORC1 by Rag GTPases in nutrient response. *Nature cell biology* **10**, 935-945 (2008)

16. Y. Sancak, T. R. Peterson, Y. D. Shaul, R. A. Lindquist, C. C. Thoreen, L. Bar-Peled, D. M. Sabatini, The Rag GTPases bind raptor and mediate amino acid signaling to mTORC1. *Science* **320**, 1496-1501 (2008)

17. V. Zinzalla, M. N. Hall, Signal transduction: Linking nutrients to growth. *Nature* **454**, 287-288 (2008)

18. L. Bar-Peled, L. D. Schweitzer, R. Zoncu, D. M. Sabatini, Ragulator is a GEF for the rag GTPases that signal amino acid levels to mTORC1. *Cell* **150**, 1196-1208 (2012)

19. Y. Sancak, L. Bar-Peled, R. Zoncu, A. L. Markhard, S. Nada, D. M. Sabatini, Ragulator-Rag complex targets mTORC1 to the lysosomal surface and is necessary for its activation by amino acids. *Cell* **141**, 290-303 (2010)

20. K. Saito, Y. Araki, K. Kontani, H. Nishina, T. Katada, Novel role of the small GTPase Rheb: its implication in endocytic pathway independent of the activation of mammalian target of rapamycin. *Journal of biochemistry* **137**, 423-430 (2005)

21. X. Long, Y. Lin, S. Ortiz-Vega, K. Yonezawa, J. Avruch, Rheb binds and regulates the mTOR kinase. *Curr Biol* **15**, 702-713 (2005)

22. Y. Sancak, C. C. Thoreen, T. R. Peterson, R. A. Lindquist, S. A. Kang, E. Spooner, S. A. Carr, D. M. Sabatini, PRAS40 is an insulin-regulated inhibitor of the mTORC1 protein kinase. *Mol Cell* **25**, 903-915 (2007)

23. Y. Zhang, X. Gao, L. J. Saucedo, B. Ru, B. A. Edgar, D. Pan, Rheb is a direct target of the tuberous sclerosis tumour suppressor proteins. *Nature cell biology* **5**, 578-581 (2003)

24. K. Inoki, Y. Li, T. Xu, K. L. Guan, Rheb GTPase is a direct target of TSC2 GAP activity and regulates mTOR signaling. *Genes & development* **17**, 1829-1834 (2003)

25. A. R. Tee, B. D. Manning, P. P. Roux, L. C. Cantley, J. Blenis, Tuberous sclerosis complex gene products, Tuberin and Hamartin, control mTOR signaling by acting as a GTPase-activating protein complex toward Rheb. *Curr Biol* **13**, 1259-1268 (2003)

26. B. A. Hemmings, D. F. Restuccia, PI3K-PKB/Akt pathway. *Cold Spring Harbor perspectives in biology* **4**, a011189 (2012)

27. E. M. Smith, S. G. Finn, A. R. Tee, G. J. Browne, C. G. Proud, The tuberous sclerosis protein TSC2 is not required for the regulation of the mammalian target of rapamycin by amino acids and certain cellular stresses. *The Journal of biological chemistry* **280**, 18717-18727 (2005)

28. M. Roccio, J. L. Bos, F. J. Zwartkruis, Regulation of the small GTPase Rheb by amino acids. *Oncogene* **25**, 657-664 (2006)

29. X. Long, S. Ortiz-Vega, Y. Lin, J. Avruch, Rheb binding to mammalian target of rapamycin (mTOR) is regulated by amino acid sufficiency. *The Journal of biological chemistry* **280**, 23433-23436 (2005)

30. D. H. Kim, D. D. Sarbassov, S. M. Ali, J. E. King, R. R. Latek, H. Erdjument-Bromage, P. Tempst, D. M. Sabatini, mTOR interacts with raptor to form a nutrient-sensitive complex that signals to the cell growth machinery. *Cell* **110**, 163-175 (2002)

31. T. Nobukuni, M. Joaquin, M. Roccio, S. G. Dann, S. Y. Kim, P. Gulati, M. P. Byfield, J. M. Backer, F. Natt, J. L. Bos, F. J. Zwartkruis, G. Thomas, Amino acids mediate mTOR/raptor signaling through activation of class 3 phosphatidylinositol 3OH-kinase. *Proceedings of the National Academy of Sciences of the United States of America* **102**, 14238-14243 (2005)

32. M. P. Byfield, J. T. Murray, J. M. Backer, hVps34 is a nutrient-regulated lipid kinase required for activation of p70 S6 kinase. *The Journal of biological chemistry* **280**, 33076-33082 (2005)

33. S. Volinia, R. Dhand, B. Vanhaesebroeck, L. K. MacDougall, R. Stein, M. J. Zvelebil, J. Domin, C. Panaretou, M. D. Waterfield, A human phosphatidylinositol 3-kinase complex related to the yeast Vps34p-Vps15p protein sorting system. *The EMBO journal* **14**, 3339-3348 (1995)

34. T. Nobukuni, S. C. Kozma, G. Thomas, hvps34, an ancient player, enters a growing game: mTOR Complex1/S6K1 signaling. *Current opinion in cell biology* **19**, 135-141 (2007)

35. Y. Yan, J. M. Backer, Regulation of class III (Vps34) PI3Ks. *Biochemical Society transactions* **35**, 239-241 (2007)

36. J. M. Backer, The regulation and function of Class III PI3Ks: novel roles for Vps34. *The Biochemical journal* **410**, 1-17 (2008)

37. C. K. Kikani, L. Q. Dong, F. Liu, "New"-clear functions of PDK1: beyond a master kinase in the cytosol? *Journal of cellular biochemistry* **96**, 1157-1162 (2005)

38. J. E. Kim, J. Chen, Cytoplasmic-nuclear shuttling of FKBP12-rapamycin-associated protein is involved in rapamycin-sensitive signaling and translation initiation. *Proceedings of the National Academy of Sciences of the United States of America* **97**, 14340-14345 (2000)

39. S. J. Kim, C. R. Kahn, Insulin stimulates p70 S6 kinase in the nucleus of cells. *Biochemical and biophysical research communications* **234**, 681-685 (1997)

40. Z. Lian, A. Di Cristofano, Class reunion: PTEN joins the nuclear crew. *Oncogene* **24**, 7394-7400 (2005)

41. M. Rosner, A. Freilinger, M. Hengstschlager, Akt regulates nuclear/cytoplasmic localization of tuberin. *Oncogene* **26**, 521-531 (2007)

42. X. Zhang, L. Shu, H. Hosoi, K. G. Murti, P. J. Houghton, Predominant nuclear localization of mammalian target of rapamycin in normal and malignant cells in culture. *The Journal of biological chemistry* **277**, 28127-28134 (2002)

43. S. Paglin, N. Y. Lee, C. Nakar, M. Fitzgerald, J. Plotkin, B. Deuel, N. Hackett, M. McMahill, E. Sphicas, N. Lampen, J. Yahalom, Rapamycin-sensitive pathway regulates mitochondrial membrane potential, autophagy, and survival in irradiated MCF-7 cells. *Cancer research* **65**, 11061-11070 (2005)

44. A. Ramanathan, S. L. Schreiber, Direct control of mitochondrial function by mTOR. *Proceedings of the National Academy of Sciences of the United States of America* **106**, 22229-22232 (2009)

45. S. M. Schieke, D. Phillips, J. P. McCoy, Jr., A. M. Aponte, R. F. Shen, R. S. Balaban, T. Finkel, The mammalian target of rapamycin (mTOR) pathway

regulates mitochondrial oxygen consumption and oxidative capacity. *The Journal of biological chemistry* **281**, 27643-27652 (2006)

46. K. Thedieck, B. Holzwarth, M. T. Prentzell, C. Boehlke, K. Klasener, S. Ruf, A. G. Sonntag, L. Maerz, S. N. Grellscheid, E. Kremmer, R. Nitschke, E. W. Kuehn, J. W. Jonker, A. K. Groen, M. Reth, M. N. Hall, R. Baumeister, Inhibition of mTORC1 by astrin and stress granules prevents apoptosis in cancer cells. *Cell* **154**, 859-874 (2013)

47. T. Takahara, T. Maeda, Transient sequestration of TORC1 into stress granules during heat stress. *Mol Cell* **47**, 242-252 (2012)

48. F. Wippich, B. Bodenmiller, M. G. Trajkovska, S. Wanka, R. Aebersold, L. Pelkmans, Dual specificity kinase DYRK3 couples stress granule condensation/dissolution to mTORC1 signaling. *Cell* **152**, 791-805 (2013)

49. T. E. Harris, A. Chi, J. Shabanowitz, D. F. Hunt, R. E. Rhoads, J. C. Lawrence, Jr., mTOR-dependent stimulation of the association of eIF4G and eIF3 by insulin. *The EMBO journal* **25**, 1659-1668 (2006)

50. M. K. Holz, B. A. Ballif, S. P. Gygi, J. Blenis, mTOR and S6K1 mediate assembly of the translation preinitiation complex through dynamic protein interchange and ordered phosphorylation events. *Cell* **123**, 569-580 (2005)

51. N. Sonenberg, A. G. Hinnebusch, Regulation of translation initiation in eukaryotes: mechanisms and biological targets. *Cell* **136**, 731-745 (2009)

52. D. Bridges, J. T. Ma, S. Park, K. Inoki, L. S. Weisman, A. R. Saltiel, Phosphatidylinositol 3,5-bisphosphate plays a role in the activation and

subcellular localization of mechanistic target of rapamycin 1. *Molecular biology of the cell* **23**, 2955-2962 (2012)

53. M. Rosner, M. Hengstschlager, Cytoplasmic and nuclear distribution of the protein complexes mTORC1 and mTORC2: rapamycin triggers dephosphorylation and delocalization of the mTORC2 components rictor and sin1. *Human molecular genetics* **17**, 2934-2948 (2008)

54. H. K. Lim, Y. A. Choi, W. Park, T. Lee, S. H. Ryu, S. Y. Kim, J. R. Kim, J. H. Kim, S. H. Baek, Phosphatidic acid regulates systemic inflammatory responses by modulating the Akt-mammalian target of rapamycin-p70 S6 kinase 1 pathway. *The Journal of biological chemistry* **278**, 45117-45127 (2003)

55. H. Nojima, C. Tokunaga, S. Eguchi, N. Oshiro, S. Hidayat, K. Yoshino, K. Hara, N. Tanaka, J. Avruch, K. Yonezawa, The mammalian target of rapamycin (mTOR) partner, raptor, binds the mTOR substrates p70 S6 kinase and 4E-BP1 through their TOR signaling (TOS) motif. *The Journal of biological chemistry* **278**, 15461-15464 (2003)

56. S. S. Schalm, D. C. Fingar, D. M. Sabatini, J. Blenis, TOS motif-mediated raptor binding regulates 4E-BP1 multisite phosphorylation and function. *Curr Biol* **13**, 797-806 (2003)

57. S. Faivre, G. Kroemer, E. Raymond, Current development of mTOR inhibitors as anticancer agents. *Nature reviews. Drug discovery* **5**, 671-688 (2006)

58. N. Sonenberg, A. C. Gingras, The mRNA 5' cap-binding protein eIF4E and control of cell growth. *Current opinion in cell biology* **10**, 268-275 (1998)

59. A. Pause, G. J. Belsham, A. C. Gingras, O. Donze, T. A. Lin, J. C. Lawrence, Jr., N. Sonenberg, Insulin-dependent stimulation of protein synthesis by phosphorylation of a regulator of 5'-cap function. *Nature* **371**, 762-767 (1994)

60. L. S. Harrington, G. M. Findlay, A. Gray, T. Tolkacheva, S. Wigfield, H. Rebholz, J. Barnett, N. R. Leslie, S. Cheng, P. R. Shepherd, I. Gout, C. P. Downes, R. F. Lamb, The TSC1-2 tumor suppressor controls insulin-PI3K signaling via regulation of IRS proteins. *The Journal of cell biology* **166**, 213-223 (2004)

61. O. J. Shah, Z. Wang, T. Hunter, Inappropriate activation of the TSC/Rheb/mTOR/S6K cassette induces IRS1/2 depletion, insulin resistance, and cell survival deficiencies. *Curr Biol* **14**, 1650-1656 (2004)

62. M. A. Frias, C. C. Thoreen, J. D. Jaffe, W. Schroder, T. Sculley, S. A. Carr, D. M. Sabatini, mSin1 is necessary for Akt/PKB phosphorylation, and its isoforms define three distinct mTORC2s. *Curr Biol* **16**, 1865-1870 (2006)

63. E. Jacinto, V. Facchinetti, D. Liu, N. Soto, S. Wei, S. Y. Jung, Q. Huang, J. Qin, B. Su, SIN1/MIP1 maintains rictor-mTOR complex integrity and regulates Akt phosphorylation and substrate specificity. *Cell* **127**, 125-137 (2006)

64. J. Huang, C. C. Dibble, M. Matsuzaki, B. D. Manning, The TSC1-TSC2 complex is required for proper activation of mTOR complex 2. *Molecular and cellular biology* **28**, 4104-4115 (2008)

65. T. Sato, A. Nakashima, L. Guo, K. Coffman, F. Tamanoi, Single amino-acid changes that confer constitutive activation of mTOR are discovered in human cancer. *Oncogene* **29**, 2746-2752 (2010)

66. K. Stemke-Hale, A. M. Gonzalez-Angulo, A. Lluch, R. M. Neve, W. L. Kuo, M. Davies, M. Carey, Z. Hu, Y. Guan, A. Sahin, W. F. Symmans, L. Pusztai, L. K. Nolden, H. Horlings, K. Berns, M. C. Hung, M. J. van de Vijver, V. Valero, J. W. Gray, R. Bernards, G. B. Mills, B. T. Hennessy, An integrative genomic and proteomic analysis of PIK3CA, PTEN, and AKT mutations in breast cancer. *Cancer research* **68**, 6084-6091 (2008)

67. J. Chung, R. E. Bachelder, E. A. Lipscomb, L. M. Shaw, A. M. Mercurio, Integrin (alpha 6 beta 4) regulation of eIF-4E activity and VEGF translation: a survival mechanism for carcinoma cells. *The Journal of cell biology* **158**, 165-174 (2002)

68. B. P. Zhou, M. C. Hu, S. A. Miller, Z. Yu, W. Xia, S. Y. Lin, M. C. Hung, HER-2/neu blocks tumor necrosis factor-induced apoptosis via the Akt/NF-kappaB pathway. *The Journal of biological chemistry* **275**, 8027-8031 (2000)

69. T. Tamguney, D. Stokoe, New insights into PTEN. *Journal of cell science* **120**, 4071-4079 (2007)

70. I. Sansal, W. R. Sellers, The biology and clinical relevance of the PTEN tumor suppressor pathway. *Journal of clinical oncology : official journal of the American Society of Clinical Oncology* **22**, 2954-2963 (2004)

71. J. L. Nakamura, E. Garcia, R. O. Pieper, S6K1 plays a key role in glial transformation. *Cancer research* **68**, 6516-6523 (2008)

72. G. Armengol, F. Rojo, J. Castellvi, C. Iglesias, M. Cuatrecasas, B. Pons, J. Baselga, S. Ramon y Cajal, 4E-binding protein 1: a key molecular "funnel factor" in human cancer with clinical implications. *Cancer research* **67**, 7551-7555 (2007)

73. A. De Benedetti, J. R. Graff, eIF-4E expression and its role in malignancies and metastases. *Oncogene* **23**, 3189-3199 (2004)

74. M. Barlund, F. Forozan, J. Kononen, L. Bubendorf, Y. Chen, M. L. Bittner, J. Torhorst, P. Haas, C. Bucher, G. Sauter, O. P. Kallioniemi, A. Kallioniemi, Detecting activation of ribosomal protein S6 kinase by complementary DNA and tissue microarray analysis. *Journal of the National Cancer Institute* **92**, 1252-1259 (2000)

75. S. Huang, P. J. Houghton, Resistance to rapamycin: a novel anticancer drug. *Cancer metastasis reviews* **20**, 69-78 (2001).

76. M. B. Dilling, P. Dias, D. N. Shapiro, G. S. Germain, R. K. Johnson, P. J. Houghton, Rapamycin selectively inhibits the growth of childhood rhabdomyosarcoma cells through inhibition of signaling via the type I insulin-like growth factor receptor. *Cancer research* **54**, 903-907 (1994)

77. B. Geoerger, K. Kerr, C. B. Tang, K. M. Fung, B. Powell, L. N. Sutton, P. C. Phillips, A. J. Janss, Antitumor activity of the rapamycin analog CCI-779 in human primitive neuroectodermal tumor/medulloblastoma models as single agent and in combination chemotherapy. *Cancer research* **61**, 1527-1532 (2001)

78. M. Grewe, F. Gansauge, R. M. Schmid, G. Adler, T. Seufferlein, Regulation of cell growth and cyclin D1 expression by the constitutively active FRAP-p70s6K pathway in human pancreatic cancer cells. *Cancer research* **59**, 3581-3587 (1999)

79. S. Muthukkumar, T. M. Ramesh, S. Bondada, Rapamycin, a potent immunosuppressive drug, causes programmed cell death in B lymphoma cells. *Transplantation* **60**, 264-270 (1995)

80. T. Ogawa, M. Tokuda, K. Tomizawa, H. Matsui, T. Itano, R. Konishi, S. Nagahata, O. Hatase, Osteoblastic differentiation is enhanced by rapamycin in rat osteoblast-like osteosarcoma (ROS 17/2.8) cells. *Biochemical and biophysical research communications* **249**, 226-230 (1998)

81. H. Pang, L. E. Faber, Estrogen and rapamycin effects on cell cycle progression in T47D breast cancer cells. *Breast cancer research and treatment* **70**, 21-26 (2001)

82. T. Seufferlein, E. Rozengurt, Rapamycin inhibits constitutive p70s6k phosphorylation, cell proliferation, and colony formation in small cell lung cancer cells. *Cancer research* **56**, 3895-3897 (1996)

83. T. L. Phung, K. Ziv, D. Dabydeen, G. Eyiah-Mensah, M. Riveros, C. Perruzzi, J. Sun, R. A. Monahan-Earley, I. Shiojima, J. A. Nagy, M. I. Lin, K. Walsh, A. M. Dvorak, D. M. Briscoe, M. Neeman, W. C. Sessa, H. F. Dvorak, L. E. Benjamin, Pathological angiogenesis is induced by sustained Akt signaling and inhibited by rapamycin. *Cancer cell* **10**, 159-170 (2006)

84. G. V. Thomas, C. Tran, I. K. Mellinghoff, D. S. Welsbie, E. Chan, B. Fueger, J. Czernin, C. L. Sawyers, Hypoxia-inducible factor determines sensitivity to inhibitors of mTOR in kidney cancer. *Nature medicine* **12**, 122-127 (2006)

85. F. J. Dumont, Q. Su, Mechanism of action of the immunosuppressant rapamycin. *Life sciences* **58**, 373-395 (1996).

86. A. C. Gingras, B. Raught, S. P. Gygi, A. Niedzwiecka, M. Miron, S. K. Burley, R. D. Polakiewicz, A. Wyslouch-Cieszynska, R. Aebersold, N. Sonenberg, Hierarchical phosphorylation of the translation inhibitor 4E-BP1. *Genes & development* **15**, 2852-2864 (2001)

87. J. E. Dancey, Therapeutic targets: MTOR and related pathways. *Cancer biology & therapy* **5**, 1065-1073 (2006)

88. B. I. Rini, Temsirolimus, an inhibitor of mammalian target of rapamycin. *Clinical cancer research : an official journal of the American Association for Cancer Research* **14**, 1286-1290 (2008)

89. D. A. Rizzieri, E. Feldman, J. F. Dipersio, N. Gabrail, W. Stock, R. Strair, V. M. Rivera, M. Albitar, C. L. Bedrosian, F. J. Giles, A phase 2 clinical trial of deforolimus (AP23573, MK-8669), a novel mammalian target of rapamycin inhibitor, in patients with relapsed or refractory hematologic malignancies. *Clinical cancer research : an official journal of the American Association for Cancer Research* **14**, 2756-2762 (2008)

90. B. M. Wolpin, A. F. Hezel, T. Abrams, L. S. Blaszkowsky, J. A. Meyerhardt, J. A. Chan, P. C. Enzinger, B. Allen, J. W. Clark, D. P. Ryan, C. S. Fuchs, Oral mTOR inhibitor everolimus in patients with gemcitabine-refractory metastatic pancreatic cancer. *Journal of clinical oncology : official journal of the American Society of Clinical Oncology* **27**, 193-198 (2009)

91. K. E. O'Reilly, F. Rojo, Q. B. She, D. Solit, G. B. Mills, D. Smith, H. Lane, F. Hofmann, D. J. Hicklin, D. L. Ludwig, J. Baselga, N. Rosen, mTOR inhibition induces upstream receptor tyrosine kinase signaling and activates Akt. *Cancer research* **66**, 1500-1508 (2006)

92. M. E. Feldman, B. Apsel, A. Uotila, R. Loewith, Z. A. Knight, D. Ruggero, K. M. Shokat, Active-site inhibitors of mTOR target rapamycin-resistant outputs of mTORC1 and mTORC2. *PLoS biology* **7**, e38 (2009)

93. C. C. Thoreen, S. A. Kang, J. W. Chang, Q. Liu, J. Zhang, Y. Gao, L. J. Reichling, T. Sim, D. M. Sabatini, N. S. Gray, An ATP-competitive mammalian target of rapamycin inhibitor reveals rapamycin-resistant functions of mTORC1. *The Journal of biological chemistry* **284**, 8023-8032 (2009)

94. A. Molckovsky, L. L. Siu, First-in-class, first-in-human phase I results of targeted agents: highlights of the 2008 American society of clinical oncology meeting. *Journal of hematology & oncology* **1**, 20 (2008)10.1186/1756-8722-1-20).

95. T. A. Yap, M. D. Garrett, M. I. Walton, F. Raynaud, J. S. de Bono, P. Workman, Targeting the PI3K-AKT-mTOR pathway: progress, pitfalls, and promises. *Current opinion in pharmacology* **8**, 393-412 (2008)

96. T. J. Liu, D. Koul, T. LaFortune, N. Tiao, R. J. Shen, S. M. Maira, C. Garcia-Echevrria, W. K. Yung, NVP-BEZ235, a novel dual phosphatidylinositol 3-kinase/mammalian target of rapamycin inhibitor, elicits multifaceted antitumor activities in human gliomas. *Molecular cancer therapeutics* **8**, 2204-2210 (2009)

97. V. Grunwald, L. DeGraffenried, D. Russel, W. E. Friedrichs, R. B. Ray, M. Hidalgo, Inhibitors of mTOR reverse doxorubicin resistance conferred by PTEN status in prostate cancer cells. *Cancer research* **62**, 6141-6145 (2002)

98. W. H. Mondesire, W. Jian, H. Zhang, J. Ensor, M. C. Hung, G. B. Mills, F. Meric-Bernstam, Targeting mammalian target of rapamycin synergistically enhances chemotherapy-induced cytotoxicity in breast cancer cells. *Clinical cancer research : an official journal of the American Association for Cancer Research* **10**, 7031-7042 (2004)

99. L. S. Steelman, P. M. Navolanic, M. L. Sokolosky, J. R. Taylor, B. D. Lehmann, W. H. Chappell, S. L. Abrams, E. W. Wong, K. M. Stadelman, D. M. Terrian, N. R. Leslie, A. M. Martelli, F. Stivala, M. Libra, R. A. Franklin, J. A. McCubrey, Suppression of PTEN function increases breast cancer chemotherapeutic drug resistance while conferring sensitivity to mTOR inhibitors. *Oncogene* **27**, 4086-4095 (2008)

100. J. Xu, Y. Dang, Y. R. Ren, J. O. Liu, Cholesterol trafficking is required for mTOR activation in endothelial cells. *Proceedings of the National Academy of Sciences of the United States of America* **107**, 4764-4769 (2010)

101. E. Lloyd-Evans, A. J. Morgan, X. He, D. A. Smith, E. Elliot-Smith, D. J. Sillence, G. C. Churchill, E. H. Schuchman, A. Galione, F. M. Platt, Niemann-Pick disease type C1 is a sphingosine storage disease that causes deregulation of lysosomal calcium. *Nature medicine* **14**, 1247-1255 (2008)

102. D. Shen, X. Wang, X. Li, X. Zhang, Z. Yao, S. Dibble, X. P. Dong, T. Yu, A. P. Lieberman, H. D. Showalter, H. Xu, Lipid storage disorders block lysosomal trafficking by inhibiting a TRP channel and lysosomal calcium release. *Nature communications* **3**, 731 (2012)10.1038/ncomms1735).

Chapter 2: Regulation of mTORC1 by Lysosomal Calcium and Calmodulin

2.1 Abstract

Blockade of lysosomal calcium release due to lysosomal lipid accumulation has been shown to inhibit mTORC1 signaling. However, the mechanism by which lysosomal calcium regulates mTORC1 has remained undefined. Herein we report that proper lysosomal calcium release through the calcium channel TRPML1 is required for mTORC1 activation. TRPML1 depletion inhibits mTORC1 activity, while overexpression or pharmacologic activation of TRPML1 has the opposite effect. Lysosomal calcium activates mTORC1 by inducing association of calmodulin (CaM) with mTOR. Blocking the interaction between mTOR and CaM by antagonists of CaM significantly inhibits mTORC1 activity. Moreover, CaM is capable of stimulating the kinase activity of mTORC1 in a calcium-dependent manner *in vitro*. These results reveal that mTOR is a new type of CaM-dependent kinase, and TRPML1, lysosomal calcium and CaM play essential regulatory roles in the mTORC1 signaling pathway.

ABBREVIATIONS

TRPML1, transient receptor potential cation channel, mucolipin subfamily, member 1; HUVEC, human umbilical vein endothelial cells; mTOR, mechanistic target of rapamycin; mTORC1, mTOR complex 1; GAPDH, glyceraldehyde 3-phosphate dehydrogenase; S6K, ribosomal s6 kinase; 4EBP1, eukaryotic translation initiation factor 4E-binding protein 1; CaM, calmodulin; MLC2, myosin light chain 2; CMDZ, calmidazolium; Rheb, Ras homolog enriched in brain.

2.2 Introduction

Mechanistic target of rapamycin (mTOR) plays an essential role in sensing a myriad of environmental cues including nutrients and growth factor stimulation to regulate cell growth and proliferation (*1*). mTOR independently associates with regulatory-associated protein of mammalian target of rapamycin (raptor) or rapamycin-insensitive companion of mTOR (rictor) to form two distinct complexes, mTORC1 and mTORC2, respectively. The two complexes share several common subunits, including the catalytic mTOR subunit, mammalian lethal with sec-13 protein 8 (mLST8), DEP domain containing mTOR-interacting protein (DEPTOR), and the Tti1/Tel2 complex(*2*). Among the remaining components, raptor and proline-rich Akt substrate 40 kDa (PRAS40) are specific to mTORC1, whereas rictor, mammalian stress-activated map kinase-interacting protein 1 (mSin1) protein observed with rictor 1 and 2 (protor1/2) are unique to mTORC2(*2*). These two complexes differ in their sensitivity to rapamycin, upstream signals and downstream outputs(*2*). The mTORC1 complex integrates different extracellular and intracellular signal inputs, such as growth factors, amino acids, stress and energy status, to regulate cellular processes such as protein and lipid synthesis and autophagy, by phosphorylating and activating p70 S6 kinase (p70S6K)(*3, 4*) and eukaryotic translation initiation factor 4E-binding protein 1 (4E-BP1)(*5, 6*). In contrast, mTORC2 is involved in Akt phosphorylation and regulation of the cellular cytoskeleton(*7*). Activation of mTORC1 by amino acids requires the translocation of mTORC1 from the cytosol to the surface of lysosomes, which is dependent on the Rag GTPase heterodimers Rag A/B and Rag C/D(*8, 9*).

The second messenger calcium has been shown to play an important role in the regulation of mTOR signaling. Earlier hints that calcium might play a key role in mTOR signaling came from observations that calcium was required for the activation of p70S6K(*10-12*). But the underlying mechanism was attributed to upstream regulators such as PI3K or isoforms of PKC. More definitive roles of calcium and its signaling mediator calmodulin (CaM) in mTORC1 signaling were demonstrated in the context of amino acid activation of the pathway(*13*). It was shown that the phosphorylation of S6K1 in response to amino acids or insulin was inhibited by the cell permeable calcium chelator BAPTA-AM while thapsigargin, which releases intracellular calcium, activated mTORC1 activity. Moreover, it was shown that the activation of mTORC1 by amino acids was inhibited by antagonists of CaM or its knockdown using siRNA, suggesting that CaM plays an essential role in mTORC1 signaling pathway. The underlying mechanism by which calcium and CaM regulate mTORC1 was attributed to the binding of calcium-activated CaM to the hVps34, leading to the activation of its kinase activity. While the sensitivity of mTORC1 to BAPTA-AM and CaM antagonists have been reproducibly seen, ensuing studies have cast some doubt on the notion that hVps34 is a key mediator of calcium and CaM in the regulation of mTORC1 in similar and other cellular systems(*14, 15*).

In a previous study, we found that the antifungal drug itraconazole inhibited mTOR due in part to its induction of lysosomal cholesterol and lipid accumulation, which mimics the phenotype of Niemann-Pick type C (NPC) disease(*16*). Moreover, other small molecules that are known to induce NPC phenotype also inhibited mTOR(*16*). Independently, it has also been reported that NPC cells showed significant defects in

lysosomal calcium homeostasis(*17, 18*). Cells that have mutant or deficient mucolipin transient receptor potential (TRP) channel 1 (TRPML1) display altered Ca^{2+} homoeostasis similar to that seen in NPC cells(*19-21*). Cells treated with chemical NPC inducers exhibited reduced TRPML1-mediated lysosomal Ca^{2+} release in response to a TRPML1 agonist, indicating dysfunction of this calcium channel. Furthermore, it has been shown that TRPML1 homolog in fly is required for TORC1 activation and fusion of amphisomes with lysosomes, and the inhibition of TORC1 can be rescued by feeding fly larvae with a high-protein diet, while TORC1 exerts reciprocal control on TRPML function, establishing the connection between TRPML and TORC1 signaling pathway in fly cells(*22, 23*). Whether TRPML1 regulates mTORC1 signaling pathway in mammalian cells remains unknown. Putting these findings together, we hypothesized that a defect in lysosomal calcium homeostasis in NPC cells might be responsible for the observed inhibition of the mTOR signaling pathway.

We validated our hypothesis by demonstrating that depletion of TRPML1 inhibits mTORC1 while overexpression or pharmacologic activation of TRPML1 activates mTORC1. We traced the likely site of regulation of mTORC1 pathway by calcium and CaM by determining the sensitivity of mTORC1 activity to BAPTA-AM and CaM antagonists in response to various upstream activators of the kinase complex and narrowed it to mTORC1 itself. We found that CaM directly binds to mTOR within its FAT domain, activating its kinase activity. Together, these findings shed significant new light on mTORC1 signaling pathway and offer a unifying mechanism that accounts for most, if not all, earlier observations implicating calcium and CaM in the regulation of mTORC1 by different upstream activators in distinct cellular context.

2.3 Materials and methods

Cell lines and tissue culture

HEK293T (ATCC) and A549 (ATCC) cells were cultured in low glucose DMEM (Life Technology) supplemented with 10% FBS (Life Technology). Healthy human fibroblasts (Coriell Insititute, GM03440) and mucolipidosis IV human fibroblasts (Coriell Insititute, GM02048) were cultured in EMEM (ATCC) supplemented with 15% FBS. HUVEC (ATCC) were cultured in EGM media (Lonza). All cells were cultured at 37°C with the presence of 5% CO_2. HEK293T cells were tested for mycoplasma contamination using a PCR mycoplasma test, and showed negative result.

Leucine starvation and stimulation of the cells

Almost confluent cultures in 6-well plates were washed once with leucine-free low glucose DMEM (US Biological), incubated in leucine-free DMEM for 3 hr, and stimulated with 52 μg/ml leucine for 10 minutes. For those cells treated with calmidazolium (CMDZ, Cayman Chemical) or BAPTA-AM (Cayman Chemical), compounds were added 1 hr prior to cell harvesting. Cells were processed for biochemical assays as described below.

Growth factor starvation and insulin stimulation of the cells

Almost confluent cultures in 6-well plates were washed once with FBS-free DMEM, incubated in FBS-free DMEM for 24 hrs, and stimulated with 600 nM insulin (Life Technology) for 10 minutes. For those cells treated with calmidazolium (CMDZ) or

BAPTA-AM, compounds were added 1 hr prior to cell harvesting. Cells were processed for biochemical assays as described below.

Immunoblotting analysis

After indicated treatments, cells were washed once with ice-cold PBS and lysed in ice-cold RIPA buffer (20 mM Tris-HCl (pH 7.5), 150 mM NaCl, 1 mM Na_2EDTA, 1 mM EGTA, 1% NP-40, 1% sodium deoxycholate, 2.5 mM sodium pyrophosphate, 1 mM beta-glycerophosphate, 1 mM Na_3VO_4, 1 μg/ml leupeptin). After brief sonication, the cell debris was removed by centrifugation at 13,000 rpm for 10 minutes in a microfuge, and the protein amount in the supernatant was quantified and mixed with a proper volume of 5x SDS loading buffer. Proteins were then separated by SDS-PAGE and transferred to nitrocellulose membranes. After blocking at room temperature for 1 hour, membranes were immunoblotted with anti-p-S6K (T389) (1:1000, Cell Signaling Technology, Cat. 9205), p-Akt (T308) (1:1000, Cell Signaling Technology, Cat. 9275), p-Akt (S473) (1:1000, Cell Signaling Technology, Cat. 9271), p-4EBP1 (S65) (1:1000, Cell Signaling Technology, Cat. 9451), p-mTOR (S2448) (1:1000, Cell Signaling Technology, Cat. 2971), mTOR (1:1000, Cell Signaling Technology, Cat. 2983), Akt (1:1000, Cell Signaling Technology, Cat. 9272), raptor (1:1000, Cell Signaling Technology, Cat. 2280), PRAS40 (1:1000, Cell Signaling Technology, Cat. 2610), hVps34 (1:1000, Cell Signaling Technology, Cat. 3811), HA tag (1:1000, Santa Cruz Biotechnology, Cat. sc-7392), myc tag (1:1000, Santa Cruz Biotechnology, Cat. sc-40), FLAG tag (1:5000, Sigma, Cat. F1804), GFP (1:1000, Santa Cruz Biotechnology, Cat. sc-9996), S6K (1:1000, Santa Cruz Biotechnology, Cat. sc8418), GAPDH (1:1000, Santa Cruz

Biotechnology, Cat. sc-20357) at 4°C overnight with the primary antibodies, followed by incubation with HRP-conjugated anti-mouse (1:10000, GE Healthcare, Cat. NXA931), anti-rabbit (1:10000, GE Healthcare, Cat. NA934V) or anti-goat IgG (1:10000, Santa Cruz Biotechnology, Cat. sc-2020) at room temperature for 1 hour. Antibody-protein complexes were detected using enhanced chemiluminescence (ECL) immunoblotting detection reagent. The band intensity was measured using ImageJ software (National Institute of Health, USA)

CaM sepharose precipitation

Cells were washed once with ice-cold wash buffer (40 mM HEPES [pH 7.4], 150 mM NaCl), and lysed in ice-cold lysis buffer (40 mM HEPES [pH 7.4], 150 mM NaCl, 0.3% CHAPS or 1% NP-40 or 1% Triton-X100, phosphatase inhibitor cocktail (Sigma) and protease inhibitor cocktail (Roche)). The cell debris was removed by centrifugation at 13,000 rpm for 10 minutes in a microfuge. Five percent of the supernatant was reserved as "input", and the rest of the supernatant was equally divided into two groups: one contained 1 mM $CaCl_2$, and another one contained 5mM EGTA. The lysates were incubated with pre-washed CaM sepharose (GE Healthcare) at 4°C for 2 hrs with rotation. The beads were washed with $CaCl_2$ (1 mM) or EGTA (5 mM) -containing CHAPS (0.3 %) buffer 3 times, and boiled at 95°C for 5 min. Elution of the protein from CaM sepharose was subjected to immunoblotting to analyze the recovery of indicated proteins or peptides.

Immunoprecipitations and *in vitro* kinase assay

Cells were washed once with ice-cold wash buffer (40 mM HEPES [pH 7.4], 150 mM NaCl), and lysed in ice-cold CHAPS buffer (40 mM HEPES [pH 7.4], 150 mM NaCl, 2mM EDTA, 0.3% CHAPS, phosphatase inhibitor cocktail and protease inhibitor cocktail). The cell debris was removed by centrifugation at 13,000 rpm for 10 minutes in a microfuge. The soluble fractions of cell lysates were mixed with anti-raptor antibody (4 μg/10cm dish, Life Technology, Cat. 42-4000), and the mixtures were incubated with rotation for 1.5 hours at 4°C. 80 μl of a 50% slurry of protein A/G plus-sepharose (Santa Cruz Biotechnology) was then added and the incubation continued for an additional 1 hour. Immunoprecipitates were washed twice with ice-cold CHAPS buffer, and once with mTOR kinase buffer (25mM HEPES [pH 7.4], 50mM KCl, 10mM $MgCl_2$). The kinase assays were performed as previously described (*24*). CaM (2 μM) or/and $CaCl_2$ (0.2 mM) were added into the kinase reaction as indicated. CMDZ (8 μM) or Torin 1 (100 nM, Cayman Chemical) was incubated with the reaction mixtures 10 min prior to initiating the reaction by addition of 250 μM ATP (Sigma). The phosphorylation states of S6K or 4EBP1 were detected by immunoblotting.

Real-time qPCR

HEK293T, HUVEC and A549 cells were transduced with lentivirus carrying scramble shRNA or TRPML1 shRNA. Total RNA was collected using RNeasy Mini Kit (QIAGEN). cDNA was generated with SuperScript III First-Strand kit (Invitrogen), and real-time PCR was carried out using TaqMan Universal Master Mix II (Life Technologies). Real-time PCR primers and probes were from Thermo Fisher Scientific:

MCOLN1 FAM (Hs01100653_m1), TPCN2 FAM (Hs01552063_m1). Human GAPDH VIC (Hs02758991_g1) was used as an endogenous control.

cDNA manipulations and mutagenesis

Myc-mTOR (Addgene plasmid # 1861), myc-mTOR (1-1482 aa) (Addgene plasmid # 21745), myc-mTOR (1271-2008 aa) (Addgene plasmid # 21746), myc-mTOR (1750-2549 aa) (Addgene plasmid # 21747), HA-GbL (Addgene plasmid # 1865), pRK5-HA GST RagA 66L (Addgene plasmid # 19300), pRK5-HA GST RagC 75L (Addgene plasmid # 19305) and HA GST PreScission p70 S6K1 (Addgene plasmid # 15511) were gifts from David Sabatini. pcDNA3-FLAG-Rheb-N153T (Addgene plasmid # 19997) was a gift from Fuyuhiko Tamanoi. pcDNA-CaM was a gift from David Yue. TRPML1-HA (Addgene plasmid # 18825) was a gift from Craig Montell. EGFP-Rab7A Q67L (Addgene plasmid # 28049) and EGFP-Rab7A T22N (Addgene plasmid # 28048) were gifts from Qing Zhong.

Myc-tagged truncated mTOR fragments were amplified by PCR and cloned into the EcoRI site of pRK5 or pEGFP vector. FLAG-tagged $Rheb^{N153T}$ was amplified by PCR and cloned into the EcoRI site of pLVX-AcGFP-N1 vector. GST-tagged 4EBP1 was amplified by PCR and cloned into a pDEST15-based vector. FLAG-tagged CaM was amplified by PCR and cloned into a pGEX6-based vector. TRPML1 was amplified by PCR and cloned into a pEGFP-based vector. All ligations were performed with Infusion Kit (Clontech Laboratories, Inc.) according to the manufacture's instruction. After sequence verification, these plasmids were used, as described below, in transient cDNA

transfections, bacterial protein expression or to produce the lentiviruses needed to generate cell lines stably expressing the proteins.

cDNA transfection-based experiments

For transfection experiments, HEK293T cells were seeded in 6-well plates or 6 cm culture dishes. After 24 hrs, cells were transfected with the pRK5-based cDNA expression plasmids indicated in the figures (500 ng of truncated mTOR fragments; 200 ng HA-GST-tagged RagA 66L or RagC 75L, 1000 ng of EGFP-tagged TRPML1, and same amount of proper empty vectors) using Lipofectamine 2000 (Life Technology) according to the manufacturer's instructions.

Preparation of p70S6K1, HA-GST-TRD3, GST-4EBP1 and FLAG-CaM for Use in mTORC1 Kinase Assays

HA-GST-PreScission-p70 S6K1 was transfected into HEK293T cells as described above, and after 48 h the cells were treated with 20 μM LY294002 for 1 hr prior to cell harvesting and lysis. HA-GST-PreSciss-S6K1 was purified as described (*25*). The purified protein was stored at -80°C in 20% glycerol.

HA-GST-TRD3 expression plasmid (pRK5-based) was transfected into HEK293T cells. After 48 h, the cells were lysed with lysis buffer (PBS, pH 7.4, 1% triton X-100, protease inhibitor cocktails, phosphatase inhibitor cocktails) in ice and HA-GST-TRD3 was tandemly purified using glutathione sepharose beads (GE healthcare) and anti-HA antibody-conjugated agarose beads (Thermo Fisher Scientific) according to the manufacturers' instructions.

GST-fused 4EBP1 protein was expressed and purified from BL21 (DE3) *Escherichia coli*. Bacteria were grown to an OD of 0.8 and induced for 16 hrs at 18°C with 0.5 mm IPTG (American Bioanalytical). Bacteria were pelleted, and lysed in ice-cold PBS containing 1% Triton X-100, 1mg/mL lysozyme (Sigma-Aldrich) and protease inhibitor cocktail by sonication. Cell debris was cleared by centrifugation. The supernatant was mixed with pre-equilibrated glutathione sepharose 4B resin for 1 hour at 4°C with rotation. After gentle centrifugation, GST-4EBP1 was eluted by 10 mM reduced glutathione, and the protein sample was desalted by PD-10 desalting columns and then eluted by the elution buffer (150mM NaCl, 40mM HEPES [pH 7.4]). The purified protein was stored at -80°C in 20% glycerol.

GST-FLAG-CaM protein was expressed and purified as GST-4EBP1. GST tag was removed by PreScission (GE Healthcare) according to the manufacturer's instruction. The purified protein was stored at -80°C in 20% glycerol.

Mammalian lentiviral shRNAs

TRC lentiviral shRNAs targeting hTRPML1, mTOR, hVps34 and raptor were obtained from Sigma. The TRC number for each shRNA is as follows:

Human mTOR shRNA #1: TRCN0000038677

Human mTOR shRNA #2: TRCN0000039785

Human raptor shRNA #1: TRCN0000039772

Human raptor shRNA #2: TRCN0000010415

Human TRPML1 shRNA #1: TRCN0000083297

Human TRPML1 shRNA #2: TRCN0000083296

Human hVps34 shRNA #1: TRCN0000037794

Human hVps34 shRNA#2: TRCN0000037795

Human TPC2 shRNA #1: TRCN0000043919

Human TPC2 shRNA #2: TRCN0000043921

Human P2X4 shRNA #1: TRCN0000044960

Human P2X4 shRNA #2: TRCN0000044962

Lentivirus production and cell transduction

HEK293T cells were seeded in 15-cm culture dishes. When 50-70% confluent, the cells were co-transfected with 9 μg lentiviral vector (empty, lentiviral vector containing sequences expressing indicated proteins, scramble shRNA or shRNA targeting indicated proteins) + 6 μg pspAX$_2$ + 3 μg pMD$_2$G using lipofectamine 2000 according to manufacturer's instructions. After 24 hrs, 48 hrs and 72 hrs, the supernatants were harvested, respectively, and concentrated using PEG6000 as described before (*26*). The concentrated virus was stored at -80°C.

HEK293T cells were seeded in 10-cm culture dishes. When cells were 40% confluent, concentrated lentiviral solutions were added into the cell culture medium. After 48 hrs, cells were treated with antibiotics to select transduced cells.

Immunostaining

Cells were fixed with 4% (wt/vol) paraformaldehyde in PBS for 20 min at room temperature (RT). After wash, cells were permeabilized by PBS/0.5% Triton X-100 and incubated at RT for 10 min. After blocking, cells were incubated with anti-mTOR

antibody (1:150, Cell Signaling Technology, Cat. 2983) at 4°C overnight, followed by incubating with Alexa Fluor® 568 (1:500, Life technologies, Cat. A11011) for 1 h at RT. Images were captured using a Zeiss LSM 700 confocal microscope.

Data analysis

All graphs were created using GraphPad Prism software, and statistical analysis was performed with GraphPad Prism. Data are presented as the mean ± s.d. Two-tail t-test statistical comparisons were made using ANOVA. A P value < 0.05 was considered statistically significant. No statistical method was used to predetermine sample size. The experiments were not randomized. The investigators were not blinded to allocation during experiments.

2.4 Results

TRPML1 is required for the activation of mTORC1

To determine whether TRPML1 is required for mTORC1 signaling, HEK293T cells were transduced with lentiviral shRNA targeting human TRPML1 (Sh1 and Sh2) or a scrambled shRNA (Scr). Due to a lack of reliable hTRPML1 antibodies, the knockdown efficiency was assessed by RT-qPCR, as well as indirectly by the expression level of ectopically expressed EGFP-TRPML1. The activity of mTORC1, as judged by the phosphorylation of S6K, was significantly inhibited upon TRPML1 knockdown, while the phosphorylation of Akt (T308) was not affected **(Figure 2.1 a)**.

To determine whether the mTOR inhibition caused by TRPML1 knockdown was due to blockade of lysososmal calcium release, we performed a rescue experiment in TRPML1 knockdown Human Umbilical Vein Endothelial Cells (HUVEC) **(Figure 2.2 a)** and HEK293T **(Figure 2.2 b)** using thapsigargin, a sarco/endoplasmic reticulum Ca^{2+}-ATPase inhibitor that increases cytosolic calcium concentrations (*27*). Indeed, the inhibition of mTORC1 activity by TRPML1 knockdown was rescued by thapsigargin, suggesting that mTORC1 inhibition was due, in large part, to the lack of lysosomal calcium release. Furthermore, we determined the phosphorylation of S6K in normal human fibroblasts (TRPML1 +/+) and fibroblasts from a mucolipidosis IV patient (TRPML1 -/-). Compared with TRPML1 +/+ human fibroblasts, TRPML1 -/- cells showed decreased phosphorylation of S6K. However, the treatment of thapsigargin fully restored the phosphorylation of S6K **(Figure 2.2 c)**.

In order to investigate whether amino acid can rescue mTORC1 inhibition caused by depletion of TRPML1, we firstly knocked down TRPML1 in HEK293T cells, then

starved the cells with leucine-free medium and restimulated cells with leucin. As shown in **figure 2.3 a**, knocking down TRPML1 attenuated the activation of mTORC1 by leucine. In addition, compared with TRPML1 +/+ human fibroblasts, TRPML1 -/- cells showed decreased phosphorylation of S6K. Interestingly, this inhibition was partially reversed by leucine compared with that in wild type cells **(Figure 2.3 b)**. Figure 2.2c and 2.3b suggest that in mammalian cells, the decrease in mTORC1 activity in TRPML1 mutant cells is not only due to the incomplete autophagy that has been reported in *Drosophila* (*22*). Have shown that depletion of TRPML1 attenuates the activation of mTORC1 by leucine, we next investigate whether overexpression of Rag GTPase can rescue this attenuation. HEK293T cells were transfected with constitutively active $RagA^{Q66L}$ and $RagC^{S75L}$ mutants and starved with leucine. The result shows that overexpression of constitutively active RagA or RagC were not able to fully rescue mTORC1 inhibition caused by depletion of TRPML1 **(Figure 2.3 c)**, indicating that the regulation of mTORC1 by TRPML1 acts parallel to amino acid/Rag GTPase axis.

Next, in order to investigate whether insulin can rescue the effect of depletion of TRPML1, HEK293T cells were transduced with lentivirus carrying shRNA targeting human TRPML1 gene, and then the cells were starved with serum, and restimulated with insulin. As shown in **Figure 2.4**, depletion of TRPML1 attenuated the activation of mTORC1 signaling by insulin, indicating that the regulation of mTORC1 by TRPML1 is parallel to the regulation by insulin.

In addition, knockdown of other lysosomal channels, such as TPC2 and P2X4, did not significantly inhibit mTORC1 signaling (**Figure 2.5**), indicating that the decreased mTOR activity upon TRPML1 knockdown was not due to the dysregulation of the

structure of the endolysosmal system, and as one of the lysosomal calcium channels, TRPML1 may play a more dominant role in the regulation of mTORC1 signaling.

Having shown that TRPML1-mediated lysosomal calcium release is necessary for mTORC1 activity, we then turned to the reciprocal question of whether an increase in lysosomal calcium release through TRPML1 could stimulate mTORC1. Thus, HEK293T cells were transfected with expression plasmids for EGFP-TRPML1 and its non-conducting pore mutant (D471K/D472K) EGFP-TRPML1 (KK), respectively. The phosphorylation of S6K was slightly but significantly increased by overexpression of wild type TRPML1 but not the non-conducting pore mutant TRPML1 (KK) **(Figure 2.6)**, suggesting that TRPML1 positively regulates mTORC1 pathway.

MLSA1 has been reported to be a TRPML1 agonist that stimulates the lysosomal Ca^{2+} release through TRPML1(*18, 28*). Therefore, in order to test whether MLSA1 also activates mTORC1 pathway, we treated HEK293T cells with different concentrations of MLSA1. The phosphorylation of S6K was increased by MLSA1 in a dose-dependent manner (**Figure 2.7 a**). In order to investigate whether this activation was due to the boost of TRPML1, we compared the effect of MLSA1 to mTORC1 between wild type and TRPML1 knockdown HEK293T cell. MLSA1 failed to increase the phosphorylation of S6K in the cells transduced with lentiviral TRPML1 shRNA, or pretreated with bafilomycin A1 or Glycyl-L-phenylalanine 2-naphthylamide (GPN), suggesting that the increase in S6K phosphorylation induced by MLSA1was mediated by TRPML1 (**Figure 2.7 b, c**).

Upon amino acids stimulation, mTOR translocated from the cytosol to the lysosome, colocalizing with EGFP-TRPML1 (**Figure 2.8**), indicating that the activation

of TRPML1 acted independently of the translocation of mTORC1 induced by amino acids.

The upregulated TRPML1 has been reported to promote autophagy (*22, 29, 30*). To determine if activation of mTORC1 in response to TRPML1 overexpression was due to up-regulated autophagy, we overexpressed constitutively active Rab7A (Q67L) and dominant negative Rab7A (T22N) in HEK293T cells (*31, 32*). As shown in revised **Figure 2.9**, neither overexpression of constitutively active nor dominant negative Rab7A affected mTORC1 signaling, while overexpression of TRPML1 plus MLSA1 treatment stimulated the phosphorylation of S6K, suggesting that the activated mTORC1 by TRPML1 stimulation was not mediated through autophagy.

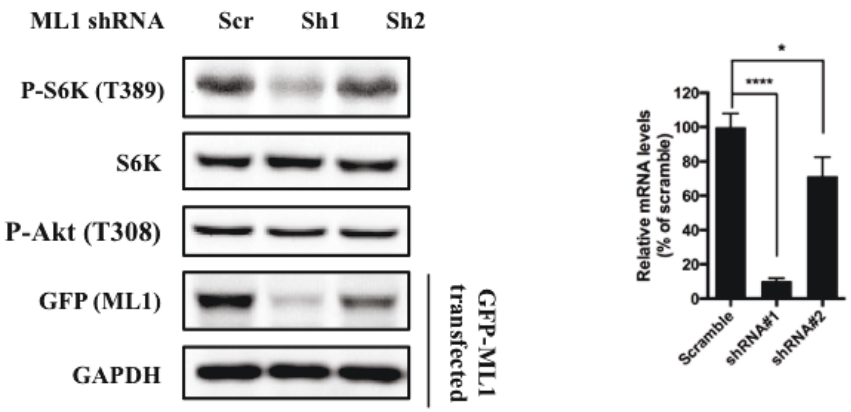

Figure 2.1: Depletion of TRPML1 inhibits mTORC1 signaling pathway in HEK293T cells.

HEK293T cells were transduced with lentiviral scrambled shRNA (Scr) and shRNA targeting human TRPML1 (Sh1 and Sh2), respectively. To assess the knockdown efficiency, a fraction of transduced cells were transfected with EGFP-TRPML1. After 24 h, transfected or untransfected cells were lysed and subjected to immunoblotting. Untransfected cells were used to detect p-S6K, S6K and p-Akt, and transfected cells were used to detect GFP and GAPDH. RT-qPCR was also performed to evaluate the knockdown efficiency (right panel) (mean ± s.d., n = 2 independent experiments).

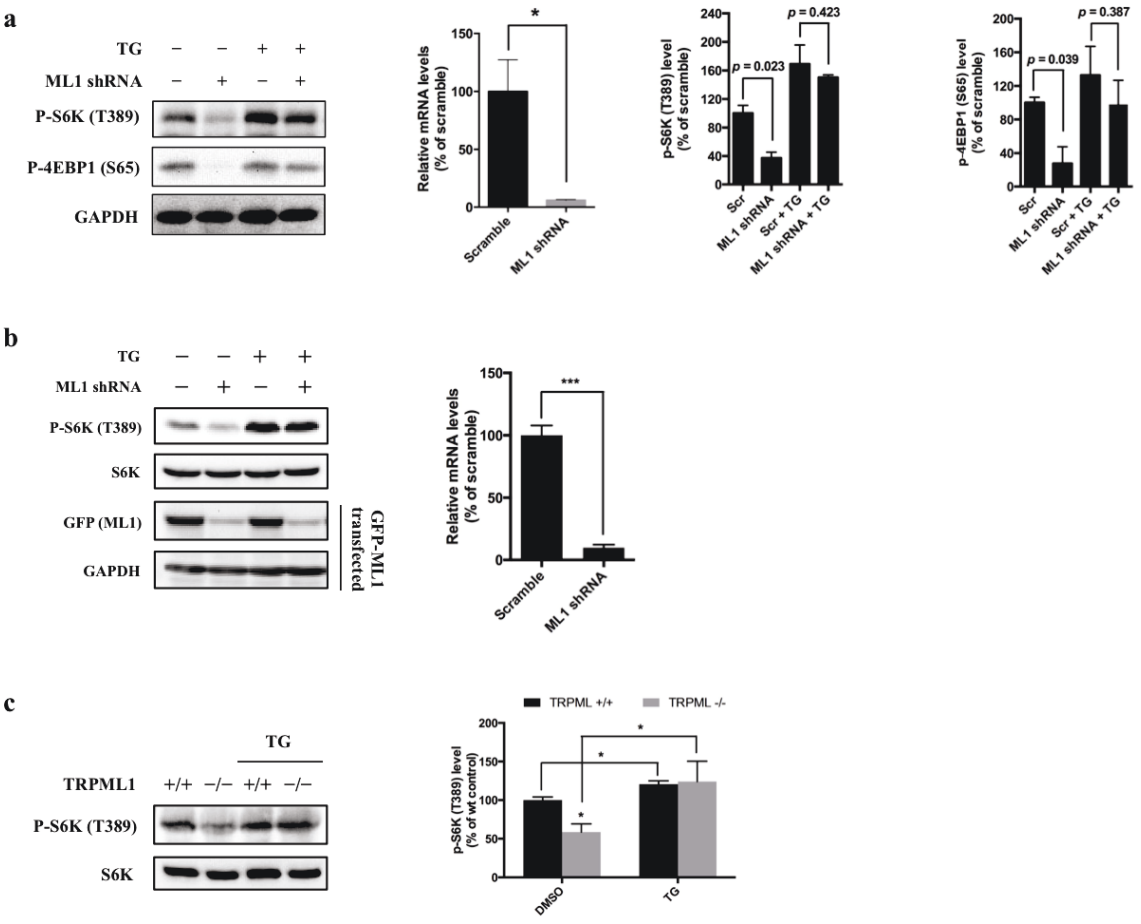

Figure 2.2: Inhibition of mTORC1 by TRPML1 depletion is rescued by thapsigargin.

Scrambled shRNA or TRPML1 shRNA-transduced **(a)** HUVEC or **(b)** HEK293T cells were treated with vehicle control or thapsigargin (5 μM) for an additional 2 h. Cells were lysed and subjected to immunoblotting. Knockdown efficiency was assessed by RT-qPCR (right panels). The right two panels of plots in (a) show the percentage of p-S6K and p-4EBP1 levels compared with scramble shRNA transduced vehicle control treated HUVEC normalized by GAPDH loading control (mean ± s.d., n = 2 independent experiments). **(c)** Healthy human fibroblast or mucolipidosis IV patient's fibroblasts

(TRPML-/-) were treated with vehicle control or thapsigargin (5 μM) for 2 h, respectively. Cells were lysed and subjected to immunoblotting. The plot shows the percentage of p-S6K level compared with vehicle control treated wild type human fibroblasts normalized by total S6K control. (mean ± s.d. for n = 3 independent experiments).

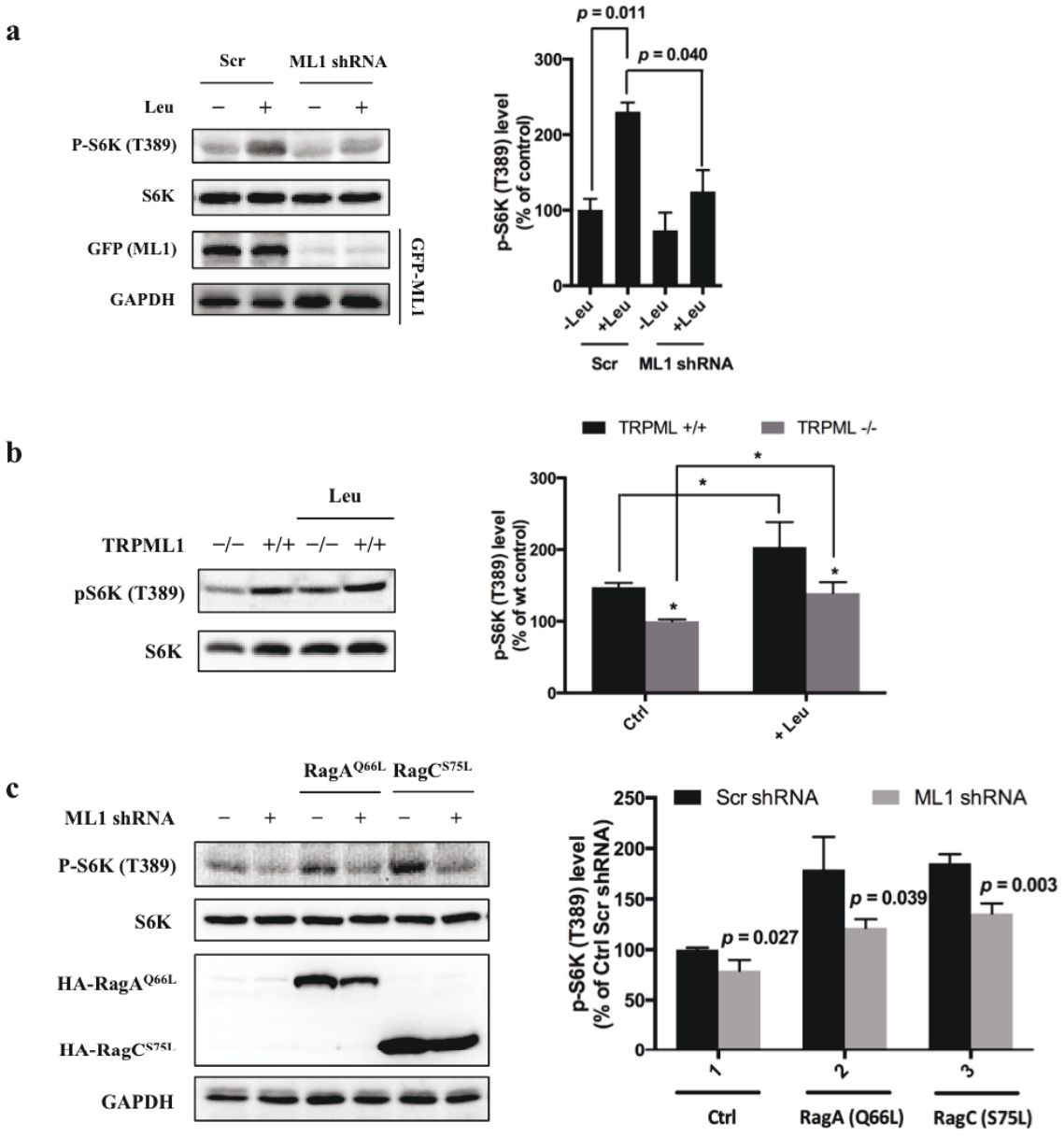

Figure 2.3: Depletion of TRPML1 attenuates mTORC1 activation by leucine.

(a) Scrambled shRNA or TRPML1 shRNA transduced HEK293T cells were deprived for 3 h of leucine, and, where indicated, were stimulated with 52 µg/ml leucine for 10 min. Simultaneously, another fraction of scrambled shRNA or TRPML1 shRNA-transduced cells were transfected with EGFP-TRPML1 for 24 h. Cells were lysed and subjected to

immunoblotting. The plot shows the percentage of p-S6K levels compared with scramble shRNA transduced leucine starved HEK293T cells normalized by total S6K control (mean ± s.d., n = 2 independent experiments, respectively). **(b)** Wild type and mucolipidosis IV patient's fibroblasts (TRPML-/-) were treated with vehicle control or leucine for 10 min. Cells were lysed and subjected to immunoblotting. The plot shows the percentage of p-S6K level compared with vehicle control treated TRPML-/- human fibroblasts normalized by total S6K control. (mean ± s.d. for n = 2 independent experiments). **(c)** Scrambled shRNA or TRPML1 shRNA-transduced HEK293T cells were transfected with Rag AQ66A or Rag CS75L for 24 h. Cells were lysed and subjected to immunoblotting. The plot shows the percentage of p-S6K level compared with scramble shRNA transduced empty vector transfected HEK293T cells normalized by total S6K control. (mean ± s.d. for n = 3 independent experiments).

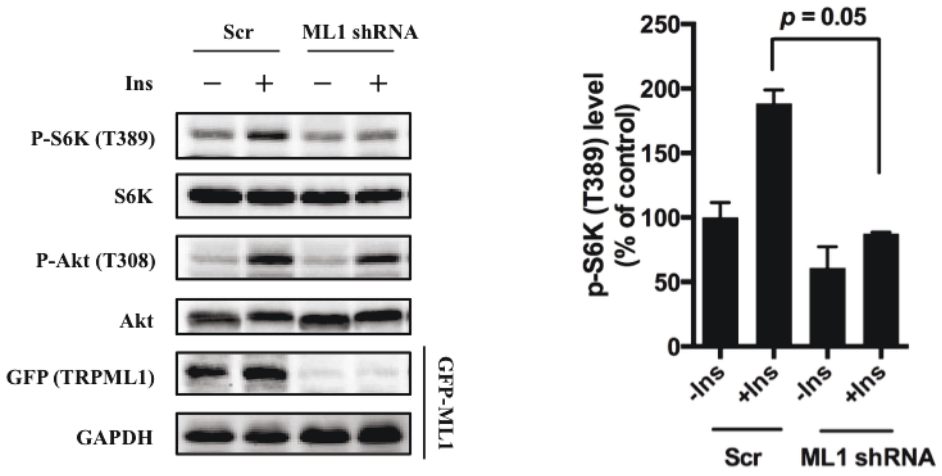

Figure 2.4: Depletion of TRPML1 attenuates mTORC1 activation by insulin.

Scrambled shRNA or TRPML1 shRNA transduced HEK293T cells were deprived for 24 h of serum and, where indicated, were stimulated with 600 nM insulin for 10 min. Simultaneously, another fraction of scrambled shRNA or TRPML1 shRNA-transduced cells were transfected with EGFP-TRPML1 for 24 h. Cells were lysed and subjected to immunoblotting. The plots show the percentage of p-S6K levels compared with scramble shRNA transduced serum starved HEK293T cells normalized by total S6K control (mean ± s.d., n = 2 independent experiments, respectively).

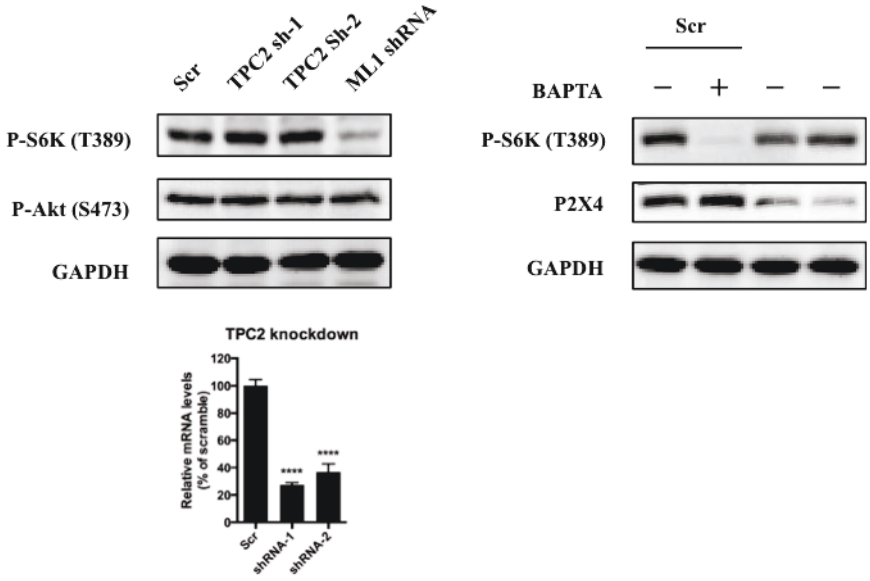

Figure 2.5: Depletion of TPC2 or P2X4 does not affect mTORC1 signaling pathway. Lentivirus carrying scrambled shRNA, TRPML1 shRNA, TPC2 shRNA or P2X4 shRNA transduced HEK293T cells were lysed and subjected to immunoblotting. RT-qPCR (bottom panel) was used to evaluate the knockdown efficiency of TPC2.

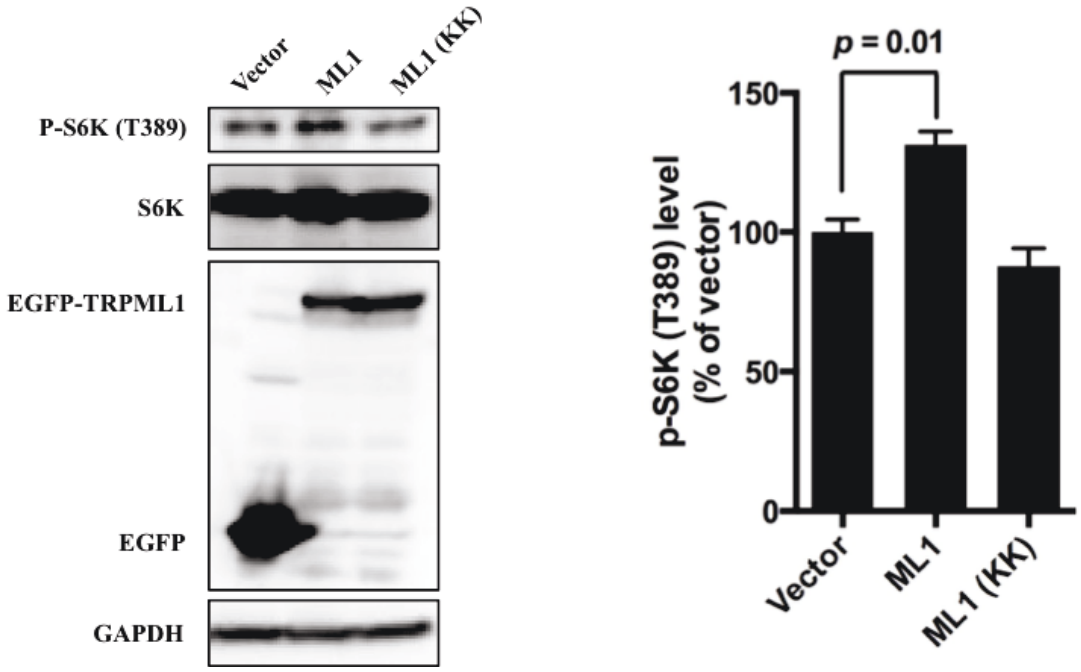

Figure 2.6: Overexpression of wild type TRPML1 but not dead mutant activates mTORC1 signaling pathway.

HEK293T cells (80% confluency) were transfected with EGFP vector, EGFP-TRPML1 or its non-conducting pore mutant (D471K/D472K) EGFP-TRPML1 (KK) for 20 h. Cells were lysed and subjected to immunoblotting. The plot shows the percentage of p-S6K levels compared with vector transfected cells normalized by total S6K control (mean ± s.d., n = 3 independent experiments).

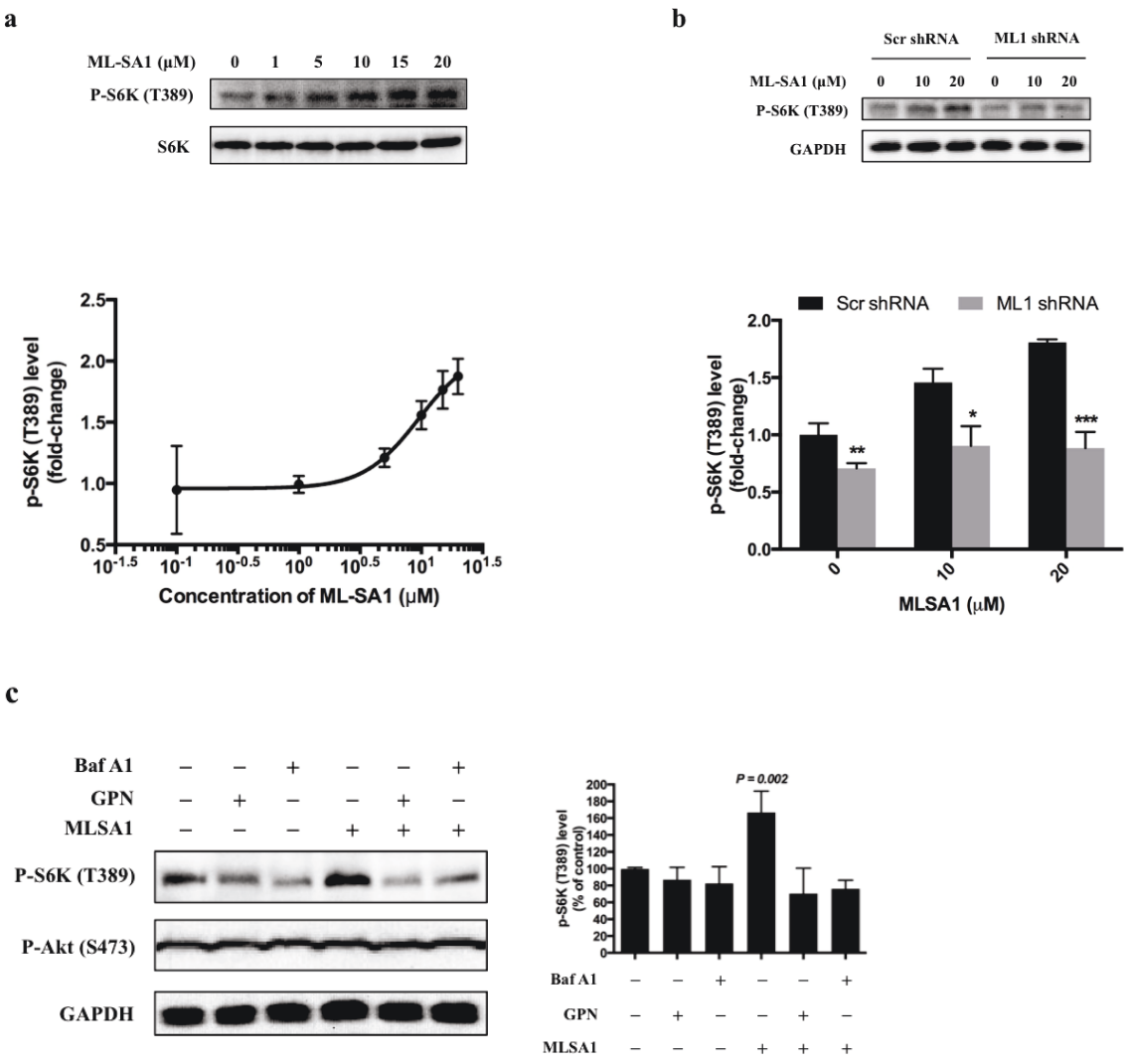

Figure 2.7: Pharmacological stimulation of TRPML1 activates mTORC1 pathway.

(a) HEK293T cells were treated with different concentrations of ML-SA1 for 3 h. Cells were lysed and subjected to immunoblotting. The plot shows the dose-response curve of ML-SA1 normalized by total S6K. (**b**) Scrambled shRNA or TRPML1 shRNA transduced HEK293T cells were treated with varying concentrations of MLSA1 for 3 h. Cells were lysed and subjected to immunoblotting. The plot shows the percentage of p-S6K levels compared with scramble shRNA transduced vehicle control treated 293T cells

normalized by GAPDH loading control (mean ± s.d., n = 3 independent experiments). **(c)** HEK293T cells were pretreated with bafilomycin A1 (1 μM) or GPN (200 μM) for 1 h, followed by treatment with or without MLSA1 for an additional 1.5 h. Cells were lysed and subjected to immunoblotting. The plot shows the percentage of p-S6K levels compared with vehicle control normalized by GAPDH loading control (mean ± s.d., n = 3 independent experiments). * $p < 0.05$, ** $p < 0.01$, n.s. no significant difference.

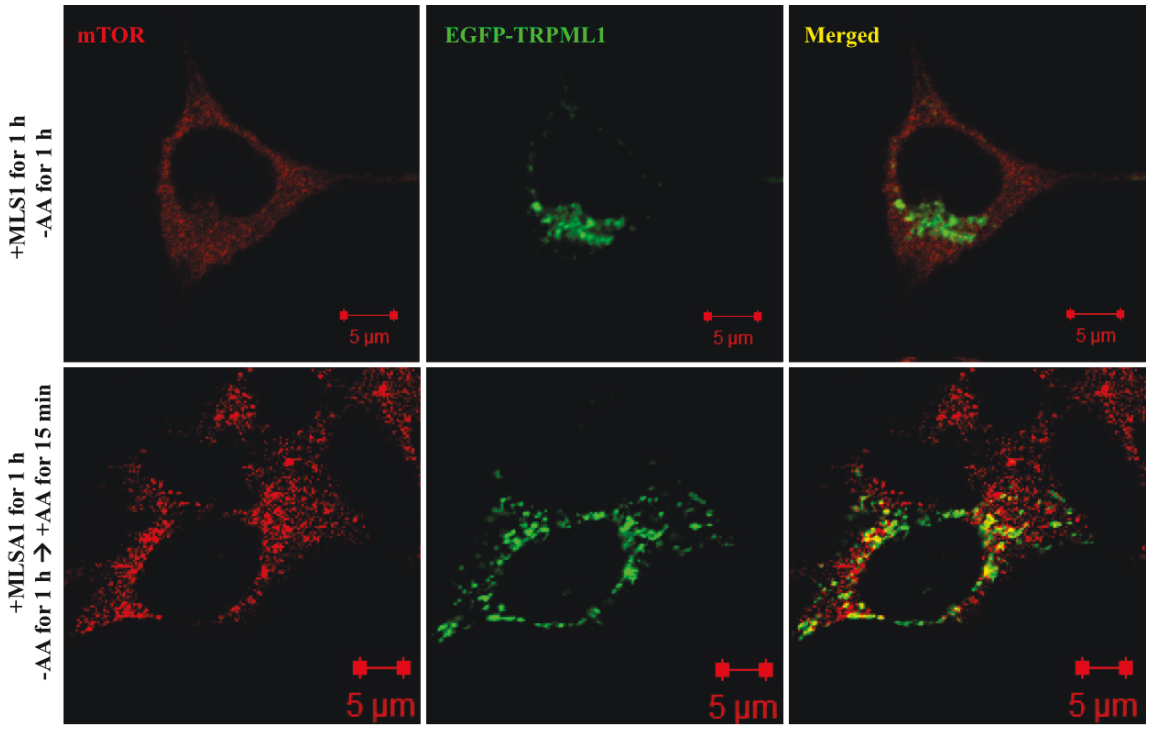

Figure 2.8: Colocalization of EGFP-TRPML1 and mTOR.

HEK293T cells were transfected with EGFP-TRPML1 expression plasmid. After 18 hours, cells were treated with MLSA1 (15 µM) for 1 hour, and starved with amino acids for 1 hour, or starved with amino acids for 1 hour and restimulated with amino acids for 15 min. Cells were fixed, stained with anti-mTOR antibody and images were captured using a Zeiss LSM510 confocal microscope.

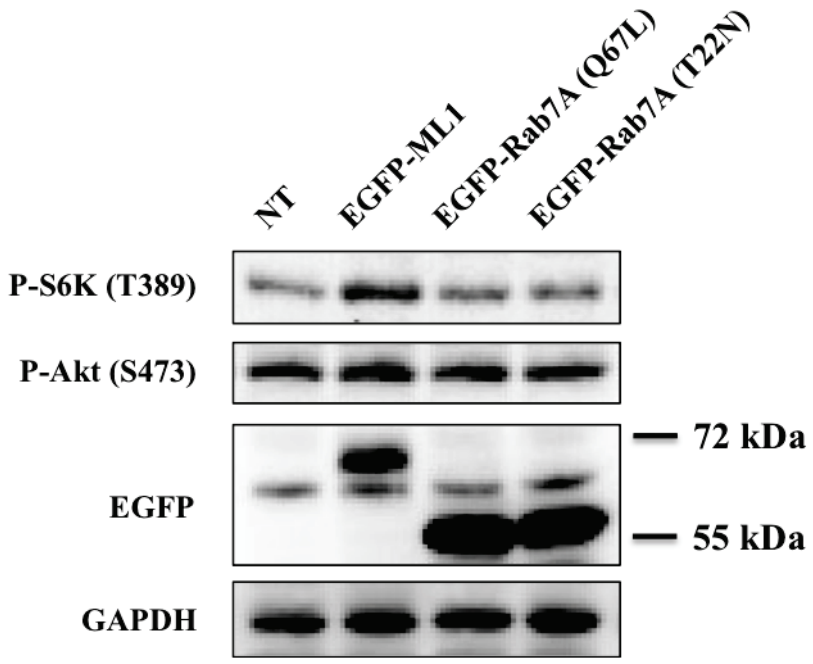

Figure 2.9: Effects of constitutively active or dominant negative Rab 7A.

HEK293T cells were transfected with EGFP-ML1, EGFP-Rab7A (Q67L) or EGFP-Rab7A (T22N). After 19 hours, the cells transfected with EGFP-ML1 were treated with MLSA1 (20 μM) for 1 hour. Cells were lysed and subjected to immunoblotting.

Calcium and CaM are required for activation of mTORC1, and the regulation of mTORC1 by cytosolic calcium and CaM occurs proximal to mTORC1 itself

Both intracellular calcium and CaM have been reported to be required for mTORC1 activity (*10-14*). We thus treated HEK293T cells with the cytosolic Ca^{2+} chelator BAPTA-AM (BAPTA) or the CaM antagonists W-7 and calmidazolium (CMDZ). In agreement with previous studies (*11, 13, 33, 34*), we observed that CMDZ, W-7 and BAPTA inhibited phosphorylation of S6K in a dose-dependent manner with IC_{50} values of 3.96 ± 1.30 μM, 21.59 ± 1.81 μM and 10.36 ± 0.59 μM, respectively (**Figure 2.10**). In comparison to S6K, phosphorylation of Akt (S473), the substrate of mTORC2, was also inhibited by CMDZ and W-7, but at much higher concentrations (EC_{50} values of 27.21 ± 9.82 μM and 45.91 ± 9.61 μM, respectively) compared with that of p-S6K, while BAPTA did not show appreciable inhibition to p-Akt (S473) (**Figure 2.10 c**). In addition, CMDZ and BAPTA also showed potent inhibitory effect on mTORC1 signaling pathway in HUVEC and A549 cells (**Figure 2.10 d, e**), suggesting that the inhibition of mTORC1 by disruption of Ca^{2+}/CaM is also observed in primary and other cancer cells.

Next, we investigated how fast mTORC1 and mTORC2 responded to BAPTA or CMDZ. As shown in **Figure 2.11**, both CMDZ and BAPTA caused appreciable inhibition of mTORC1 activity within 0.5-1 hour as judged by the phosphorylation of S6K and 4EBP1. In contrast, the phosphorylation of Akt (T308) and its substrate, mTOR (S2448), was not significantly affected by CMDZ until 6 hours post treatment. In addition, CMDZ did not cause significant inhibition of phosphorylation of Akt (S473) until 3 hours after treatment, indicating that the response of mTORC2 to the CaM

antagonist has a much slower onset than that of mTORC1 (**Figure 2.11 a left panel, b and c**). Although the onset of the effect of BAPTA on 4EBP1 phosphorylation was slightly slower than that of CMDZ, BAPTA did not significantly affect the phosphorylation of either Akt (S473, T308) or mTOR even after 6 hours (**Figure 2.11 a right panel, d and e**). These results suggest that CaM regulates both mTORC1 and mTORC2, but the two complexes differ in their sensitivity to CaM and calcium. Interestingly, after a 6-hour treatment with BAPTA, the inhibition to phosphorylation of S6K and 4EBP1 was partially reversed (**Figure 2.11 a and d**), which is consistent with a previous report that with the treatment time of BAPTA, a gradual increase of intracellular Ca^{2+} was seen (*35*). The relatively short time required for CMDZ and BAPTA to exert their effects on mTORC1 and their faster onset than those on mTORC2 suggested that the inhibition of mTORC1 likely occurred independently of its upstream signaling events, such as phosphorylation of Akt (T308).

To further explore the level at which Ca^{2+} and CaM regulate mTORC1 signaling, we determined the effects of CMDZ and BAPTA on mTORC1 activation in response to various upstream activating stimuli of mTORC1. Similar to previous observations (*13*), we found that leucine-stimulated mTORC1 activation was inhibited by BAPTA and CMDZ **(Figure 2.12 a, Lanes 4 vs. 2 and 6 vs. 2)**. The activation of mTORC1 by leucine has been shown to be mediated by the small GTPases RagA/B and RagC/D (*8*), and overexpression of constitutively active $RagA^{Q66L}$/$RagC^{S75N}$ can bypass leucine to activate mTORC1. We found that activation of mTORC1 in response to either $RagA^{Q66L}$ or $RagC^{S75N}$ was still inhibited by CMDZ **(Figure 2.12 b)**.

Next, we determined whether activation of mTORC1 by insulin was also sensitive to CaM blockade. Although insulin strongly increased the phosphorylation of Akt (T308) **(Figure 2.13 a)**, the mTORC1 activity remained sensitive to CMDZ as well as BAPTA-AM **(Figure 2.13 a, Lanes 4 and 6)**. It has been reported that mTOR is directly bound to and activated by Rheb-GTP (*36*). Thus, we used HEK293T, HUVEC and A549 to produce stable cell lines overexpressing constitutively active $Rheb^{N153T}$ as previously described (*37*), and determined their sensitivity to BAPTA and CMDZ. $Rheb^{N153T}$-induced phosphorylation of S6K remained sensitive to inhibition by BAPTA and CMDZ in HEK293T, HUVEC and A549 cells **(Figure 2.13 b, c, d, e)**. Together, these results suggested that the site of regulation of mTORC1 by Ca^{2+} and CaM lies proximal to mTORC1 itself.

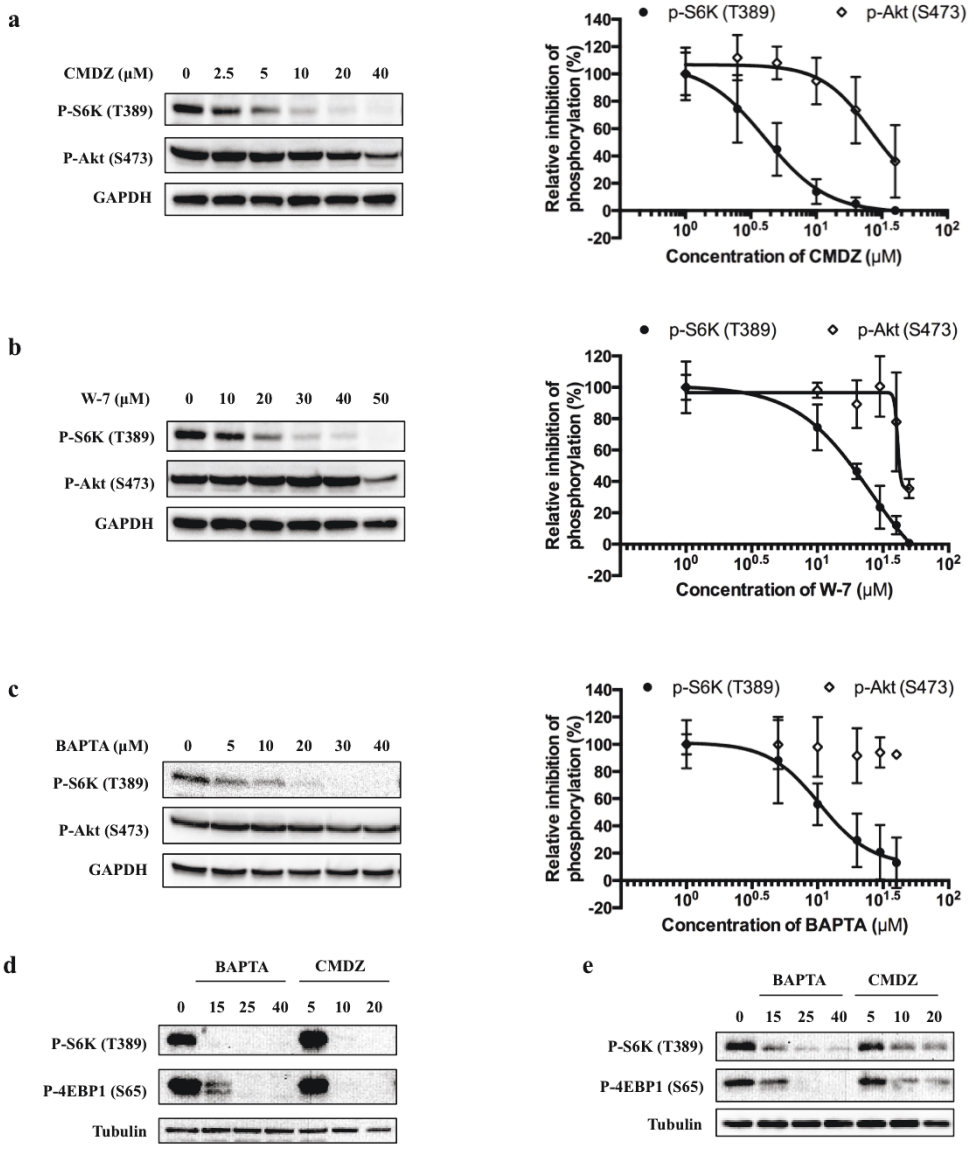

Figure 2.10: Calmodulin antagonists and cytosolic calcium chelator inhibit mTORC1 pathway in a dose-dependent manner.

Effects of calmodulin antagonist **(a)** calmidazolium (CMDZ), **(b)** W-7 and **(c)** cytosolic Ca^{2+} chelator BAPTA-AM on phosphorylation state of S6K (T389) and Akt (S473). HEK293T cells were treated with different concentrations of indicated compound for 1 hr. The phosphorylation state of S6K and Akt was analyzed by immunoblotting. The plots

show the dose-response curve of CMDZ, W-7 and BAPTA normalized by total S6K, respectively. HUVEC **(d)** and A549 **(e)** cells were treated with different concentrations of BAPTA or CMDZ for 1 h. The phosphorylation state of S6K and 4EBP1 was analyzed by immunoblotting.

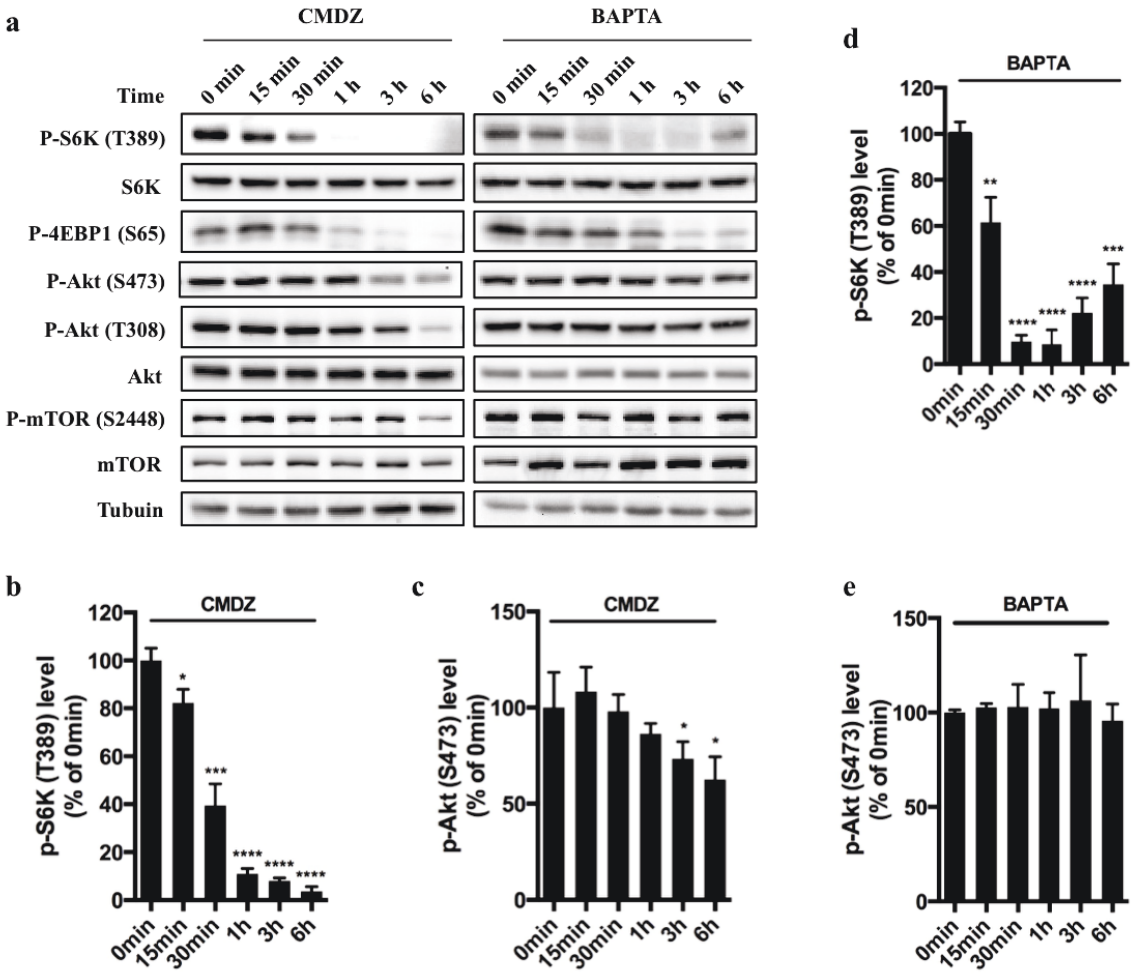

Figure 2.11: Calmodulin antagonist and cytosolic calcium chelator inhibit mTORC1 pathway within a short time treatment.

(a) Effects of 10 μM CaM antagonist calmidazolium (CMDZ) or 25 μM cytosolic Ca^{2+} chelator BAPTA-AM (BAPTA) on the phosphorylation of different proteins of the mTOR signaling pathway at different time points. The percentage of p-S6K **(b and d)** and p-Akt (S473) **(c and e)** levels compared with 0 min treated 293T cells normalized by total S6K and total Akt control, respectively (mean ± s.d., n = 3 independent experiments). * $p < 0.05$, ** $p < 0.01$, *** $p < 0.001$, **** $p < 0{,}0001$.

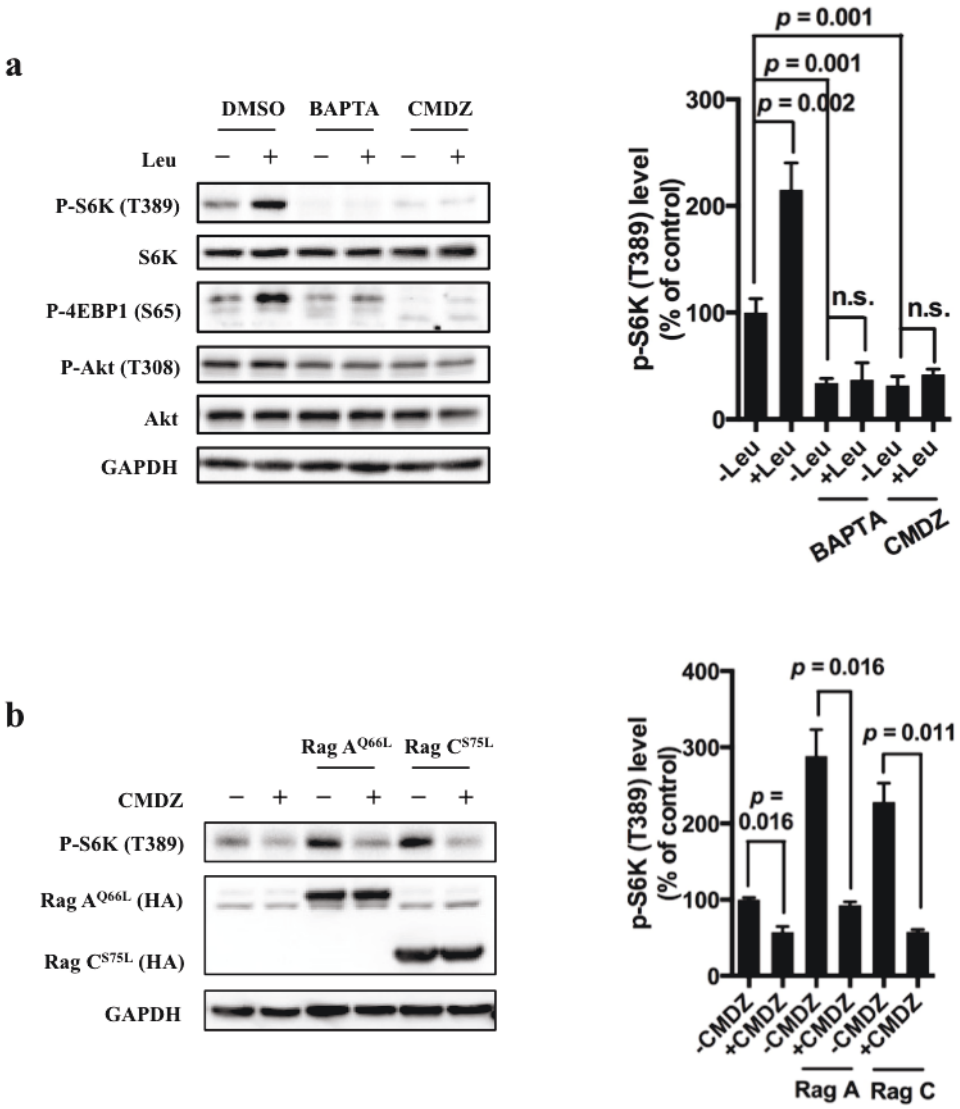

Figure 2.12: Calmodulin antagonist and cytosolic calcium chelator inhibit the activation of mTORC1 through amino acid/Rag GTPase axis.

(a) Effects of CMDZ (10 μM) or BAPTA-AM (25 μM) on the phosphorylation of indicated proteins in response to deprivation and stimulation with leucine. Cell lysates were prepared from HEK293T cells deprived for 3 h of leucine and, where indicated, stimulated with 52 μg/ml leucine for 10 min. CMDZ (10 μM) or BAPTA-AM (25 μM) was added 1 h prior to cell harvesting. The plot shows the percentage of p-S6K levels compared with vehicle control treated leucine starved HEK293T cells normalized by total

S6K control (mean ± s.d., n = 3 independent experiments, respectively). **(b)** Effects of CMDZ (10 μM) on the phosphorylation of S6K in HEK293T cells transfected with constitutively active RagA or RagC in expression vectors. Cell lysates were prepared and subjected to immunoblotting. The plot shows the percentage of p-S6K levels compared with vector transfected vehicle control treated 293T cells normalized by GAPDH loading control (mean ± s.d., n = 3 independent experiments).

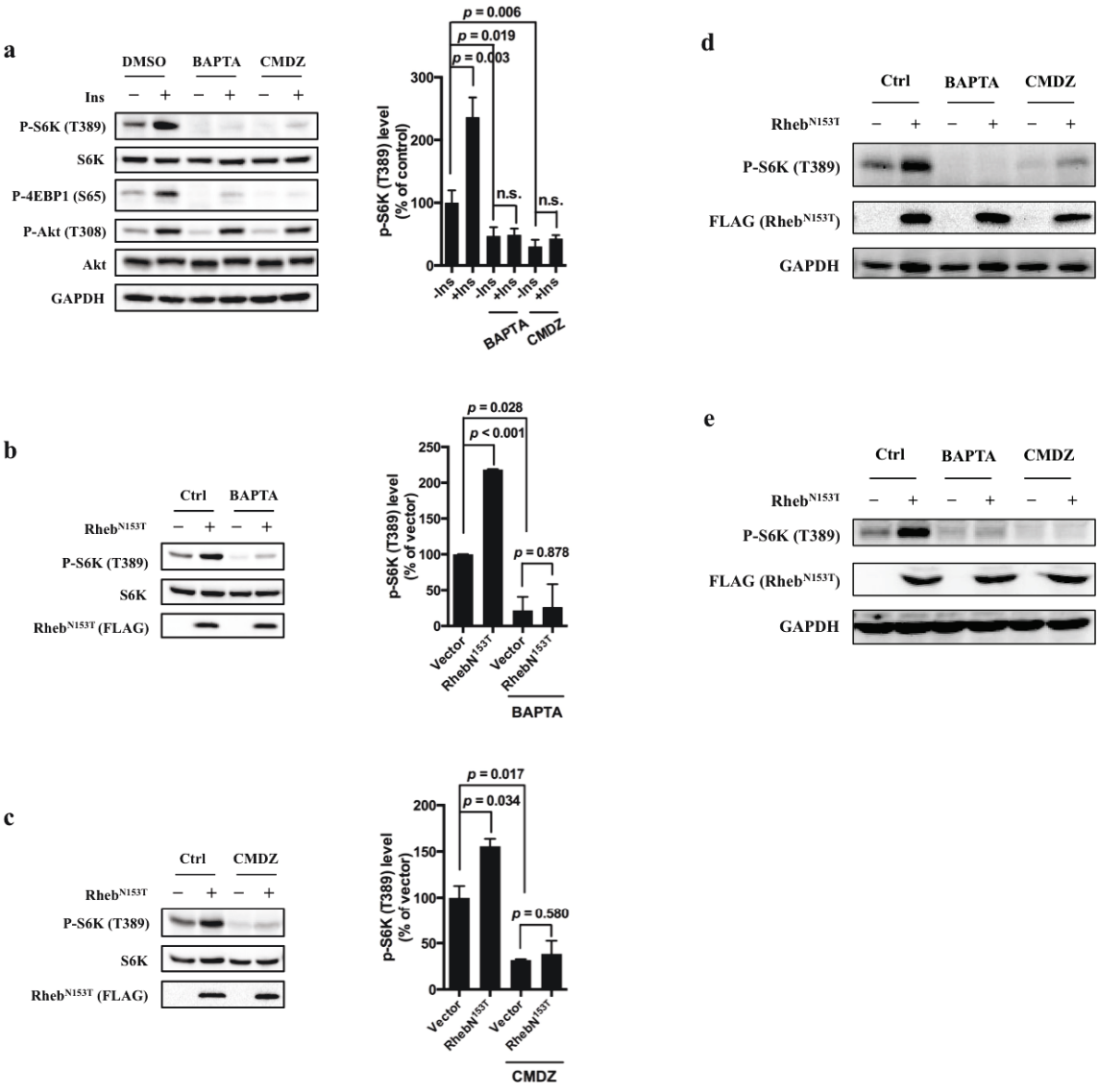

Figure 2.13: Calmodulin antagonist and cytosolic calcium chelator inhibit the activation of mTORC1 through insulin/Rheb axis.

(a) Effects of CMDZ (10 μM) or BAPTA-AM (25 μM) on the phosphorylation of indicated proteins in response to deprivation and stimulation with insulin. Cell lysates were prepared from HEK293T cells deprived for 24 h of serum and, where indicated, stimulated with 600 nM insulin for 10 min. CMDZ (10 μM) or BAPTA-AM (25 μM) was

added 1 h prior to cell harvesting. The plot shows the percentage of p-S6K levels compared with vehicle control treated serum starved HEK293T cells normalized by total S6K control (mean ± s.d., n = 3 independent experiments, respectively). **(b)** and **(c)** Effects of 25 μM BAPTA-AM (b) and 10 μM CMDZ (c) on the phosphorylation state of S6K in HEK293T cells stably expressing constitutively active Rheb as indicated. HEK293T cells were transduced with lentiviral FLAG-tagged $Rheb^{N153T}$, and treated with indicated compounds for 1 h. Cell lysates were prepared and used for immunoblotting. The plots show the percentage of p-S6K levels compared with vehicle control treated empty lentiviral vector transduced 293T cells normalized by total S6K control (mean ± s.d., n = 2 independent experiments). HUVEC **(d)** and A549 **(e)** cells were transduced with lentivirus carrying constitutively active $Rheb^{N153T}$. The transduced cells were treated with BAPTA or CMDZ for 1 h. The phosphorylation state of S6K was analyzed by immunoblotting. * $p < 0.05$, ** $p < 0.01$, *** $p < 0.001$, **** $p < 0{,}0001$.

CaM interacts with mTOR

First, we determined whether CaM intereacted with mTORC1. As shown in **Figure 2.14**, CaM could pull down mTOR and raptor, but not PRAS40, in a Ca^{2+}-dependent manner, and the binding is sensitive to detergents and CaM antagonist W-7. CaM has been previously reported to indirectly interact with mTORC1, and human vacuolar protein sorting 34 (hVps34) was shown to mediate the interaction between CaM and mTORC1 in HeLa cells (*13*). To our surprise, when hVps34 was knocked down in HEK293T cells, binding of CaM to mTOR was not affected (**Figure 2.15**), neither was the sensitivity of mTORC1 to CaM (**Figure 2.16**), ruling out hVps34 as a mediator of CaM-mTOR interaction in HEK293T cells. These results raised the possibility that CaM may directly interact with a subunit of the mTORC1 complex, thereby regulating its kinase activity. However, Ca^{2+} did not affect the assembly of mTORC1 complex (**Figure 2.17**), suggesting that one of the interactions of CaM sepharose with mTOR and raptor could be indirect. To identify the subunit in mTORC1 that interacts with CaM, we knocked down raptor and mTOR, respectively, and determined the remaining interaction between each subunit and CaM sepharose (**Figure 2.15**). Knockdown of raptor had no effect on the pulldown of mTOR by CaM sepharose. In contrast, knockdown of mTOR significantly reduced the binding of raptor as well as mTOR to CaM (**Figure 2.15**), suggesting that the interaction between mTOR and CaM is independent of raptor.

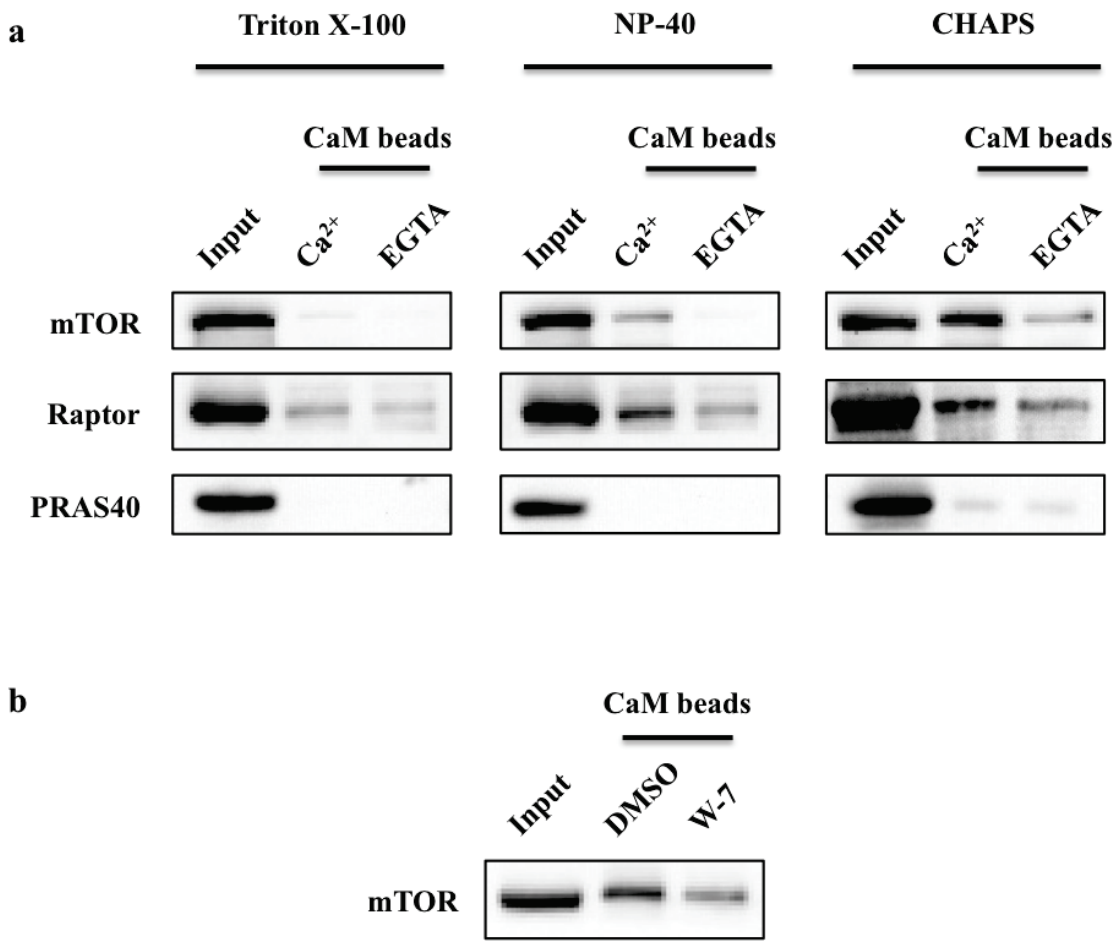

Figure 2.14: Calmodulin interacts with mTORC1 in a Ca^{2+}-dependent manner.

(a) Endogenous mTORC1 was pulled down by CaM sepharose in a Ca^{2+}-dependent manner. HEK293T cells were lysed in Triton X-100, NP-40 or CHAPS buffer, and the lysates were incubated with CaM sepharose in the presence of $CaCl_2$ (1 mM) or EGTA (5 mM). The precipitates were analyzed by immunoblotting. **(b)** The interaction between CaM and mTOR is inhibited by the CaM antagonist W-7. Cell lysates were prepared from HEK293T cells in CHAPS buffer, and endogenous mTOR was precipitated by CaM sepharose in the presence of W-7 or vehicle control.

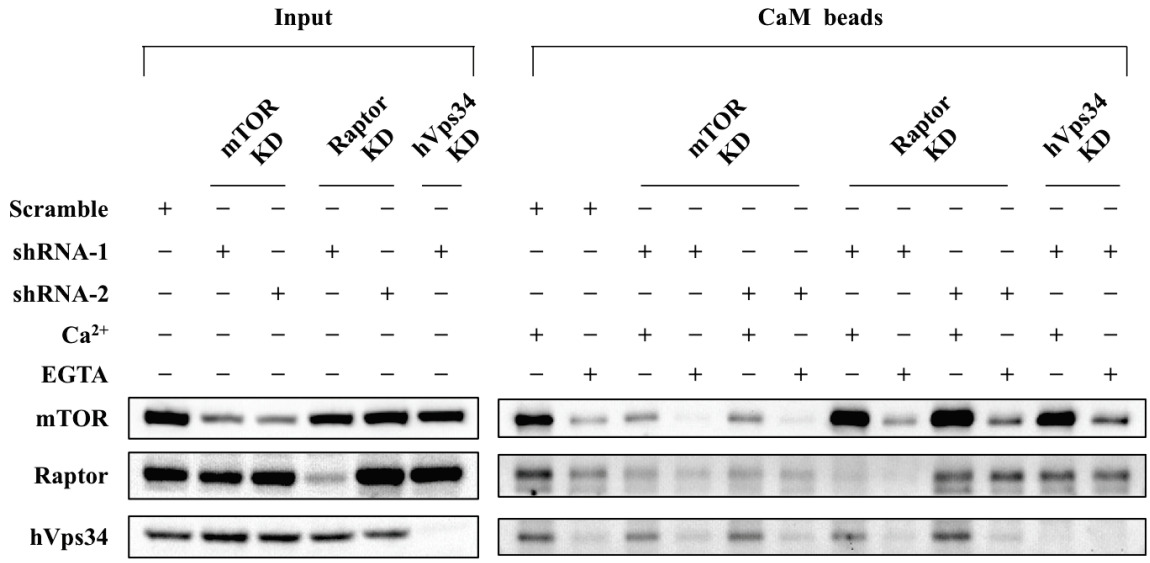

Figure 2.15: CaM interacts with mTOR independent of hVps34 or raptor.

Cell lysates were prepared from HEK293T cells transduced with lentiviral shRNAs targeting human mTOR, raptor, hVps34 or scrambled shRNA, followed by CaM sepharose precipitation in the presence of $CaCl_2$ (1 mM) or EGTA (5 mM). The cell lysates and precipitates were analyzed by immunoblotting to detect the indicated proteins.

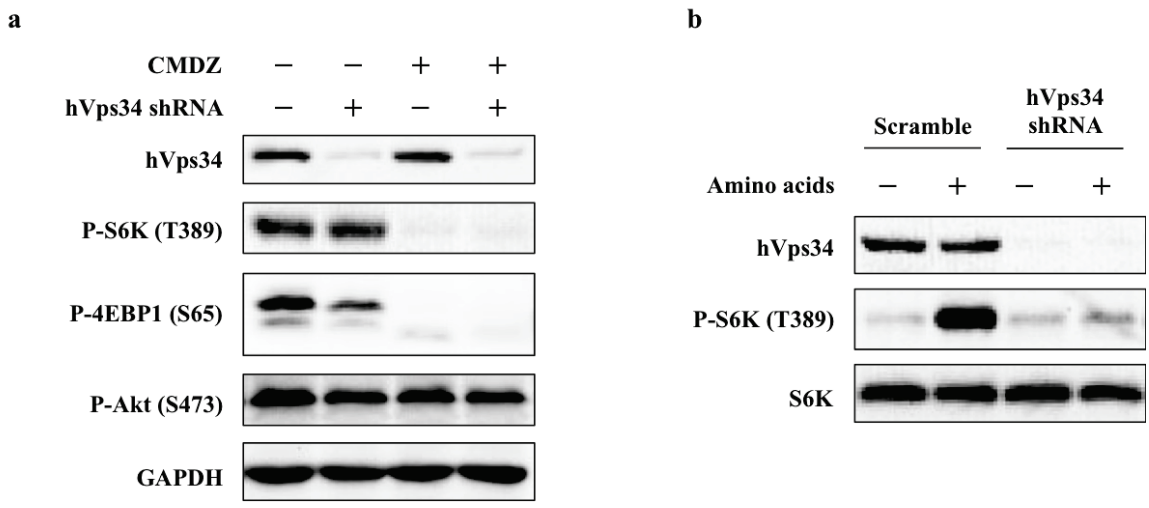

Figure 2.16: Effects of calmidazolium (CMDZ) on hVps34 depleted cells.

(a) HEK 293T cells were transduced with lentivirus carrying scramble shRNA or shRNA targeting hVps34. 96 hours after puromycin selection, cells were treated with vehicle control or CMDZ (10 μM) for 1 hour. **(b)** The same cells in (a) were starved with amino acids for 1 hours, and re-stimulated with amino acids for 10 min. Cells were lysed and subjected to immunoblotting.

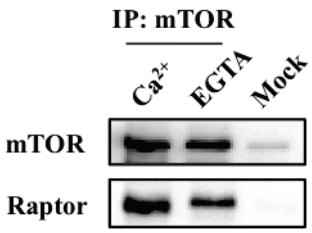

Figure 2.17: The presence or absence of Ca^{2+} does not affect the association of mTORC1.

Cell lysates were prepared from HEK293T in CHAPS buffer, and endogenous mTORC1 was immunoprecipitated by mTOR antibody. Rabbit IgG was used as mock immunoprecipitation.

Ca^{2+} and CaM activate the mTORC1 kinase activity *in vitro*

Having shown that CaM-binding fragment of mTOR (TRD3) exerted a dominant negative effect on mTORC1 activity in cells, we asked the question of whether CaM and Ca^{2+} had a direct effect on the intrinsic kinase activity of isolated mTORC1 complex *in vitro*. Thus, endogenous mTORC1 complex was immunoprecipitated by an anti-raptor antibody, and an *in vitro* kinase assay was performed using purified recombinant 4EBP1 as a substrate (*38*). As shown in **Figure 2.18 a**, the phosphorylation of 4EBP1 by immunoprecipitated mTORC1 complex was significantly increased in the presence of both $CaCl_2$ (0.2 mM) and CaM (2 μM), but not CaM alone, indicating that CaM activates mTORC1 kinase activity *in vitro* in a Ca^{2+}-dependent manner **(Figure 2.18 a, top left and top right panels, Lanes 1-3, respectively)**. Importantly, the activation of mTORC1 by Ca^{2+}/CaM was inhibited by Torin 1 **(Figure 2.18 a, top left panel, Lane 4)**, a TOR kinase inhibitor, and CMDZ **(Figure 2.18 a, top right panel, Lane 4)**, indicating that the phosphorylation of 4EBP1 was dependent on TOR kinase activity and CaM. Similar results were obtained from the *in vitro* kinase assay using purified recombinant S6K as the substrate **(Figure 2.18 b)**. These results demonstrated that CaM binding to mTOR leads to the stimulation of kinase activity of the mTORC1 complex.

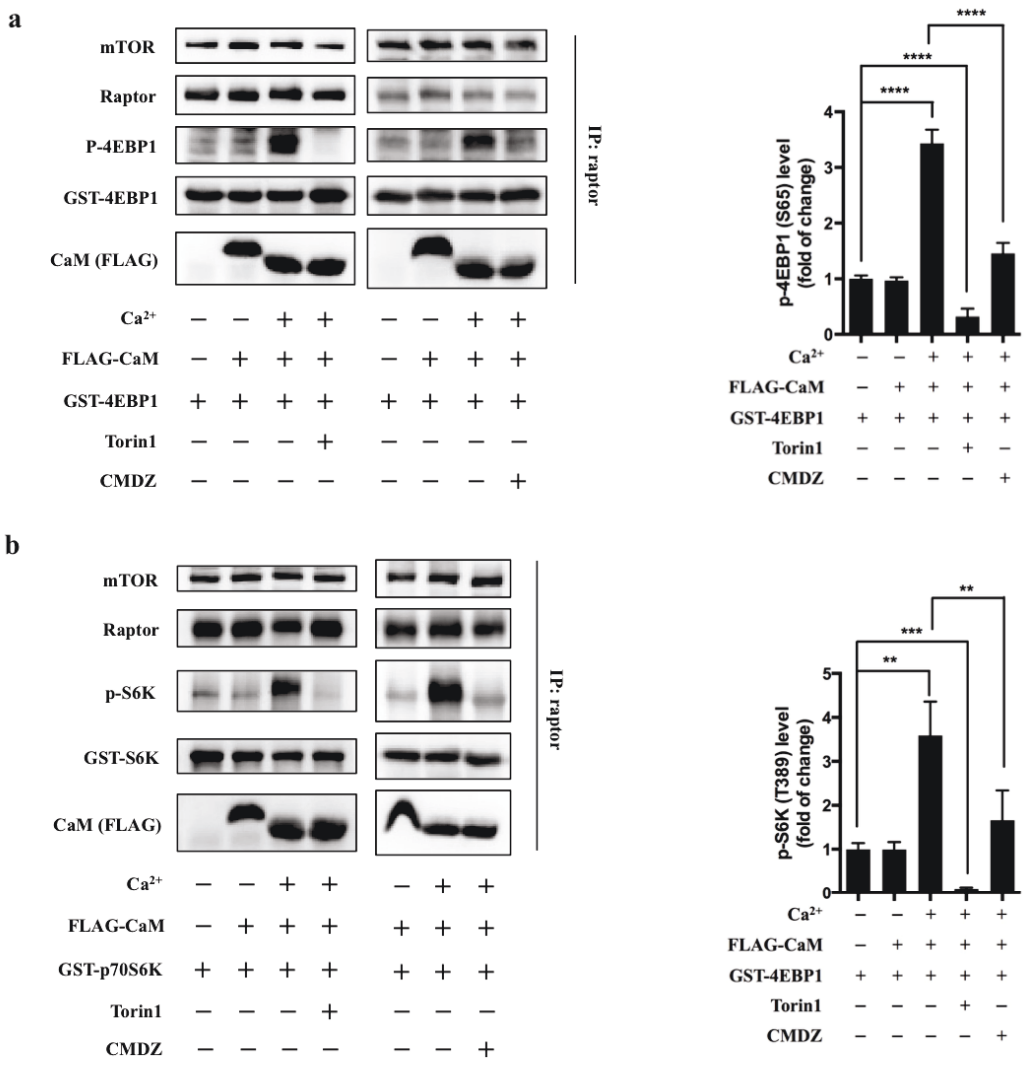

Figure 2.18: Calmodulin interacts with mTORC1 in a Ca^{2+}-dependent manner.

Cell lysates were prepared from HEK293T cells in CHAPS buffer, and endogenous mTORC1 was immunoprecipitated by a raptor antibody. ATP (250 μM), Torin1 (100 nM), CMDZ (8 μM), CaM (2 μM) or/and $CaCl_2$ (0.2 mM) were added into the kinase reaction as indicated. Phosphorylation of 4EBP1 **(a)** and S6K **(b)** were detected by immunoblotting. The plots show the fold of change of phosphorylation of 4EBP1 **(a)** or S6K **(b)** compared with control group (first lane) normalized by total GST-tagged protein control. (mean ± s.d., n = 6 and 5 independent experiments, respectively).

2.5 Discussion

The work described in this manuscript reveals a novel mechanism of regulation of mTORC1 by lysosomal calcium and CaM, shedding new light on the mTOR signaling pathway **(Figure 2.19)**. In the current model of mTORC1 activation (*39-42*), growth factors, energy, and other inputs signal to mTORC1 primarily through the TSC-Rheb axis; amino acids act by regulating the nucleotide state of the heterodimeric Rag GTPases and promoting the translocation of mTORC1 onto lysosomes, where it interacts with and becomes activated by lysosomally-localized, GTP-bound Rheb (*9*). Our results have uncovered another role of lysosomal localization of mTORC1, i.e., to receive localized lysosomal calcium stimulation. Integrating our previous observations (*16*) and the results from the present study, we propose an addition to the current model of mTOR signaling pathway: upon the translocation of mTORC1 onto the lysosome, properly released lysosomal calcium enriches local Ca^{2+} concentration, prompting Ca^{2+} binding to a local population of CaM, which in turn binds mTORC1 and stimulates the kinase activity of the mTORC1 complex.

The depletion of the homolog of TRPML1, TRPML in *Drosophila*, results in decreased TORC1 signaling, which was attributed to incomplete autophagy, and was completely reversed by feeding fly larvae with a high-protein diet (*22, 23*). However, we showed that in TRPML1-knockdown mammalian cells or mucolipidosis IV human fibroblasts, the inhibited mTORC1 signaling was only partially reversed by leucine or overexpression of constitutively active Rag GTPase, suggesting that there is a difference in the mechanisms of regulation of mTOR by Ca^{2+}/CaM between mammalian and fly cells. Interestingly, thapsigargin, which increases cytosolic Ca^{2+}, could completely

restore phosphorylation of S6K in TRPML1 deficient cells to the control level. Given that increased cytosolic Ca^{2+} also positively regulates the Ca^{2+}-dependent fusion of late-endosomes and autophagosomes to lysosomes (*17, 22, 43*), the rescue effect of thapsigargin might be due to the combined effects of autophagy as well as the direct stimulation of mTORC1 by Ca^{2+}/CaM in mammalian cells. On the other hand, TRPML1 is significantly upregulated under amino acids starvation (*29*), when mTORC1 dissociates from the lysosomal surface and becomes inactive, indicating that mTORC1 and TRPML1 may form reciprocal regulation loop. In addition, it has been recently reported that under starvation, lysosomal Ca^{2+} release through TRPML1 activates local calcineurin, a Ca^{2+}, CaM-dependent protein phosphatase, which dephosphorylates TFEB and promotes its nuclear translocation as well as regulates lysosomal biogenesis (*30*), suggesting another local function of lysosomal Ca^{2+}.

Our model of regulation of mTORC1 by Ca^{2+} and CaM differs from that proposed in a previous report (*13*), even though some of the experimental observations are in agreement. Similar to previous reports (*11, 13, 33*), we found that mTORC1 activity is sensitive to inhibition by BAPTA-AM and CaM antagonist CMDZ (Figure 3), suggesting that both intracellular calcium and CaM are required for mTORC1 activation. However, the precise mechanism of regulation of mTORC1 by calcium and CaM is distinct in our new model. First, we demonstrated that the lysosomal pool of calcium plays a unique and critical role in mTORC1 activation in mammalian cells. In earlier studies, however, the sources of calcium have been only suggested to be extracellular (*10, 13*) or conventional intracellular calcium stores such as the ER (*11, 33, 34*). Second, a previous study showed the CaM associates with mTORC1 complex through hVps34, and calcium and CaM

activate mTORC1 via hVps34 activation (*13*). In an independent study, it was shown that hVps15, but not Ca^{2+}/CaM, activates hVps34 (*15*). Similarly, we also found that knockdown of hVps34 had no effect on the interaction between CaM and mTORC1 in HEK293T cells, ruling out involvement of hVps34 in the regulation of mTORC1 via Ca^{2+}/CaM, at least in this cell type. We surmise that most of the previous results implicating calcium or CaM in the regulation of mTORC1 may be explained by our current model.

In previous studies, *in vitro* kinase assay of mTORC1 used EDTA in immunoprecipitation buffer (*24, 44*), which precluded the detection of any regulatory effect of calcium and CaM. By performing the mTOR kinase assay in the absence or presence of calcium and CaM *in vitro*, we were able to observe a dramatic activation of mTORC1 by calcium and CaM, revealing the functional consequence of the binding of CaM to mTOR--activation of its intrinsic kinase activity. As such, mTOR is a new type of atypical CaM-dependent kinase. The newly uncovered roles of lysosomal calcium and CaM in the regulation of mTOR signaling not only fill a gap in our understanding of this fundamental signaling pathway, but also offer new molecular targets for discovering and developing novel mTOR inhibitors.

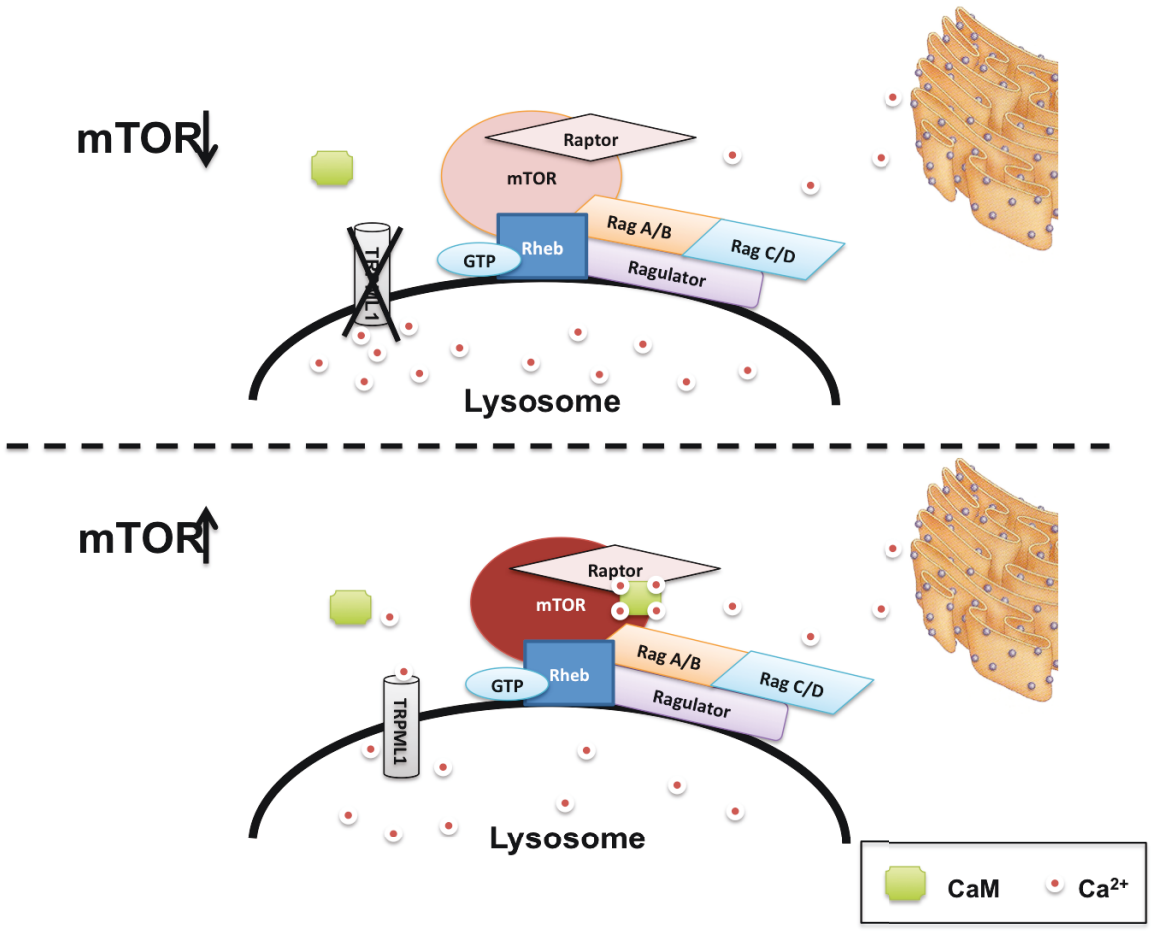

Figure 2.19: Proposed model of regulation of mTORC1 by TRPML1, lysosomal calcium and CaM.

Upon the translocation of mTORC1 onto the lysosome through binding to GTP-Rheb, lysosomal Ca^{2+} released through TRPML1 enriches the local Ca^{2+} concentration, prompting the binding to and activation of CaM, which in turn interacts with mTORC1 and leading to a fully activation of the kinase activity.

2.6 References

1. S. Wullschleger, R. Loewith, M. N. Hall, TOR signaling in growth and metabolism. *Cell* **124**, 471-484 (2006)
2. M. Laplante, D. M. Sabatini, mTOR signaling in growth control and disease. *Cell* **149**, 274-293 (2012)
3. J. Chung, C. J. Kuo, G. R. Crabtree, J. Blenis, Rapamycin-FKBP specifically blocks growth-dependent activation of and signaling by the 70 kd S6 protein kinases. *Cell* **69**, 1227-1236 (1992)
4. D. J. Price, J. R. Grove, V. Calvo, J. Avruch, B. E. Bierer, Rapamycin-induced inhibition of the 70-kilodalton S6 protein kinase. *Science* **257**, 973-977 (1992)
5. T. A. Lin, X. Kong, A. R. Saltiel, P. J. Blackshear, J. C. Lawrence, Jr., Control of PHAS-I by insulin in 3T3-L1 adipocytes. Synthesis, degradation, and phosphorylation by a rapamycin-sensitive and mitogen-activated protein kinase-independent pathway. *The Journal of biological chemistry* **270**, 18531-18538 (1995)
6. S. R. von Manteuffel, A. C. Gingras, X. F. Ming, N. Sonenberg, G. Thomas, 4E-BP1 phosphorylation is mediated by the FRAP-p70s6k pathway and is independent of mitogen-activated protein kinase. *Proceedings of the National Academy of Sciences of the United States of America* **93**, 4076-4080 (1996)
7. P. T. Bhaskar, N. Hay, The two TORCs and Akt. *Developmental cell* **12**, 487-502 (2007)

8. E. Kim, P. Goraksha-Hicks, L. Li, T. P. Neufeld, K. L. Guan, Regulation of TORC1 by Rag GTPases in nutrient response. *Nature cell biology* **10**, 935-945 (2008)

9. Y. Sancak, T. R. Peterson, Y. D. Shaul, R. A. Lindquist, C. C. Thoreen, L. Bar-Peled, D. M. Sabatini, The Rag GTPases bind raptor and mediate amino acid signaling to mTORC1. *Science* **320**, 1496-1501 (2008)

10. N. M. Conus, B. A. Hemmings, R. B. Pearson, Differential regulation by calcium reveals distinct signaling requirements for the activation of Akt and p70S6k. *The Journal of biological chemistry* **273**, 4776-4782 (1998)

11. L. M. Graves, Y. He, J. Lambert, D. Hunter, X. Li, H. S. Earp, An intracellular calcium signal activates p70 but not p90 ribosomal S6 kinase in liver epithelial cells. *The Journal of biological chemistry* **272**, 1920-1928 (1997)

12. K. M. Hannan, G. Thomas, R. B. Pearson, Activation of S6K1 (p70 ribosomal protein S6 kinase 1) requires an initial calcium-dependent priming event involving formation of a high-molecular-mass signalling complex. *The Biochemical journal* **370**, 469-477 (2003)

13. P. Gulati, L. D. Gaspers, S. G. Dann, M. Joaquin, T. Nobukuni, F. Natt, S. C. Kozma, A. P. Thomas, G. Thomas, Amino acids activate mTOR complex 1 via Ca2+/CaM signaling to hVps34. *Cell Metab* **7**, 456-465 (2008)

14. F. Mercan, H. Lee, S. Kolli, A. M. Bennett, Novel role for SHP-2 in nutrient-responsive control of S6 kinase 1 signaling. *Molecular and cellular biology* **33**, 293-306 (2013)

15. Y. Yan, R. J. Flinn, H. Wu, R. S. Schnur, J. M. Backer, hVps15, but not Ca2+/CaM, is required for the activity and regulation of hVps34 in mammalian cells. *The Biochemical journal* **417**, 747-755 (2009)

16. J. Xu, Y. Dang, Y. R. Ren, J. O. Liu, Cholesterol trafficking is required for mTOR activation in endothelial cells. *Proceedings of the National Academy of Sciences of the United States of America* **107**, 4764-4769 (2010)

17. E. Lloyd-Evans, A. J. Morgan, X. He, D. A. Smith, E. Elliot-Smith, D. J. Sillence, G. C. Churchill, E. H. Schuchman, A. Galione, F. M. Platt, Niemann-Pick disease type C1 is a sphingosine storage disease that causes deregulation of lysosomal calcium. *Nature medicine* **14**, 1247-1255 (2008)

18. D. Shen, X. Wang, X. Li, X. Zhang, Z. Yao, S. Dibble, X. P. Dong, T. Yu, A. P. Lieberman, H. D. Showalter, H. Xu, Lipid storage disorders block lysosomal trafficking by inhibiting a TRP channel and lysosomal calcium release. *Nature communications* **3**, 731 (2012)

19. X. Cheng, D. Shen, M. Samie, H. Xu, Mucolipins: Intracellular TRPML1-3 channels. *FEBS letters* **584**, 2013-2021 (2010)

20. X. P. Dong, D. Shen, X. Wang, T. Dawson, X. Li, Q. Zhang, X. Cheng, Y. Zhang, L. S. Weisman, M. Delling, H. Xu, PI(3,5)P(2) controls membrane trafficking by direct activation of mucolipin Ca(2+) release channels in the endolysosome. *Nature communications* **1**, 38 (2010)

21. D. Shen, X. Wang, H. Xu, Pairing phosphoinositides with calcium ions in endolysosomal dynamics: phosphoinositides control the direction and specificity of membrane trafficking by regulating the activity of calcium channels in the

endolysosomes. *BioEssays : news and reviews in molecular, cellular and developmental biology* **33**, 448-457 (2011)

22. C. O. Wong, R. Li, C. Montell, K. Venkatachalam, Drosophila TRPML is required for TORC1 activation. *Curr Biol* **22**, 1616-1621 (2012)

23. K. Venkatachalam, C. O. Wong, C. Montell, Feast or famine: role of TRPML in preventing cellular amino acid starvation. *Autophagy* **9**, 98-100 (2013)

24. D. H. Kim, D. D. Sarbassov, S. M. Ali, J. E. King, R. R. Latek, H. Erdjument-Bromage, P. Tempst, D. M. Sabatini, mTOR interacts with raptor to form a nutrient-sensitive complex that signals to the cell growth machinery. *Cell* **110**, 163-175 (2002)

25. P. E. Burnett, R. K. Barrow, N. A. Cohen, S. H. Snyder, D. M. Sabatini, RAFT1 phosphorylation of the translational regulators p70 S6 kinase and 4E-BP1. *Proceedings of the National Academy of Sciences of the United States of America* **95**, 1432-1437 (1998)

26. R. H. Kutner, X. Y. Zhang, J. Reiser, Production, concentration and titration of pseudotyped HIV-1-based lentiviral vectors. *Nat Protoc* **4**, 495-505 (2009)

27. J. Lytton, M. Westlin, M. R. Hanley, Thapsigargin inhibits the sarcoplasmic or endoplasmic reticulum Ca-ATPase family of calcium pumps. *The Journal of biological chemistry* **266**, 17067-17071 (1991)

28. X. Feng, J. Xiong, Y. Lu, X. Xia, M. X. Zhu, Differential mechanisms of action of the mucolipin synthetic agonist, ML-SA1, on insect TRPML and mammalian TRPML1. *Cell Calcium* **56**, 446-456 (2014)

29. W. Wang, Q. Gao, M. Yang, X. Zhang, L. Yu, M. Lawas, X. Li, M. Bryant-Genevier, N. T. Southall, J. Marugan, M. Ferrer, H. Xu, Up-regulation of lysosomal TRPML1 channels is essential for lysosomal adaptation to nutrient starvation. *Proceedings of the National Academy of Sciences of the United States of America* **112**, E1373-1381 (2015)

30. D. L. Medina, S. Di Paola, I. Peluso, A. Armani, D. De Stefani, R. Venditti, S. Montefusco, A. Scotto-Rosato, C. Prezioso, A. Forrester, C. Settembre, W. Wang, Q. Gao, H. Xu, M. Sandri, R. Rizzuto, M. A. De Matteis, A. Ballabio, Lysosomal calcium signalling regulates autophagy through calcineurin and TFEB. *Nature cell biology* **17**, 288-299 (2015)

31. S. Jager, C. Bucci, I. Tanida, T. Ueno, E. Kominami, P. Saftig, E. L. Eskelinen, Role for Rab7 in maturation of late autophagic vacuoles. *Journal of cell science* **117**, 4837-4848 (2004)

32. J. M. Hyttinen, M. Niittykoski, A. Salminen, K. Kaarniranta, Maturation of autophagosomes and endosomes: a key role for Rab7. *Biochimica et biophysica acta* **1833**, 503-510 (2013)

33. Z. Ke, D. Liang, Q. Zeng, Q. Ren, H. Ma, L. Gui, S. Chen, M. Guo, Y. Xu, W. Gao, S. Zhang, L. Chen, hsBAFF promotes proliferation and survival in cultured B lymphocytes via calcium signaling activation of mTOR pathway. *Cytokine* **62**, 310-321 (2013)

34. X. Zhou, D. S. Lin, F. Zheng, M. A. Sutton, H. Wang, Intracellular calcium and calmodulin link brain-derived neurotrophic factor to p70S6 kinase

phosphorylation and dendritic protein synthesis. *Journal of neuroscience research* **88**, 1420-1432 (2010)

35. H. Wei, W. Wei, D. E. Bredesen, D. C. Perry, Bcl-2 protects against apoptosis in neuronal cell line caused by thapsigargin-induced depletion of intracellular calcium stores. *Journal of neurochemistry* **70**, 2305-2314 (1998)

36. X. Long, Y. Lin, S. Ortiz-Vega, K. Yonezawa, J. Avruch, Rheb binds and regulates the mTOR kinase. *Curr Biol* **15**, 702-713 (2005)

37. L. Yan, G. M. Findlay, R. Jones, J. Procter, Y. Cao, R. F. Lamb, Hyperactivation of mammalian target of rapamycin (mTOR) signaling by a gain-of-function mutant of the Rheb GTPase. *The Journal of biological chemistry* **281**, 19793-19797 (2006)

38. D. D. Sarbassov, S. M. Ali, D. H. Kim, D. A. Guertin, R. R. Latek, H. Erdjument-Bromage, P. Tempst, D. M. Sabatini, Rictor, a novel binding partner of mTOR, defines a rapamycin-insensitive and raptor-independent pathway that regulates the cytoskeleton. *Curr Biol* **14**, 1296-1302 (2004)

39. C. C. Dibble, L. C. Cantley, Regulation of mTORC1 by PI3K signaling. *Trends Cell Biol* **25**, 545-555 (2015)

40. C. Buerger, B. DeVries, V. Stambolic, Localization of Rheb to the endomembrane is critical for its signaling function. *Biochemical and biophysical research communications* **344**, 869-880 (2006)

41. A. Efeyan, D. M. Sabatini, Nutrients and growth factors in mTORC1 activation. *Biochemical Society transactions* **41**, 902-905 (2013)

42. K. Saito, Y. Araki, K. Kontani, H. Nishina, T. Katada, Novel role of the small GTPase Rheb: its implication in endocytic pathway independent of the activation of mammalian target of rapamycin. *Journal of biochemistry* **137**, 423-430 (2005)

43. A. Grotemeier, S. Alers, S. G. Pfisterer, F. Paasch, M. Daubrawa, A. Dieterle, B. Viollet, S. Wesselborg, T. Proikas-Cezanne, B. Stork, AMPK-independent induction of autophagy by cytosolic Ca2+ increase. *Cellular signalling* **22**, 914-925 (2010)

44. D. H. Kim, D. D. Sarbassov, S. M. Ali, R. R. Latek, K. V. Guntur, H. Erdjument-Bromage, P. Tempst, D. M. Sabatini, GbetaL, a positive regulator of the rapamycin-sensitive pathway required for the nutrient-sensitive interaction between raptor and mTOR. *Mol Cell* **11**, 895-904 (2003)

Chapter 3: Divergence of antiangiogenic activity and hepatotoxicity of different stereoisomers of itraconazole

3.1 Abstract

In Chapter 2, I described a fundamental study of the regulation of mTOR signaling pathway by discovering that lysosomal calcium and calmodulin are required for mTORC1 activation using the methods involving chemical biology and genetic manipulation. In this chapter, I will describe a chemical biology study to study the divergence of antiangiogenesis activity and hepatotoxicity of different stereoisomers of itraconazole. Itraconazole is a triazole antifungal drug that has recently been found to inhibit angiogenesis. Itraconazole is a relatively well-tolerated drug but shows hepatotoxicity in a small subset of patients. Itraconazole contains three chiral centers and the commercial itraconazole is composed of four cis-stereoisomers (named IT-A, IT-B, IT-C, and IT-D). However, whether the stereoisomers of itraconazole are differ in their antiangiogenic activity and hepatotoxicity remains unknown. Here, we assessed *in vitro* antiangiogenic activity of itraconazole and each stereoisomer using human umbilical vein endothelial cell (HUVEC) proliferation and tube formation assays. We also determined their hepatotoxicity using primary human hepatocytes *in vitro* and a mouse model *in vivo*. Mouse Matrigel plug and tumor xenograft models were used to evaluate *in vivo* antiangiogenic and antitumor activities of the stereoisomers. Of the four stereoisomers contained in commercial itraconazole, we found that IT-A (2S,4R,20R) and IT-C (2S,4R,20S) were more potent for inhibition of angiogenesis than IT-B (2R,4S,20R) and IT-D (2R,4S,20S). Interestingly, IT-A and IT-B were more hepatotoxic than IT-C and IT-

D. In mouse models, IT-C showed more potent antiangiogenic/antitumor activity with lower hepatotoxicity compared with itraconazole and IT-A. These results demonstrate the segregation of influence of stereochemistry at different positions of itraconazole on its antiangiogenic activity and hepatotoxicity, with the 2 and 4 positions affecting the former and the 20 position affecting the latter. They also suggest that IT-C may be superior to the racemic mixture of itraconazole as an anticancer drug candidate due to its lower hepatotoxicity and improved antiangiogenic activity.

ABBREVIATIONS

HUVEC, human umbilical vein endothelial cells; mTOR, mechanistic target of rapamycin; mTORC1, mTOR complex 1; GAPDH, glyceraldehyde 3-phosphate dehydrogenase; S6K, ribosomal s6 kinase; VEGF, vascular endothelial growth factor; NPC, Niemann-Pick Disease Type C; CYP3A4, cytochrome P450 3A4; ALT, alanine aminotransaminase; LDL, low-density lipoprotein.

3.2 Introduction

Angiogenesis, the formation of new blood vessels from preexisting vasculature, has been shown to play a critical role in both normal physiologic and pathologic processes. It is essential during development and wound healing, and is tightly regulated by endogenous pro- and antiangiogenic factors. It has also been implicated in a number of diseases including cancer, rheumatoid arthritis and macular degeneration (*1-3*). Since the angiogenesis hypothesis was first proposed by Judah Folkman in 1971 (*4*), a number of angiogenesis inhibitors have been discovered and developed into antiangiogenic drugs (*5-7*). A monoclonal antibody against VEGF, bevacizumab, was first approved by the FDA in 2004 for the treatment of metastatic colon cancer in combination with standard chemotherapy. Subsequently, several small-molecule angiogenesis inhibitors have been entered the clinic, including sorafenib (Nexavar), sunitinib (Sutent), and pazopanib (Votrient). However, most of these small-molecule antiangiogenic drugs are kinase inhibitors that lack specificity or lead to a high frequency of drug resistance (*8-10*), necessitating the development of small-molecule angiogenesis inhibitors with novel mechanisms of action. In an effort to accelerate drug discovery and development, we assembled the Johns Hopkins Drug Library over a decade ago and screened it for new antiangiogenic activity among existing drugs using a proliferation assay with primary human umbilical vein endothelial cells (HUVEC). Among the most interesting hits was the antifungal drug itraconazole (*11*). Interestingly, itraconazole was also found to be an inhibitor of the hedgehog signaling pathway in a separate screen, rendering itraconazole a novel anticancer drug candidate capable of inhibiting the growth of both tumor vasculature and tumor cells themselves (*12*). A series of tests of itraconazole in

preclinical angiogenesis and cancer models confirmed the antiangiogenic and anticancer activity of itraconazole in vivo (*11-13*). On the basis of these promising preclinical results, itraconazole entered multiple Phase II human clinical studies for treating different types of cancer. (http://www.clinicaltrials.gov/). Positive clinical results have been reported for advanced lung cancer, metastatic prostate cancer, and basal cell carcinoma (*14-16*). Moreover, itraconazole was found to increase progression or overall survival among late-stage ovarian, triplenegative breast and metastatic pancreatic cancer patients upon retrospective analysis of previous clinical data (*17-19*). Together, these encouraging results strongly suggest that itraconazole is a promising new anticancer drug lead. Although the precise mechanism for the antiangiogenic and anti-hedgehog activities remains unknown, preliminary evidence suggests that the mode of action of itraconazole is distinct from any other known inhibitors of angiogenesis or the hedgehog signaling pathway. Early on, we ruled out the cholesterol biosynthetic enzyme, lanosterol 14a-demethylase, which mediates the antifungal activity of itraconazole, as the relevant target for its antiangiogenic activity (*11*). Subsequently, we serendipitously discovered that itraconazole blocks the traffic of cholesterol and likely lipids out of the lysosome, causing a phenotype similar to Niemann-Pick Disease Type C (NPC) in endothelial cells. We also found that itraconazole is a potent inhibitor of the mTOR pathway in endothelial cells (*20*). Importantly, the blockade of cholesterol trafficking through the endolysosome can only partially explain the inhibition of mTOR by itraconazole, suggesting that there exist unidentified molecular target(s) for itraconazole. Similarly, the mechanism underlying the inhibition of hedgehog signaling also remains unclear, even though it has been shown to block the translocation of Smoothened from intracellular vesicles into the

primary cilium (*12*). Using a number of synthetic analogs of itraconazole, we explored the structure-activity relationship of itraconazole for its two distinct activities and found no correlation between the two, further suggesting that the antiangiogenic and anti-hedgehog activity of itraconazole are likely to be mediated by different molecular mechanisms (*21*). Itraconazole has been widely used to treat fungal infections.

Although itraconazole is known to be relatively well tolerated, about 7% of patients who received the drug experience hepatotoxicity (*22*). In addition to lanosterol 14 alpha-demethylase (*23*), itraconazole is also known to be a potent inhibitor of human liver cytochrome P450 3A4 (CYP3A4), accounting for its extensive drug–drug interactions with other medications (*24*). It is believed that the effect of itraconazole on CYP3A4 is responsible for the human hepatotoxicity (*25*). The commercial itraconazole consists of four cis-stereoisomers of itraconazole, including IT-A (2S,4R,2'R), IT-B (2R,4S,2'R), IT-C (2S,4R,2'S), and IT-D (2R,4S,2'S). All four isomers are known to be ligands of CYP3A4 (*26*). However, only IT-B and IT-D among the four isomers were metabolized by CYP3A4 (*26*). To assess the antiangiogenic activity of the different stereoisomers, we previously synthesized each of cis-stereoisomers and determined their effects on both fungi and endothelial cells (*27*). In this study, we conducted a large-scale purification of each stereoisomer from the racemic itraconazole mixture using the preparative supercritical fluid chromatography (SFC) and obtained gram quantities of each purified stereoisomer. Using the purified stereoisomers, we compared the antiangiogenic activity and hepatotoxicity of each stereoisomer of itraconazole and the racemic itraconazole both in vitro and in vivo. We found that ITA and IT-C are more potent at inhibiting angiogenesis compared to the others, whereas IT-C and IT-D are less hepatotoxic

compared to IT-A, IT-B and racemic itraconazole. Together, these results suggest that IT-C is the most potent antiangiogenic and anticancer agent with the least hepatotoxicity among the four stereoisomers of itraconazole.

3.3 Materials and methods

Cells

HUVECs (Lonza) were grown in endothelial cell growth medium-2 (EGM-2) using the EGM-2 bullet kit (Lonza) per manufacturer's instructions. HUVEC phenotype was verified by morphological observation throughout serial passage by the manufacturer. Human pericytes (placental derived) were purchased from Zen-Bio (Research Triangle Park, NC) and were grown in the complete pericyte growth medium (Zen-Bio). HCC1954 human breast cancer and CWR22Rv1 human prostate cancer cells were grown in RPMI-1640 medium containing 10% fetal bovine serum (FBS, Invitrogen, Carlsbad, CA) and 1% antibiotic (penicillin and streptomycin) solution (Invitrogen). The cells were maintained in a humidified incubator at 37°C adjusted to 5% CO_2.

Reagents

Racemic itraconazole and filipin were purchased from Sigma-Aldrich (St Louis, MO). Four individual cis-stereoisomers of itraconazole (IT-A, IT-B, IT-C, and IT-D) were obtained using preparative supercritical fluid chromatography (SFC) separation of commercial itraconazole, which was performed by WuXi AppTec. Quality control of each purified stereoisomer was conducted by chiral HPLC and optical rotation using previously synthesized stereoisomer samples as standards (*27*). Low-density lipoprotein (LDL) from human plasma was purchased from Fisher Scientific.

HUVEC proliferation assay

HUVEC (5,000 cells/well) were seeded in 96-well plates containing 0.2 mL of EGM-2 medium and allowed to adhere at 37°C for 24 hours. The cells were then treated with various concentrations of each compound for 24 hours. Cells were pulsed with 0.5 mCi [3H]-thymidine (PerkinElmer) for 16 hours, before the cells were treated with 1 × trypsin-EDTA (Invitrogen). The detached cells were harvested onto FilterMat A glass fiber filters (Wallac) using a Harvester 96 cell harvester (Tomtec). [3H]-thymidine counts were determined using a MicroBeta plate reader (PerkinElmer). Each treatment was done in triplicate and the experiments were conducted four times independently. The IC_{50} values of each compound and their95%confidence intervals were calculated using the GraphPad Prism 5.0 software (GraphPad Software).

Immunobloting

Immunobloting assays were performed as described in Chapter 2.

Filipin staining

HUVEC were seeded at 3×10^4 cells per well in a Nunc Lab-Tek II Chamber Slide (Thermo Fisher Scientific) and allowed to adhere overnight. Following drug treatment for 24 hours, cells were fixed in 4% paraformaldehyde in PBS (pH 7.4) for 20 minutes and then washed with PBS three times. The slides were incubated with PBS containing filipin (at a final concentration of 50 mg/mL) in the dark for 1 hour at room temperature. The cells were then washed with PBS three times, mounted with Immumount (Thermo Fisher Scientific), and stored in the dark before imaging with a Zeiss 510 Meta confocal microscope (Carl Zeiss).

HUVEC tube formation assay

The tube formation assay, a model for assessment of angiogenesis in vitro, was conducted as previously described (*28*). Briefly, a 96-well plate was coated with Matrigel (BD Biosciences) by adding 50 mL of ice-cold Matrigel solution per well followed by incubation at 37°C for 1 hour. HUVEC were then seeded on the Matrigel-coated wells (2×10^4 cells/well). Cells were treated with compound alone or in combination with LDL and then incubated in a CO_2 incubator for 16 hours. For the posttreatment experiments, compounds were added to the cells 6 hours after seeding on Matrigel and the incubation was continued for 18 hours. The cells were washed carefully with PBS once, and Calcein-AM (BD Biosciences) solution in PBS (2 mmol/L final concentration) was added. After incubation at 37°C for an additional 30 minutes, the cells were washed with PBS and the fluorescence-labeled HUVEC tubes were observed under the Nikon Eclipse TS100 fluorescence microscope (485-nm excitation and 520-nm emission) at magnification ×100. Each treatment was done in triplicate and the experiments were conducted three times independently. The total tube length, size, and number of junctions from the fluorescence images were quantified using the AngioQuant v1.33 software (The MathWorks).

HUVEC-pericyte co-culture tube formation

Growing pericytes in a 6-cm cell culture dish were labeled with Calcein-AM for 30 minutes before the tube formation experiments. Ibidi m-Slide angiogenesis chamber (Ibidi) was coated with Matrigel by adding 10 mL of ice-cold Matrigel solution per well followed by incubation at 37°C for 1 hour. HUVEC (1.5×10^4 cells/well) and pericytes

(500 cells/well) were mixed at a ratio of 30:1 in complete EGM-2 media, seeded on the Matrigel-coated wells and then treated with compounds. After 20 hours of incubation, the co-culture tube formation was analyzed under a Zeiss AxioObserver Z1 fluorescence microscope with ApoTome apparatus (Carl Zeiss) at magnification ×50. The total tube lengths of the fluorescence-labeled pericytes were quantified using the AngioQuant v1.33 software.

Determination of hepatotoxicity in primary human hepatocytes

Fresh primary human hepatocytes (6-well plates) with Matrigel overlay from three donors were obtained from XenoTech, LLC. Ages and genders of donors were as follows: 22-year-old male, 54-year-old male, and 63-year-old male. Hepatocyte viability from each donor was at least 74%. Upon receipt of the hepatocytes, the shipping medium was replaced with Williams' Medium E supplemented with 10% FBS (Invitrogen), penicillin–streptomycin (Sigma-Aldrich), and L-glutamine (Invitrogen). The hepatocytes were then incubated overnight at 37°C in a 5% CO_2 humidified environment. Following the overnight incubation the medium was replaced with fresh William's Medium E supplemented as described above and the hepatocytes were incubated with DMSO (vehicle control, 0.1% final volume), racemic itraconazole (2 mmol/L or 10 mmol/L) as well as stereoisomers denoted as IT-A, IT-B, IT-C, and IT-D at a final concentration of either 2 or 10 mmol/L for 72 hours. Following incubation, to monitor hepatocyte function, the medium was removed and alanine aminotransaminase (ALT) levels were measured using an alanine aminotransaminase activity assay kit purchased from BioVision Inc. Cell viability following treatment with itraconazole and stereoisomers was

determined using the Cell Death Detection ELISA Kit according to the manufacturer's instructions (Roche Diagnostics Corporation) as we have reported previously (*29*). Intracellular glutathione (GSH) was measured using HPLC by quantification of the 5-thio-2-nitrobenzoic acid formed following the addition of Ellman's reagent to hepatocyte lysates as previously described (*30*).

Determination of hepatotoxicity in mice

Female mice (BALB/c, AnNCr) ages 6 to 8 weeks were purchased from the National Cancer Institute (Frederick, MD) and treated in accordance with Johns Hopkins Animal Care and Use Committee procedures. Mice (n = 5/group) were treated intraperitoneally (i.p.) with vehicle (saline with 5% DMSO, 5% PEG500, and 5% tween-80), 60 mg/kg itraconazole, 60 mg/kg IT-A, and 60 mg/kg IT-C once daily for 10 days. Mice were sacrificed and livers from each group were isolated, photographed, and fixed in 10% neutral- buffered formalin (Sigma-Aldrich). Fixed liver tissues were embedded in paraffin, processed for histology sections and stained with hematoxylin and eosin (H&E).

***In vivo* Matrigel plug angiogenesis assay**

Female mice (BALB/c, AnNCr) ages 6 to 8 weeks were used for the Matrigel plug angiogenesis assay. Mice (n = 5/group) were pretreated i.p. with vehicle (saline with 5% DMSO, 5% PEG500, and 5% tween-80), itraconazole (20 and 50 mg/kg), IT-A (20 and 50 mg/kg), and IT-C (20 and 50 mg/kg) once daily for 2 days before Matrigel implantation. Matrigel (0.5 mL/injection) containing 200 ng/mL VEGF and 500 ng/mL basic fibroblast growth factor (bFGF) was implanted subcutaneously into mice. The drug

treatment was continued once daily for an additional 8 days. Mice were sacrificed and whole Matrigel plugs with mouse skin were excised, fixed in 10% neutral-buffered formalin, embedded in paraffin. For staining infiltrated cells in the Matrigel, the fixed Matrigel plugs were processed for histochemical staining using Masson trichrome staining, which stains the Matrigel blue and the infiltrated cells and vessels red.

For staining functional vasculatures, the fixed Matrigel plugs were stained with anti-CD31 (BD Pharmingen), a blood vessel marker, and anti-NG2 (Abcam), a pericyte marker, to assess Matrigel plug angiogenesis. A cross-section of the Matrigel plug was photographed at ×100 magnification under a Nikon Eclipse TS100 microscope and CD31-positive blood vessels and NG2-stained cells were counted per field for quantification of angiogenesis.

In vivo tumor xenograft assay

Female athymic nude mice (BALB/c, nu/nu-NCr) ages 6 to 8 weeks were purchased from the National Cancer Institute (NCI)-Frederick and treated in accordance with Johns Hopkins AnimalCare and Use Committee procedures. HCC1954 human breastcancer cells (2×10^6) were implanted subcutaneously into the mice. After tumors became palpable, the mice (n = 7/group) were treated i.p. with vehicle (saline with 5% DMSO, 5% PEG500, and 5% tween-80), itraconazole (25 and 50 mg/kg), and IT-C (25 and 50 mg/kg) once daily for 30 days. For CWR22Rv1 human prostate cancer xenografts, male athymic nude mice (BALB/c, nu/nu-NCr) ages 6 to 8 weeks (NCI-Frederick) were used for tumor cell implantation (2×10^6 cells/injection). The tumor-bearing mice (n = 6/group) were treated i.p. with vehicle, itraconazole (20 and 60 mg/kg)

and IT-C (20 and 60 mg/kg) once daily for 24 days. The tumor volume was measured periodically using a vernier caliper and calculated according to the modified ellipsoid formula: tumor volume (mm^3) = $(width)^2 \times (length) \times \pi/6$. After treatment, the mice were sacrificed and whole tumor tissues from the HCC1954 xenograft were excised. Tumor tissues were then fixed in 10% neutral-buffered formalin, embedded in paraffin and sliced to obtain 5-mm sections. The blood vessels in the tumor tissue sections were stained with an anti-CD31 antibody (BD Pharmingen), a blood vessel marker, to assess tumor angiogenesis angiogenesis. A cross-section of the tumor tissue was photographed at magnification ×100 under the Nikon Eclipse TS100 microscope and blood vessels stained with anti-CD31 antibody were counted per field for the quantification of tumor angiogenesis. The lumen sizes of the blood vessels were also quantified using the Zen image analysis tool (Carl Zeiss).

Statistical analysis

Statistical analysis of the data was performed using Graph-Pad Prism version 5.0. Statistical significance, determined by the two-tailed Student t test (between two groups) and twotailed single sample t test (test group vs. hypothetical control value), is indicated throughout by the following: *, $P \leq 0.05$

and **, $P \leq 0.01$.

3.4 Results

Racemic itraconazole and its stereoisomers inhibited HUVEC proliferation with different potencies

Racemic itraconazole and each of the four purified cis-stereoisomers were tested for HUVEC proliferation by measuring the ability of the cells to incorporate [3H]-thymidine into DNA. Itraconazole dose-dependently inhibited the thymidine incorporation of HUVEC with an IC_{50} value of 137 nmol/L **(Table 3.1)**. Under the same assay conditions, the 2S4R stereoisomers, including IT-A and IT-C, showed more potent inhibition against HUVEC proliferation compared with itraconazole with IC_{50} values of 103 and 98 nmol/L, respectively. However, the 2R4S stereoisomers including IT-B and IT-D were less potent than itraconazole with IC_{50} values of 223 and 199 nmol/L, respectively. Collectively, 2S4R stereoisomers were roughly two times more potent than 2R4S stereoisomers in HUVEC proliferation. A one-to-one combination of IT-A and IT-C or IT-B and IT-D showed no synergy in HUVEC proliferation, suggesting that they might share the same mechanism of action to inhibit HUVEC proliferation **(Table 3.1)**.

Table 3.1 Chemical structures of itraconazole *cis*-stereoisomers and their antiproliferative activities against HUVEC

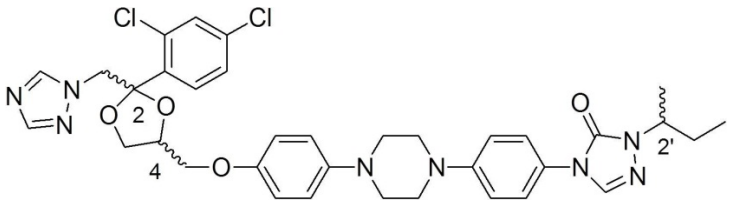

Compound	Stereochemistry	IC_{50} (nmol/L)	95% CI (nmol/L)	Inhibitory index*	$P^{\#}$
Itraconazole	Racemic	137.8	127.6 to 148.9	1	-
IT-A	2S4R2'R	103.6	91.3 to 117.5	0.75	0.042
IT-B	2R4S2'R	223.1	199.4 to 249.6	1.62	0.001
IT-C	2S4R2'S	98.3	86.8 to 111.4	0.71	0.003
IT-D	2R4S2'S	199.5	182.6 to 218.0	1.45	0.005
IT-A + IT-C (1:1)		101.2	91.4 to 112.0	0.73	0.013
IT-B + IT-D (1:1)		211.0	187.4 to 237.5	1.53	0.009

Mean IC_{50} values and their 95% confidence intervals (CI) from 4 independent experiments are shown. *Inhibitory index represents the ratio of IC_{50} of stereoisomers or mixtures to racemic itraconazole. $^{\#}P$ values of IC_{50}s for stereoisomers vs racemic itraconazole.

Itraconazole stereoisomers inhibited VEGFR2 glycosylation, mTOR activity, and cholesterol trafficking in HUVEC

We next determined whether all stereoisomers still share a common mechanism of action to inhibit endothelial cell proliferation by assessing three previously identified activities of itraconazole, that is, inhibition of VEGFR2 glycosylation, mTOR, and cholesterol trafficking (NPC phenotype). Itraconazole inhibited VEGFR2 glycosylation in HUVEC as evidenced by the dose-dependent shift of high-molecular weight, hyperglycosylated form of VEGFR2 to the low-molecular weight, hypo-glycosylated form. All four stereoisomers inhibited VEGFR2 glycosylation with slight different potencies. All four stereoisomers as well as racemic itraconazole dose-dependently inhibited mTOR activity as measured by S6 kinase (S6K) phosphorylation, a downstream target of mTOR. It was apparent that IT-A and IT-C (2S4R series) were more potent than IT-B and IT-D (2R4S series) for the inhibition of VEGFR2 glycosylation and mTOR activity **(Figure 3.1 a)**.

Next, we determined the effects of itraconazole and the stereoisomers on cholesterol trafficking in HUVEC. Cellular cholesterol was fluorescently labeled by filipin and the cholesterol distribution was observed under a confocal microscope. HUVEC were treated with either vehicle (DMSO) or 50 nmol/L of itraconazole or stereoisomers. The concentration of 50 nmol/L that we used here was the lowest concentration of itraconazole that is sufficient to induce an NPC phenotype. At this concentration, IT-A and IT-C as well as itraconazole showed an NPC phenotype as judged by the accumulation of cholesterol fluorescence in the perinuclear region of HUVEC. However, IT-B and IT-D failed to show NPC phenotype at this concentration

(Figure 3.1 b). Thus, for inhibition of cholesterol trafficking, mTOR activity and VEGFR2 glycosylation, 2S4R series were more potent than 2R4S series, which correlated with the relative potency of the stereoisomers against HUVEC proliferation.

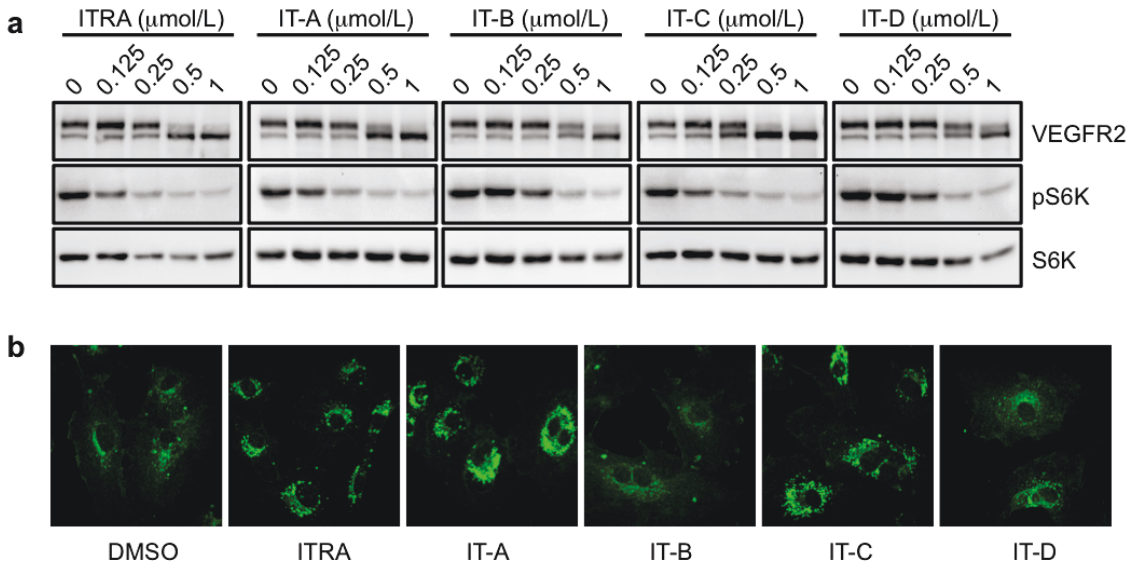

Figure 3.1: Itraconazole and stereoisomers inhibit VEGFR2 glycosylation, mTOR activity and cholesterol trafficking.

(a) HUVEC were treated with itraconazole (ITRA) and its stereoisomers at various concentrations (0, 0.125, 0.25, 0.5, and 1 mmol/L) for 24 hours. Whole-cell lysates were subjected to western blot analysis using antibodies specific for VEGFR2, phospho-S6K (pS6K), and total S6K. In the VEGFR2 Western blots, the top and the bottom bands correspond to hyperglycosylated and hypoglycosylated forms, respectively. **(b)** HUVEC were treated with 50 nmol/L of itraconazole and stereoisomers for 24 hours. The cells were stained with filipin and the fluorescent images were captured under a confocal microscope.

Inhibition of angiogenesis by itraconazole stereoisomers is dependent on cholesterol

We next used an in vitro tube formation assay to assess the activity of the stereoisomers. Upon seeding on top of solidified Matrigel, individual endothelial cells migrate and elongate to form tubule-like networks, reminiscent of new blood vessel formation. Treatment of HUVEC with 3 mmol/L itraconazole, IT-A and IT-C strongly inhibited HUVEC tube formation **(Figure 3.2)**. However, treatment with IT-B and IT-D showed little or no inhibition of HUVEC tube formation at the same concentration **(Figure 3.2)**, again demonstrating that IT-A and IT-C are more potent than the other two stereoisomers.

To see whether the compounds are able to inhibit pre-formed tubes of HUVEC, itraconazole and stereoisomers were added 6 hours after cell seeding on Matrigel and the incubation was continued for an additional 18 hours. At a higher concentration (6 mmol/L), itraconazole and the two potent stereoisomers (IT-A and IT-C) significantly inhibited the pre-formed tubes of HUVEC, again verifying that IT-A and IT-C are more potent anti angiogenic agents than IT-B and IT-D **(Figure 3.3)**.

As the antiproliferative activity of itraconazole was shown to be dependent on cholesterol trafficking (*20*), we conducted a rescue experiment of angiogenesis inhibition by itraconazole and stereoisomers with LDL. Treatment of HUVEC with LDL slightly enhanced the tube formation of HUVEC. When HUVEC was treated with itraconazole or stereoisomers together with LDL, the inhibition of tube formation formation was completely reversed to the control level **(Figure 3.4 a and b)**. Furthermore, inhibition of VEGFR2 glycosylation by itraconazole or stereoisomers was also completely reversed by LDL **(Figure 3.4 c and d)**. These results indicated that, similar to itraconazole, the

antiangiogenic activity of the different stereoisomers is dependent on their ability to inhibit cholesterol trafficking.

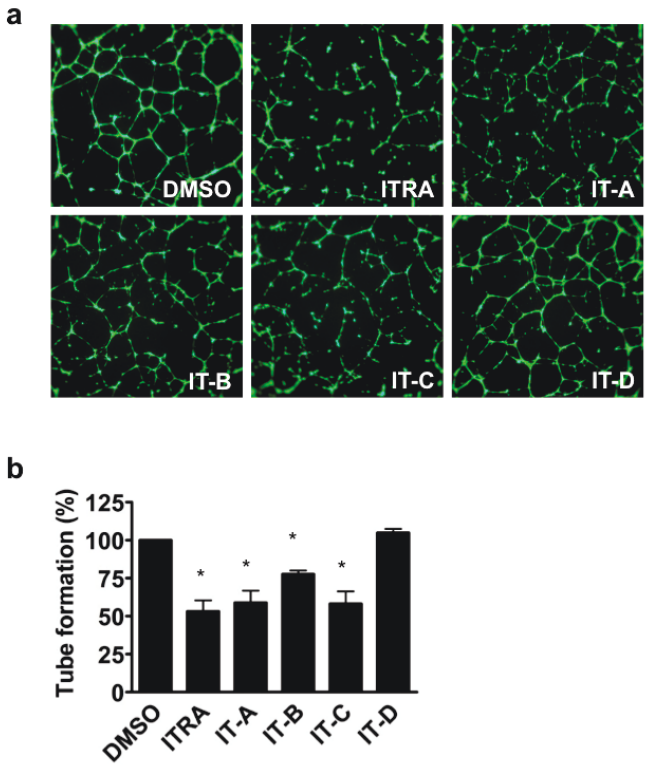

Figure 3.2: Effect of itraconazole and its stereoisomers on HUVEC tube formation.

(a) HUVEC were seeded on Matrigel and treated with itraconazole and stereoisomers at the concentration of 3 μmol/L for 16 hours. Cells were then stained with Calcein-AM and the tube formation was observed under a fluorescent microscope. **(b)** Total tube length, size and number of junctions from the fluorescence images were quantified using the AngioQuant software and plotted using the Graphpad prism. Data represent the mean ± SE of three independent experiments. *, $P \leq 0.05$ for the drug versus DMSO control (two-tailed Single Sample t-test).

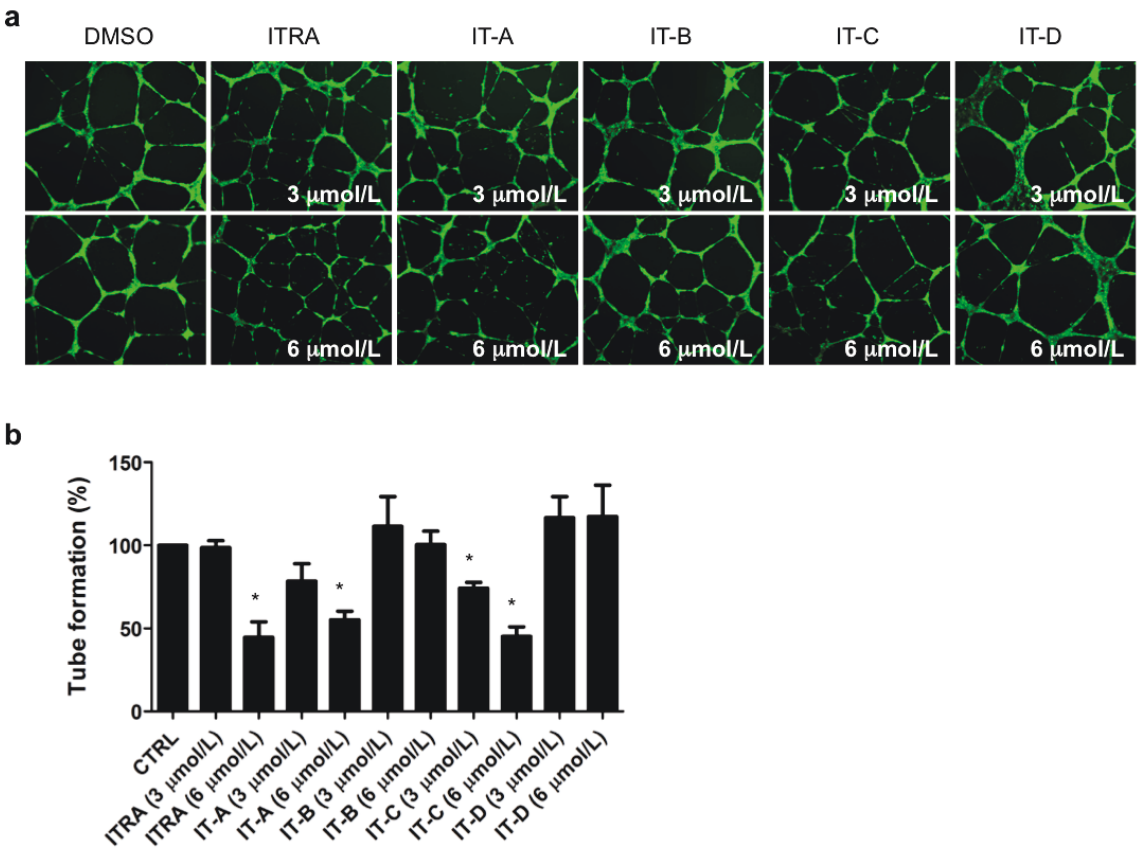

Figure 3.3: Effect of itraconazole and its stereoisomers on pre-formed HUVEC tube formation.

(a) HUVEC were seeded on Matrigel and allowed for tube formation for 6 hours. The pre-formed tubes were then treated with itraconazole and stereoisomers at the concentration of 3 and 6 µmol/L and incubated for additional 18 hours. Cells were then stained with Calcein-AM and the tube formation was observed under a fluorescent microscope. **(b)** Average tube length, size and number of junctions from the fluorescence images were quantified using the AngioQuant software and plotted using the Graphpad prism. Data represent the mean ± SE of three independent experiments. *, $P \leq 0.05$ for the drug versus DMSO control (two-tailed Single Sample t-test).

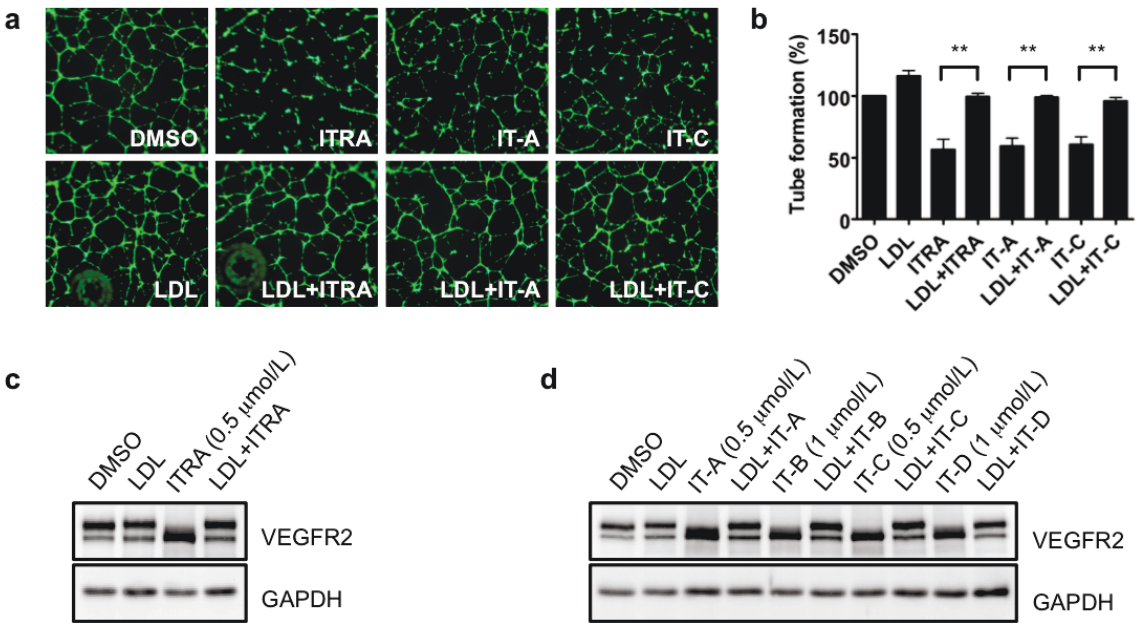

Figure 3.4: LDL rescued angiogenesis inhibition by itraconazole and stereoisomers.

(a) HUVEC were seeded on Matrigel and treated with itraconazole and stereoisomers at the concentration of 3 mmol/L and LDL (50 mg/mL) for 16 hours. Cells were then stained with Calcein-AM and the tube formation was observed under a fluorescent microscope. **(b)** Total tube lengths, sizes and number of junctions from the fluorescence images were quantified using the AngioQuant software and plotted using GraphPad Prism. Data, mean ± SE of three independent experiments. **, $P \leq 0.01$ for drug alone versus drug + LDL. **(c)** and **(d)**, HUVEC were treated with indicated concentrations of itraconazole and stereoisomers with or without LDL (50 mg/mL) for 24 hours. Western blot analysis was done using antibodies specific for VEGFR2 and GAPDH as a loading control.

Racemic itraconazole and its stereoisomers inhibited HUVEC-pericyte co-culture tube formation

Pericytes are vascular-supporting cells that interact with endothelial cells and play an important role in initiation of angiogenesis by guiding the endothelial cell sprouting and stabilizing the vessels (*31*). Therefore, pericytes, together with endothelial cells, have been recognized as a putative target in cancer treatment (*32*). To examine the effects of racemic itraconazole and its stereoisomers on pericyte angiogenesis, we performed pericyte alone and pericyte-HUVEC co-culture tube formation experiments. Under our experimental conditions, and as shown in other reports, pericytes alone could not form tubular networks on Matrigel. We therefore used HUVEC-pericyte co-culture tube formation at a ratio of 30:1 of HUVEC and pericytes, respectively. At a concentration of 3 mmol/L, racemic itraconazole, IT-A and IT-C significantly inhibited pericyte tube networks as well as overall co-culture tube formation on Matrigel **(Figure 3.5)**. In contrast, IT-B and IT-D showed negligible effects on co-culture tube formation. These results indicated that racemic itraconazole and the two stereoisomers IT-A and IT-C inhibited angiogenesis in the presence of pericytes.

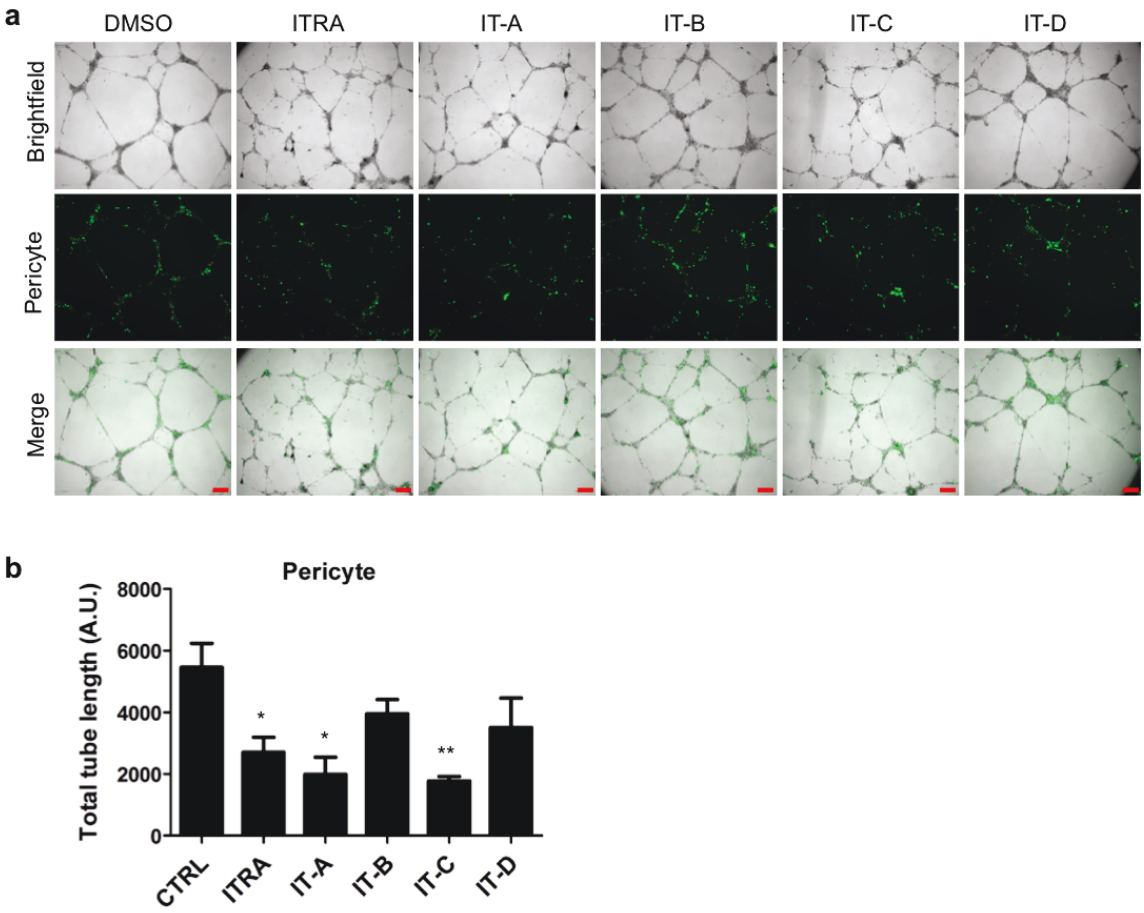

Figure 3.5: Itraconazole and stereoisomers inhibit the tube formation of HUVEC-pericyte co-culture.

(a) Pericytes were labeled with Calcein-AM for 30 minutes before being harvested for tube formation. HUVEC and pericyte mixture (30:1 ratio) were treated with compounds at 3 mmol/L, seeded on Matrigel and allowed to form tube networks for 20 hours. Total cells (HUVEC and pericytes) are shown in the brightfield images and pericytes are shown in the green fluorescent images; scale bar, 200 μm. **(b)** total tube length from the green fluorescence images were quantified as the pericyte tube formation using the AngioQuant software and plotted using Graphpad Prism. Data, mean ± SE of three independent experiments. *, $P \leq 0.05$; **, $P \leq 0.01$ for control versus drug.

Itraconazole stereoisomers possess distinct hepatotoxicity profiles

Having shown that the 2S4R pair of itraconazole stereoisomers are more potent than 2R4S pair in all in vitro angiogenesis-related assays, we wondered whether the stereochemistry had a similar influence on the relative hepatotoxicity of the different stereoisomers. Using freshly prepared human primary hepatocytes, we determined three representative markers of hepatotoxicity, including hepatocyte death, intracellular GSH depletion, and alanine transaminase (ALT) release. As expected, incubation with 2 and 10 mmol/L itraconazole increased primary human hepatocyte death 1.6- and 1.8-fold ($P \leq 0.\ 1$), respectively, as compared with vehicle control **(Figure 3.6 a)**. Similarly, itraconazole effects on GSH depletion (76%; $P \leq 0.01$) and ALT levels in the cell culture medium (92.5 IU/L; $P \leq 0.01$) were consistent with the hepatotoxicity **(Figure 3.6 b and c)**. Interestingly, IT-A and IT-B (both have a 2' R stereochemistry) appeared to have slightly higher hepatotoxicity than racemic itraconazole as judged by induction of cell death by 2.2- ($P \leq 0.01$) and 2.0-fold ($P \leq 0.01$), respectively, at a final concentration of 10 mmol/L as well as increases in GSH depletion [70% ($P \leq 0.01$) and 67% ($P \leq 0.01$), respectively] and extracellular ALT levels [117 IU/L ($P \leq 0.01$) and 128 IU/L ($P \leq 0.01$), respectively]. In contrast, ITC and IT-D (both have a 2'S stereochemistry) did not show appreciable hepatotoxicity, as judged by cell death, hepatic GSH levels or the concentration of ALT in the culture medium **(Figure 3.6 a-c)**. These results were quite unexpected as the hepatotoxicity profile is totally different from the antiangiogenic profile of stereoisomers. Thus, the stereochemistry at the C2 and C4 chiral centers of itraconazole appeared to be important for the antiangiogenic activity whereas that of the C2' chiral center influences hepatotoxicity.

We next assessed the hepatotoxicity of the stereoisomers in mice. Female mice were administered with vehicle or itraconazole stereoisomers (60 mg/kg) i.p. once daily for 10 days. After drug treatment, we first determined the ALT levels in the blood samples of the mice, but found no significant change in blood ALT levels from the mice treated with stereoisomers (data not shown). Next, livers from each mouse were isolated and processed for H&E staining. The livers from vehicle or IT-C–treated mice appeared normal, whereas those from IT-A–treated mice showed abnormalities, that is, white colored and quite sticky to surrounding tissues. In comparison, livers in mice treated with itraconazole looked partially abnormal (data not shown). From the H&E staining of the liver sections, we found that IT-A caused severe fatty liver in the mice **(Figure 3.7)**. Mice treated with racemic itraconazole had partial fatty liver, whereas livers from those treated with vehicle or IT-C were normal **(Figure 3.7)**. Once again, IT-C showed less hepatotoxicity in mice than either IT-A or the racemic itraconazole, consistent with the results from human hepatocytes.

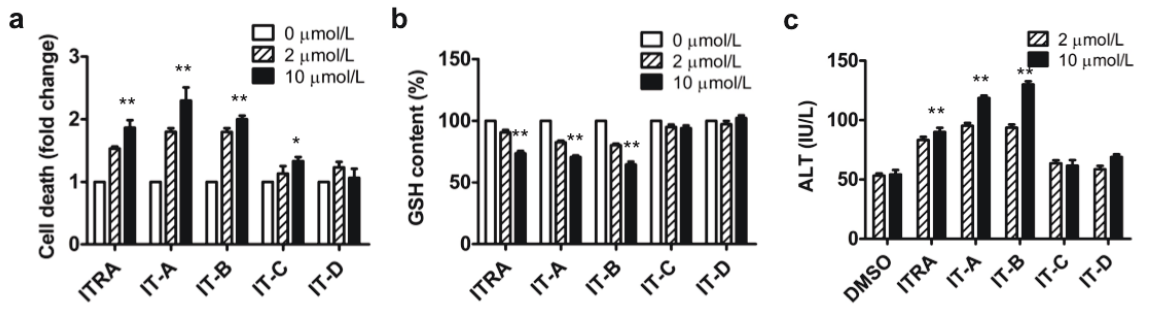

Figure 3.6: Itraconazole and each stereoisomer have distinct hepatotoxicity profiles.

(a) to **(c)** Freshly prepared human primary hepatocyteswere incubated with itraconazole and stereoisomers at the indicated concentrations for 72 hours. Cell viability of the hepatocytes (a), intracellular glutathione levels from the hepatocyte lysates (b), and the alanine aminotransaminase (ALT) levels from the hepatocyte culture media (c) were measured as described in the Materials and Methods. *, $P \leq 0.05$; **, $P \leq 0.01$ for 10 mmol/L versus 0 mmol/L (for a and b, two-tailed single sample t test). **, $P \leq 0.01$ for drug versus DMSO control (for c, two-tailed Student t test).

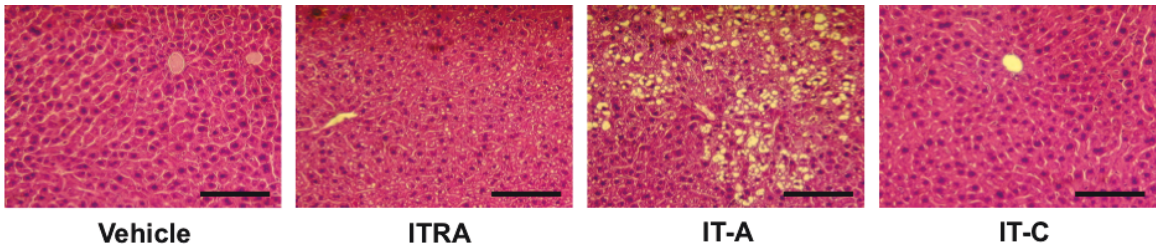

Figure 3.7: Itraconazole and each stereoisomer have distinct hepatotoxicity.

Female BALB/cAnNCr mice were treated i.p. with itraconazole and stereoisomers at the dosage of 60 mg/kg for 10 days. Livers from each mouse were isolated and processed for H&E staining. Representative images from five mice per group are shown; scale bar, 100 μm.

IT-C inhibited angiogenesis *in vivo*

We next determined and compared the in vivo antiangiogenic activity of IT-A and IT-C along with racemic itraconazole as a control. We excluded the 2R4S series (IT-B and IT-D) from these experiments because they had lower antiangiogenic activity than 2S4R series. Female mice were pre-treated with IT-A, ITC, or itraconazole at the doses of 20 and 50 mg/kg for each compound for 2 days. The mice were then implanted subcutaneously with Matrigel plugs containing angiogenic factors, including bFGF and VEGF. Treatment with vehicle or compounds was continued once daily for additional 8 days. Mice were sacrificed and Matrigel plugs were isolated from the mice for the immunohistologic analysis of blood vessel infiltration into the Matrigel using anti-CD31 (endothelial cell marker) and anti-NG2 (pericyte marker) antibodies. In addition to the antibody staining, entire population of cells infiltrated into the Matrigel plugs was analyzed using Masson's trichrome staining **(Figure 3.8)**. Compared with the vehicle control, itraconazole inhibited the number of CD31-positive blood vessels infiltrated into the Matrigel by 19% and 46% at the dosage of 20 and 50mg/kg, respectively **(Figure 3.9 a and b)**. IT-A also inhibited the CD31-positive blood vessels by 19% and 48%. IT-C showed more significant inhibition on CD31-positive Matrigel angiogenesis, with 41%and 60% inhibition at 20 and 50 mg/kg, respectively **(Figure 3.9 a and b)**. Similar results were observed in NG2-positive pericyte staining. IT-C exhibited the strongest inhibition on the infiltration and vessel formation by NG2-positive pericytes, with 47% and 70% inhibition at 20 and 50 mg/kg, respectively **(Figure 3.9 c and d)**. These results suggested that IT-C is more active than IT-A for the antiangiogenic activity.

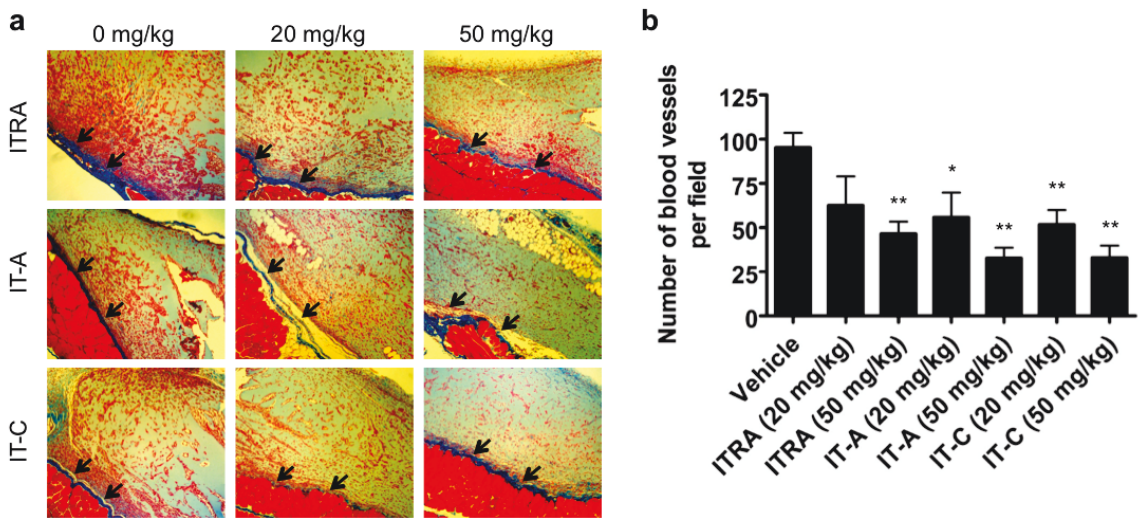

Figure 3.8: Effect of itraconazole and the 2S4R series of stereoisomers on in vivo Matrigel angiogenesis in mice.

(a) Female BALB/cAnNCr mice with Matrigel implantation were treated i.p. with itraconazole, IT-A and IT-C at dosages of 20 and 50 mg/kg for total of 10 days (2-day pre-treatment and 8-day post-treatment of Matrigel implantation). Matrigel plugs with mouse inner skin were isolated and processed for Masson trichrome staining which stains Matrigel blue and the endothelial cells and vessels red. Representative Matrigel images from 5 mice per group are shown. Arrows indicate mouse inner skin (a layer of dark blue color) where blood vessels begin to penetrate into the Matrigel. **(b)** The number of erythrocyte-containing blood vessels were counted from photos taken under a bright-field microscope and plotted using Graphpad Prism. Data represent mean ± SE of four independent Matrigel images per group. *, $P \leq 0.05$; **, $P \leq 0.01$ for each drug versus vehicle control.

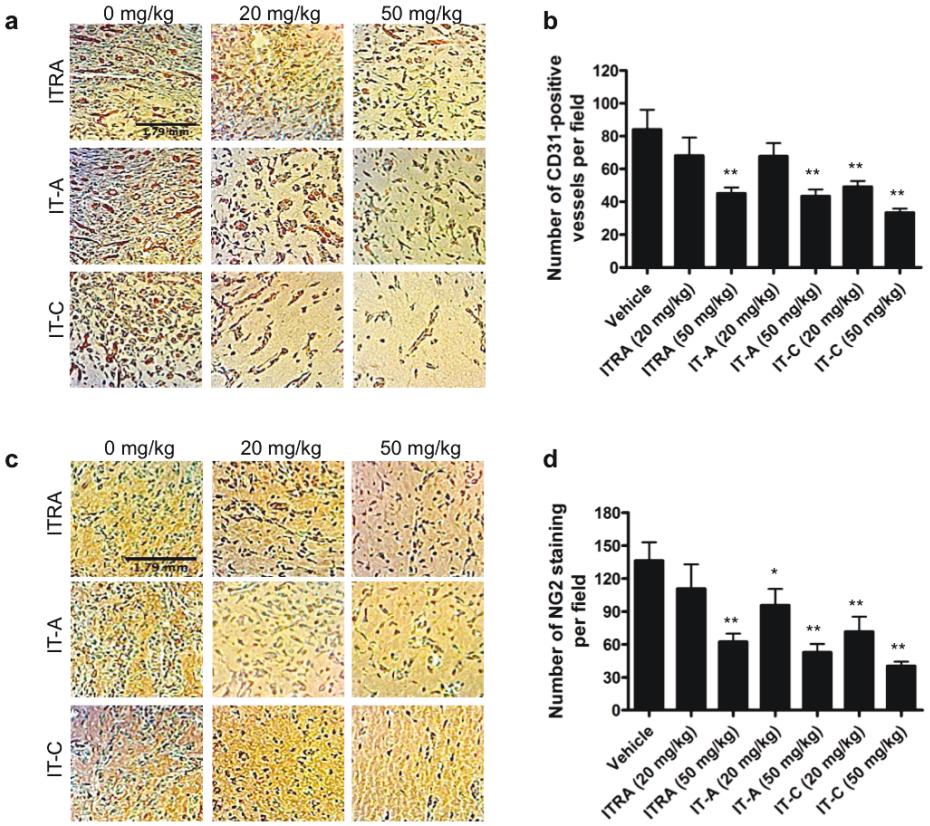

Figure 3.9: Itraconazole and the 2S4R series of stereoisomers inhibit Matrigel angiogenesis in vivo.

(a) and **(c)** Female BALB/cAnNCr mice with Matrigel implantationwere treated i.p. with itraconazole, IT-A and IT-C at dosages of 20 and 50 mg/kg for total of 10 days (2-day pre-treatment and 8-day post-treatment of Matrigel implantation). Matrigel plugs with mouse inner skin were isolated and processed for immunohistochemical (IHC) staining of CD31 (endothelial cell marker) and NG2

(pericyte marker). Representative IHC images of CD31 staining (a) and NG2 staining (c) are shown. **(b)** and **(d)** The number of CD31-positive vessels (b) and NG2-positive cells (d) were counted from the IHC samples and plotted using Graphpad Prism. Data, mean ± SE of three independent IHC samples per group. *, $P \leq 0.05$; **, $P \leq 0.01$ for each drug versus vehicle control; scale bar, 1.79 mm.

IT-C inhibited tumor growth and tumor-induced angiogenesis in mice

Taking into consideration both the antiangiogenic activity and hepatotoxicity, IT-C was deemed superior to all other stereoisomers due to a combination of its higher antiangiogenic potency and lack of hepatotoxicity in both human cells and mice. We thus assessed the antitumor activity of IT-C in two tumor xenograft models (breast cancer and prostate cancer) in parallel with racemic itraconazole. We also took the opportunity to determine the effect of IT-C on tumor-induced angiogenesis. For the breast cancer xenograft model, female athymic nude mice bearing HCC1954 cells were treated i.p. with vehicle, itraconazole, or IT-C at 25 and 50 mg/kg for each compound, once daily, for 30 days. Racemic itraconazole at 50 mg/kg significantly inhibited the growth of HCC1954 xenografts compared with the vehicle alone **(Figure 3.10 a)**. Tumor volume was reduced by 40% at day 28 of treatment with 50 mg/kg itraconazole compared with the vehicle control. Importantly, IT-C showed more pronounced inhibition of the tumor xenograft growth than itraconazole at both 25 and 50 mg/kg **(Figure 3.10 b)**. It inhibited the tumor volume by 53% at day 28 at 50 mg/kg. There were no apparent toxicities associated with itraconazole or IT-C based on assessment of mouse body weight **(Figure 3.10 c)**. Similar results were observed in the CWR22Rv1 prostate cancer xenograft model. Treatment of male athymic nude mice with either itraconazole (60 mg/kg) or IT-C (60 mg/kg) significantly inhibited the tumor growth **(Figure 3.10 d and e)**. To assess tumor-associated angiogenesis in the breast cancer xenografts, the tumor tissues were harvested from the mice and processed for immunohistochemical analysis of CD31, a blood vessel marker. Compared with the vehicle, both racemic itraconazole and

IT-C significantly inhibited angiogenesis in the HCC1954 xenografts **(Figure 3.11)**, with IT-C being more potent than itraconazole.

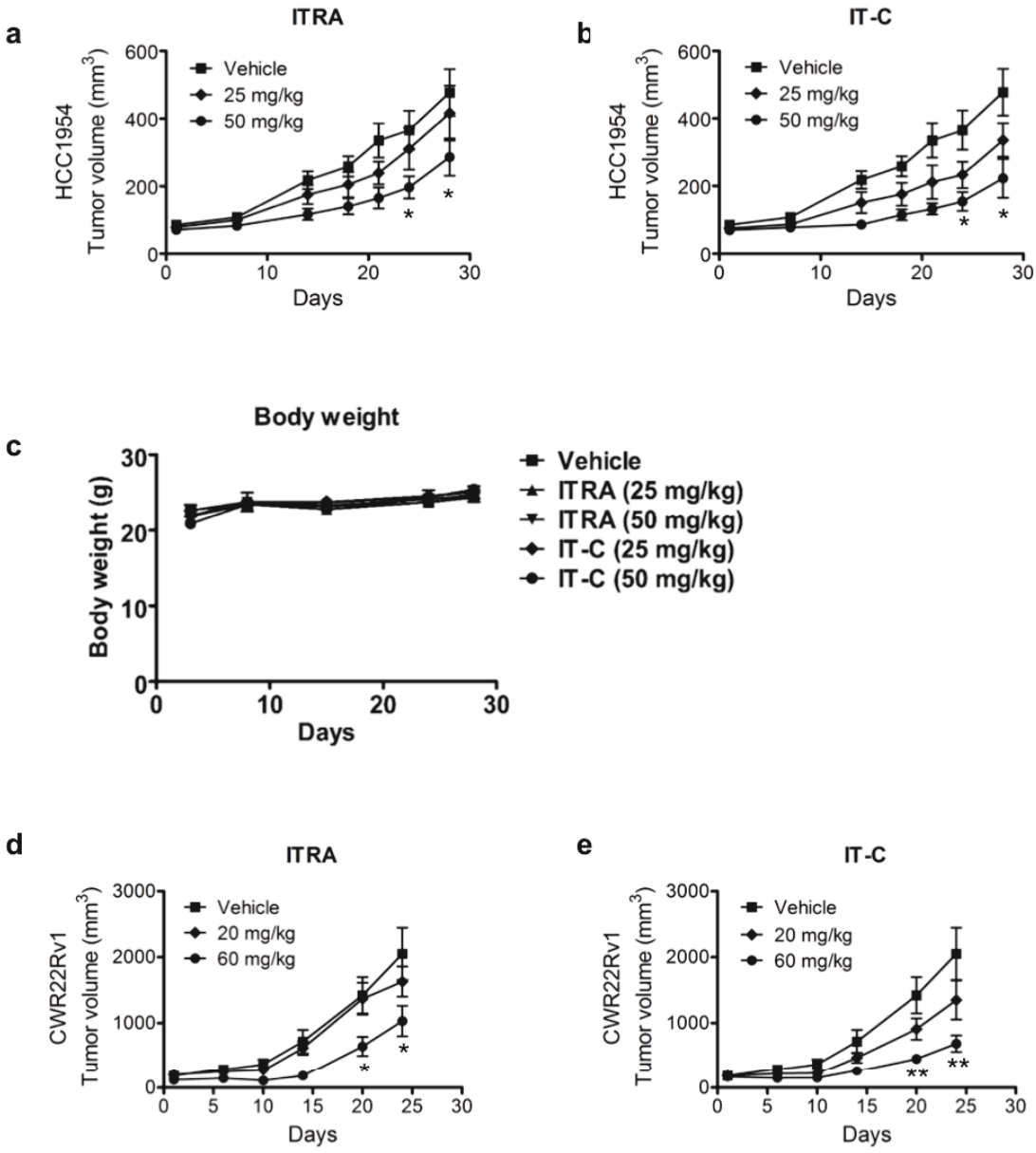

Figure 3.10: Itraconazole and IT-C inhibit the tumor growth *in vivo*.

(a) and **(b)** Female athymic nude mice (BALB/c, nu/nu-NCr) bearing HCC1954 human breast cancer cells were treated with itraconazole (ITRA, a) or IT-C (b) for 30 days. **(c)** Female athymic nude mice bearing breast cancer xenograft were given indicated drugs daily for 30 days and the body weight was measured periodically. **(d)** and **(e)** Male athymic nude mice (BALB/c, nu/nu-NCr) bearing CWR22Rv1 human prostate cancer

cells were treated with itraconazole (ITRA, d) or IT-C (e) for 24 days. Tumor volume was measured periodically by a vernier caliper and plotted using GraphPad prism. Data, mean ± SE of tumor volumes in each group (n = 6-7mice). *, $P \leq 0.05$; **, $P \leq 0.01$ for the drug versus vehicle control at each time point.

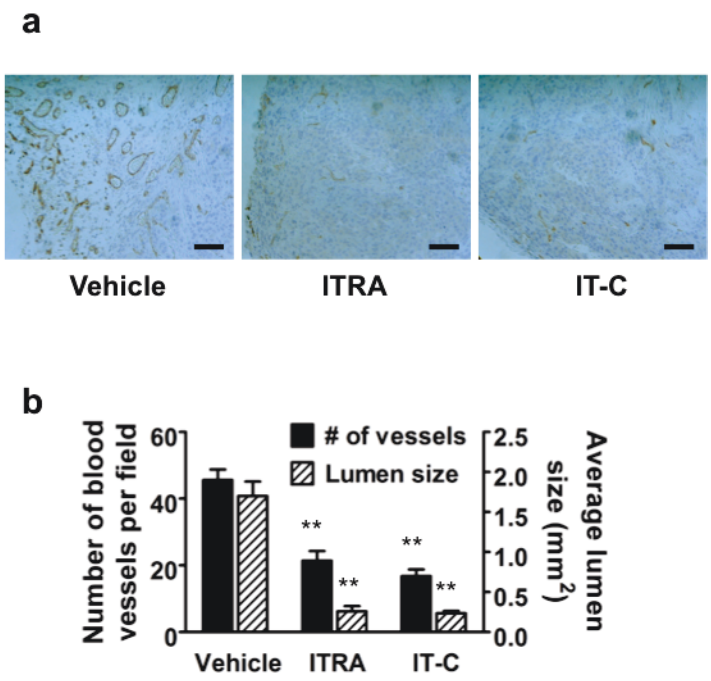

Figure 3.11: Itraconazole and IT-C inhibit the angiogenesis *in vivo*.

(a) HCC1954 tumor xenograft tissues were processed for immunohistochemical (IHC) staining of a blood vessel marker, CD31. Representative images of CD31 staining of tumor sections from each group are shown; scale bar, 100 mm. **(b)** The number of CD31-positive blood vessels were counted from photos taken under a bright-field microscope and plotted using GraphPad Prism. The lumen size of blood vessels were measured using the Zen image analysis tool. Data, mean ± SE of the number and the lumen size of blood vessels from the IHC images (n = 5/group). **, $P \leq 0.01$ for each drug versus vehicle control.

3.5 Discussion

Although itraconazole has been widely used to treat fungal infections, several adverse effects have been reported. The most frequent side effects associated with itraconazole are gastrointestinal complaints including nausea, vomiting, diarrhea, flatulence and constipation (*33*). Fortunately, these adverse effects are mostly transient and mild, and thus are tolerable to patients (*34*). However, rare but severe hepatoxicity associated with itraconazole has also been reported. Up to 7% of patients receiving itraconazole have elevated ALT levels (*22*). Moreover, fatalities due to hepatic failure have been reported in patients receiving itraconazole (*35*). Major efforts have been made to overcome the adverse effects of itraconazole on the liver. A pulse therapy of itraconazole (typically, 400mgitraconazole twice daily for 1 week followed by a three-weeks holiday) was introduced in superficial fungal infections based on the pharmacokinetic (PK) properties of itraconazole (*36*). Upon cessation of drug intake, itraconazole is rapidly cleared from systemic circulation (7–10 days), but persists for 3 to 4 weeks in the stratum corneum and for up to 6 to 12 months in the nail (*37*). This PK property of itraconazole makes pulse therapy for onychomycosis and dermatomycoses possible, which could significantly reduce the hepatotoxicityrelated adverse effects while showing therapeutic efficacies similar to continuous therapy (*38*). However, this strategy may not be applicable for the cancer therapy, which requires a high dose of itraconazole in systemic circulation. Thus, the hepatotoxicity associated with itraconazole still poses a significant challenge for the long-term, high-dose treatment of cancer patients with itraconazole.

Hepatotoxicity associated with itraconazole has long been recognized, but the mechanism underlying the liver toxicity of itraconazole has remained obscure. Cytochrome P450, specifically CYP3A4, is a main liver enzyme responsible for the metabolism of itraconazole (*39*). Itraconazole also inhibits the enzyme activity of CYP3A4 (*24*). When rats were pretreated with phenobarbital, an inducer of cytochrome P450, hepatotoxicity induced by itraconazole was significantly reduced (*25, 34*). On the other hand, pretreatment of rats with SKF 525A, an inhibitor of cytochrome P450, significantly enhanced itraconazole-induced hepatoxicity (*25*). These results suggest that inhibition of cytochrome P450, probably CYP3A4, by itraconazole is, at least in part, responsible for itraconazoleinduced hepatotoxicity. Commercial itraconazole currently used in the clinic is a racemic mixture of four cis-stereoisomers. It is interesting to note that CYP3A4 metabolizes itraconazole in a stereoselective manner. Only IT-B and IT-D are metabolized by CYP3A4 among the four stereoisomers. Although all four stereoisomers are strong binders and inhibitors of CYP3A4, IT-B, and IT-D have 2- to 4-fold stronger binding affinity for CYP3A4 and 2- to 4-fold lower IC50 values for inhibition of the enzymatic activity of CYP3A4 in comparison with IT-A and IT-C (*26*). In the present study, we confirmed that IT-A and IT-C were more potent inhibitors of angiogenesis than IT-B and IT-D. In contrast, IT-A and IT-B were much more hepatotoxic than IT-C and IT-D both in mice and in human hepatocytes. These results suggest that inhibition of CYP3A4 by itraconazole or metabolism of itraconazole by CYP3A4 may not be solely responsible for its hepatotoxicity. One interesting possibility is that a cytochrome P450 enzyme with specificity for the C20 chiral center of itraconazole could be the main enzyme mediating the hepatotoxicity of itraconazole. In

addition, the segregation of antiangiogenic activity and hepatotoxicity of the four stereoisomers of itraconazole suggests that the cellular target protein(s) responsible for angiogenesis inhibition and hepatotoxicity might be different. Answers to these questions may become clear upon identification of the molecular targets mediating the different effects of itraconazole.

Although itraconazole was shown to elevate serum ALT levels in rats, it did not increase the levels in mice in this study. Instead, itraconazole and IT-A induced moderate to severe fatty liver in mice. Rats and mice have shown different hepatotoxicity responses to certain compounds, such as coumarin (*40*). Interstrain differences of hepatotoxicity responses have also been observed in mice treated with cocaine and phenobarbital (*41*). This is thought to be due to the different liver metabolic enzymes present in different strains and animal species. Itraconazole has shown similar hepatotoxicity profiles in humans and rats, suggesting that they respond similarly to this compound. In mice, the compound did not show ALT elevation, but induced fatty liver, suggesting that racemic itraconazole and IT-A still have negative impact on mice liver but in a way different from rats or humans. However, IT-C at doses up to 60 mg/kg did not cause apparent adverse effects on the mouse liver. In the experiments using human primary hepatocytes, ITC showed no apparent signs of hepatotoxicity at concentrations up to 10 mmol/L for all three hepatotoxicity markers. In contrast, IT-A was strongly hepatotoxic and racemic itraconazole showed a medium degree of hepatotoxicity. Together, these results points to IT-C as the most promising candidate for future clinical development with improved potency and decreased hepatotoxicity in comparison with racemic itraconazole.

That the C20 stereochemistry has a major influence on the hepatotoxicity of itraconazole should also facilitate the development of next generations of itraconazole analogs as new leads of antiangiogenic and anticancer drugs.

Several antiangiogenic agents, such as sunitinib and sorafenib, have successfully entered into the clinic as targeted cancer therapies. Although these agents have dramatically changed the management of cancer in patients these days, many clinical challenges still remain, including the huge financial burden to patients and the emergence of drug resistance that occurs with most of the kinase inhibitor drugs. Development of new antiangiogenic and anticancer agents from existing non-cancer drugs (the drug repositioning strategy) offers the possibility of reducing the financial burden to patients (*42*). In addition, this approach can also diversify molecular targets as exemplified with itraconazole, which is not a kinase inhibitor. Development of agents with diverse molecular targets provides better opportunities to find drug combinations with standard chemotherapy or current targeted drugs to reduce the emergence of cancer drug resistance. As evidenced from recent clinical investigations, itraconazole has shown positive clinical outcome in patients with non–small cell lung cancer, metastatic prostate cancer, and basal cell carcinoma. It also showed prolonged survival in patients with late-stage ovarian, triple-negative breast, and metastatic pancreatic cancer. IT-C, as an equipotent isomer of itraconazole with reduced hepatotoxicity, will have a wider range of therapeutic window than racemic itraconazole, and thus is a promising lead for future development as an antiangiogenic and anticancer drug.

3.6 References

1. N. Ashton, Retinal angiogenesis in the human embryo. *British medical bulletin* **26**, 103-106 (1970)
2. P. R. Colville-Nash, D. L. Scott, Angiogenesis and rheumatoid arthritis: pathogenic and therapeutic implications. *Annals of the rheumatic diseases* **51**, 919-925 (1992)
3. J. Folkman, E. Merler, C. Abernathy, G. Williams, Isolation of a tumor factor responsible for angiogenesis. *The Journal of experimental medicine* **133**, 275-288 (1971)
4. J. Folkman, Tumor angiogenesis: therapeutic implications. *The New England journal of medicine* **285**, 1182-1186 (1971)
5. J. Folkman, R. Langer, R. J. Linhardt, C. Haudenschild, S. Taylor, Angiogenesis inhibition and tumor regression caused by heparin or a heparin fragment in the presence of cortisone. *Science* **221**, 719-725 (1983)
6. D. Ingber, T. Fujita, S. Kishimoto, K. Sudo, T. Kanamaru, H. Brem, J. Folkman, Synthetic analogues of fumagillin that inhibit angiogenesis and suppress tumour growth. *Nature* **348**, 555-557 (1990)
7. P. Twardowski, W. J. Gradishar, Clinical trials of antiangiogenic agents. *Current opinion in oncology* **9**, 584-589 (1997)
8. J. M. Llovet, S. Ricci, V. Mazzaferro, P. Hilgard, E. Gane, J. F. Blanc, A. C. de Oliveira, A. Santoro, J. L. Raoul, A. Forner, M. Schwartz, C. Porta, S. Zeuzem, L. Bolondi, T. F. Greten, P. R. Galle, J. F. Seitz, I. Borbath, D. Haussinger, T. Giannaris, M. Shan, M. Moscovici, D. Voliotis, J. Bruix, S. I. S. Group, Sorafenib

in advanced hepatocellular carcinoma. *The New England journal of medicine* **359**, 378-390 (2008)

9. R. Rajendra, R. L. Jones, S. M. Pollack, Targeted treatment for advanced soft tissue sarcoma: profile of pazopanib. *OncoTargets and therapy* **6**, 217-222 (2013)
10. I. Sakai, H. Miyake, M. Fujisawa, Acquired resistance to sunitinib in human renal cell carcinoma cells is mediated by constitutive activation of signal transduction pathways associated with tumour cell proliferation. *BJU international* **112**, E211-220 (2013)
11. C. R. Chong, J. Xu, J. Lu, S. Bhat, D. J. Sullivan, Jr., J. O. Liu, Inhibition of angiogenesis by the antifungal drug itraconazole. *ACS chemical biology* **2**, 263-270 (2007)
12. J. Kim, J. Y. Tang, R. Gong, J. Kim, J. J. Lee, K. V. Clemons, C. R. Chong, K. S. Chang, M. Fereshteh, D. Gardner, T. Reya, J. O. Liu, E. H. Epstein, D. A. Stevens, P. A. Beachy, Itraconazole, a commonly used antifungal that inhibits Hedgehog pathway activity and cancer growth. *Cancer cell* **17**, 388-399 (2010)
13. B. T. Aftab, I. Dobromilskaya, J. O. Liu, C. M. Rudin, Itraconazole inhibits angiogenesis and tumor growth in non-small cell lung cancer. *Cancer research* **71**, 6764-6772 (2011)
14. E. S. Antonarakis, E. I. Heath, D. C. Smith, D. Rathkopf, A. L. Blackford, D. C. Danila, S. King, A. Frost, A. S. Ajiboye, M. Zhao, J. Mendonca, S. K. Kachhap, M. A. Rudek, M. A. Carducci, Repurposing itraconazole as a treatment for advanced prostate cancer: a noncomparative randomized phase II trial in men

with metastatic castration-resistant prostate cancer. *The oncologist* **18**, 163-173 (2013)

15. D. J. Kim, J. Kim, K. Spaunhurst, J. Montoya, R. Khodosh, K. Chandra, T. Fu, A. Gilliam, M. Molgo, P. A. Beachy, J. Y. Tang, Open-label, exploratory phase II trial of oral itraconazole for the treatment of basal cell carcinoma. *Journal of clinical oncology : official journal of the American Society of Clinical Oncology* **32**, 745-751 (2014)
16. C. M. Rudin, J. R. Brahmer, R. A. Juergens, C. L. Hann, D. S. Ettinger, R. Sebree, R. Smith, B. T. Aftab, P. Huang, J. O. Liu, Phase 2 study of pemetrexed and itraconazole as second-line therapy for metastatic nonsquamous non-small-cell lung cancer. *Journal of thoracic oncology : official publication of the International Association for the Study of Lung Cancer* **8**, 619-623 (2013)
17. H. Tsubamoto, T. Sonoda, K. Inoue, Impact of itraconazole on the survival of heavily pre-treated patients with triple-negative breast cancer. *Anticancer research* **34**, 3839-3844 (2014)
18. H. Tsubamoto, T. Sonoda, M. Yamasaki, K. Inoue, Impact of combination chemotherapy with itraconazole on survival for patients with recurrent or persistent ovarian clear cell carcinoma. *Anticancer research* **34**, 2007-2014 (2014)
19. H. Tsubamoto, T. Sonoda, M. Yamasaki, K. Inoue, Impact of combination chemotherapy with itraconazole on survival of patients with refractory ovarian cancer. *Anticancer research* **34**, 2481-2487 (2014)

20. J. Xu, Y. Dang, Y. R. Ren, J. O. Liu, Cholesterol trafficking is required for mTOR activation in endothelial cells. *Proceedings of the National Academy of Sciences of the United States of America* **107**, 4764-4769 (2010)

21. W. Shi, B. A. Nacev, B. T. Aftab, S. Head, C. M. Rudin, J. O. Liu, Itraconazole side chain analogues: structure-activity relationship studies for inhibition of endothelial cell proliferation, vascular endothelial growth factor receptor 2 (VEGFR2) glycosylation, and hedgehog signaling. *Journal of medicinal chemistry* **54**, 7363-7374 (2011)

22. A. Restrepo, J. Robledo, I. Gomez, A. M. Tabares, R. Gutierrez, Itraconazole therapy in lymphangitic and cutaneous sporotrichosis. *Archives of dermatology* **122**, 413-417 (1986)

23. Y. Yoshida, Y. Aoyama, Interaction of azole antifungal agents with cytochrome P-45014DM purified from Saccharomyces cerevisiae microsomes. *Biochemical pharmacology* **36**, 229-235 (1987)

24. T. Varis, K. T. Kivisto, J. T. Backman, P. J. Neuvonen, The cytochrome P450 3A4 inhibitor itraconazole markedly increases the plasma concentrations of dexamethasone and enhances its adrenal-suppressant effect. *Clinical pharmacology and therapeutics* **68**, 487-494 (2000)

25. N. Somchit, C. W. Wong, A. Zuraini, A. Ahmad Bustamam, A. H. Hasiah, H. M. Khairi, M. R. Sulaiman, D. A. Israf, Involvement of phenobarbital and SKF 525A in the hepatotoxicity of antifungal drugs itraconazole and fluconazole in rats. *Drug and chemical toxicology* **29**, 237-253 (2006)

26. K. L. Kunze, W. L. Nelson, E. D. Kharasch, K. E. Thummel, N. Isoherranen, Stereochemical aspects of itraconazole metabolism in vitro and in vivo. *Drug metabolism and disposition: the biological fate of chemicals* **34**, 583-590 (2006)

27. W. Shi, B. A. Nacev, S. Bhat, J. O. Liu, Impact of Absolute Stereochemistry on the Antiangiogenic and Antifungal Activities of Itraconazole. *ACS medicinal chemistry letters* **1**, 155-159 (2010)

28. J. S. Shim, Y. Matsui, S. Bhat, B. A. Nacev, J. Xu, H. E. Bhang, S. Dhara, K. C. Han, C. R. Chong, M. G. Pomper, A. So, J. O. Liu, Effect of nitroxoline on angiogenesis and growth of human bladder cancer. *Journal of the National Cancer Institute* **102**, 1855-1873 (2010)

29. N. N. Bumpus, Efavirenz and 8-hydroxyefavirenz induce cell death via a JNK- and BimEL-dependent mechanism in primary human hepatocytes. *Toxicology and applied pharmacology* **257**, 227-234 (2011)

30. W. Chen, Y. Zhao, T. Seefeldt, X. Guan, Determination of thiols and disulfides via HPLC quantification of 5-thio-2-nitrobenzoic acid. *Journal of pharmaceutical and biomedical analysis* **48**, 1375-1380 (2008)

31. D. Ribatti, B. Nico, E. Crivellato, The role of pericytes in angiogenesis. *The International journal of developmental biology* **55**, 261-268 (2011).

32. G. Bergers, S. Song, N. Meyer-Morse, E. Bergsland, D. Hanahan, Benefits of targeting both pericytes and endothelial cells in the tumor vasculature with kinase inhibitors. *The Journal of clinical investigation* **111**, 1287-1295 (2003)

33. R. M. Tucker, Y. Haq, D. W. Denning, D. A. Stevens, Adverse events associated with itraconazole in 189 patients on chronic therapy. *The Journal of antimicrobial chemotherapy* **26**, 561-566 (1990)

34. N. Somchit, A. R. Norshahida, A. H. Hasiah, A. Zuraini, M. R. Sulaiman, M. M. Noordin, Hepatotoxicity induced by antifungal drugs itraconazole and fluconazole in rats: a comparative in vivo study. *Human & experimental toxicology* **23**, 519-525 (2004)

35. C. M. van der Horst, M. S. Saag, G. A. Cloud, R. J. Hamill, J. R. Graybill, J. D. Sobel, P. C. Johnson, C. U. Tuazon, T. Kerkering, B. L. Moskovitz, W. G. Powderly, W. E. Dismukes, Treatment of cryptococcal meningitis associated with the acquired immunodeficiency syndrome. National Institute of Allergy and Infectious Diseases Mycoses Study Group and AIDS Clinical Trials Group. *The New England journal of medicine* **337**, 15-21 (1997)

36. J. Heykants, A. Van Peer, V. Van de Velde, P. Van Rooy, W. Meuldermans, K. Lavrijsen, R. Woestenborghs, J. Van Cutsem, G. Cauwenbergh, The clinical pharmacokinetics of itraconazole: an overview. *Mycoses* **32 Suppl 1**, 67-87 (1989).

37. A. K. Gupta, R. K. Scher, P. De Doncker, Current management of onychomycosis. An overview. *Dermatologic clinics* **15**, 121-135 (1997)

38. A. Gupta, J. Lambert, J. Revuz, N. Shear, Update on the safety of itraconazole pulse therapy in onychomycosis and dermatomycoses. *European journal of dermatology : EJD* **11**, 6-10 (2001)

39. C. C. Peng, W. Shi, J. D. Lutz, K. L. Kunze, J. O. Liu, W. L. Nelson, N. Isoherranen, Stereospecific metabolism of itraconazole by CYP3A4: dioxolane ring scission of azole antifungals. *Drug metabolism and disposition: the biological fate of chemicals* **40**, 426-435 (2012)

40. B. G. Lake, P. Grasso, Comparison of the hepatotoxicity of coumarin in the rat, mouse, and Syrian hamster: a dose and time response study. *Fundamental and applied toxicology : official journal of the Society of Toxicology* **34**, 105-117 (1996)

41. C. S. Boyer, D. Ross, D. R. Petersen, Sex and strain differences in the hepatotoxic response to acute cocaine administration in the mouse. *Journal of biochemical toxicology* **3**, 295-307 (1988)

42. A. Saxena, D. Becker, I. Preeshagul, K. Lee, E. Katz, B. Levy, Therapeutic Effects of Repurposed Therapies in Non-Small Cell Lung Cancer: What Is Old Is New Again. *The oncologist* **20**, 934-945 (2015)

Chapter 4: Inhibition of angiogenesis by selective estrogen receptor modulators through blockade of cholesterol trafficking rather than estrogenreceptor antagonism

4.1 Abstract

In Chapter 3, I described a pharmacological study of the itraconazole and its stereoisomers to distinguish their differences in anti-angiogenesis effect and hepatotoxicity. As I mentioned in above chapter, itraconazole and its stereosiomers block membrane and cholesterol trafficking and inhibit angiogenesis and tumor growth. In this chapter, I will describe another pharmacological study to demonstrate the inhibition of angiogenesis by selective estrogen receptor modulators, such as tamoxifen, through blockade of cholesterol trafficking rather than estrogen receptor antagonism. Selective estrogen receptor modulators (SERM) including tamoxifen are known to inhibit angiogenesis. However, the underlying mechanism, which is independent of their action on the estrogen receptor (ER), has remained largely unknown. In the present study, we found that tamoxifen and other SERM inhibited cholesterol trafficking in endothelial cells, causing a hyper-accumulation of cholesterol in late endosomes/lysosomes. Inhibition of cholesterol trafficking by tamoxifen was accompanied by abnormal subcellular distribution of vascular endothelial growth factor receptor-2 (VEGFR2) and inhibition of the terminal glycosylation of the receptor. Tamoxifen also caused perinuclear positioning of lysosomes, which in turn trapped the mammalian target of rapamycin (mTOR) in the perinuclear region of endothelial cells. Abnormal distribution

of VEGFR2 and mTOR and inhibition of VEGFR2 and mTOR activities by tamoxifen were significantly reversed by addition of cholesterol cyclodextrin complex to the culture media of endothelial cells. Moreover, high concentrations of tamoxifen inhibited endothelial and breast cancer cell proliferation in a cholesterol-dependent, but ER-independent, manner. Together, these results unraveled a previously unrecognized mechanism of angiogenesis inhibition by tamoxifen and other SERM, implicating cholesterol trafficking as an attractive therapeutic target for cancer treatment.

ABBREVIATIONS

SERM, selective estrogen receptor modulators; HUVEC, human umbilical vein endothelial cells; mTOR, mechanistic target of rapamycin; GAPDH, glyceraldehyde 3-phosphate dehydrogenase; S6K, ribosomal s6 kinase; ER, estrogen receptor; LDL, low-density lipoprotein; NPC, Niemann-Pick Disease Type C; VEGFR2, vascular endothelial growth factor receptor 2; AIBP, apoA-I binding protein; PDGFRβ, platelet-derived growth factor receptor β; FGFR1, fibroblast growth factor receptor 1; LAMP1, lysosomal associated membrane protein 1; CD, cyclodextrin; TMX, tamoxifen; TRM, toremifene; CLM, clomifene; RLX, raloxifene; TUM, tunicamycin; ITRA, itraconazole.

4.2 Introduction

Tamoxifen and selective estrogen receptor modulators (SERM) have been used to treat hormone responsive, estrogen receptor (ER)-positive breast cancers since the 1980s. It has generally been accepted that the anticancer activity of tamoxifen is mainly attributable to its competitive antagonism to ER, thereby inhibiting the proliferation of ER-positive breast cancer cells (*1*). However, whether this is the only mechanism of action underlying the anticancer activity of SERM has been questioned since tamoxifen and other SERM also showed anticancer activity in ER-negative breast cancers (*2-4*). Since the 1990s, several groups have found that tamoxifen and SERM strongly inhibited angiogenesis by mechanisms independent of ER (*5-7*). Based on these findings, tamoxifen and other SERM are now being actively investigated as anti-angiogenic agents in clinical trials for cancer treatment (*8-10*). However, the underlying molecular mechanism by which tamoxifen inhibits angiogenesis has remained largely unknown.

Cholesterol is an essential component of cellular membranes and plays a key role in membrane permeability and fluidity. In addition to a structural role, it also functions in intracellular transport and cell signaling (*11, 12*). Serum cholesterol is delivered throughout the body in the form of low-density lipoprotein (LDL) and transported into cells through receptor-mediated endocytosis (*13*). Endocytosed LDL is transported to the late endosomes and lysosomes (endolysosomes) where cholesteryl esters are hydrolyzed and free cholesterol is released from the endosomal system for delivery to other compartments, including the plasma membrane and endoplasmic reticulum (*14*). One of the most important machineries of cholesterol trafficking in the endolysosomes is the Niemann-Pick type C (NPC) proteins (NPC1 and NPC2), which help acid lipasemediated

hydrolysis of cholesteryl esters and deliver free cholesterol out of the endolysosomes (*15*). Inhibition of NPC1 or 2 causes accumulation of cholesterol and glycolipids in the endolysosomes, a phenotype called NPC after the genetic disease of the same name (*16*).

We have previously reported that a newly identified antiangiogenic drug itraconazole inhibited cholesterol trafficking and induced NPC-like phenotype in endothelial cells (*17*). Inhibition of cholesterol trafficking by itraconazole is accompanied by inhibition of mTOR signaling and VEGFR2 glycosylation, both of which are essential signaling components for endothelial cell proliferation (*17, 18*). Recently, Fang et al. showed that upon over-expression, apoA-I binding protein (AIBP), which is responsible for cholesterol efflux from endothelial cells, inhibited angiogenesis by depleting cholesterol from the plasma membrane, thereby inhibiting the VEGFR2 signaling pathway in endothelial cells and animal models (*19*). Similar to AIBP over-expression, cells with NPC phenotype induced by small molecules showed accumulation of cholesterol in the endolysosomes leading to cholesterol depletion in plasma membrane and inhibition of the VEGFR2 signaling pathway (*17, 18*). These results strongly suggest that cholesterol trafficking in endothelial cells is critical for proper angiogenesis.

In the present study, we found that tamoxifen and other SERM inhibited cholesterol trafficking in endothelial cells. Blockade of cholesterol trafficking by SERM fled to an abnormal subcellular distribution of mTOR and VEGFR2 and caused inhibition of their signaling pathways in a cholesterol-dependent manner. These data suggest that tamoxifen and other SERM inhibit angiogenesis by interfering with cholesterol

trafficking in endothelial cells and that cholesterol trafficking is a novel target for anti-angiogenesis therapy.

4.3 Materials and methods

Cells and reagents

Pooled human umbilical vein endothelial cells (HUVEC) were purchased from Lonza (Allendale, NJ) and were grown in endothelial cell growth medium-2 (EGM-2) using the EGM-2 bullet kit (Lonza). MCF-7 (ER-positive) breast cancer cellswere grown in Roswell Park Memorial Institute (RPMI)-1640 medium containing 10% fetal bovine serum (FBS, Life Technologies, Grand Island, NY) and 1% antibiotics (penicillin and streptomycin) solution (Life Technologies).MDA-MB-231 (triple negative) breast cancer cells were grown in high-glucose Dulbecco's Modified Eagle's Medium (DMEM) with 10% FBS (Life Technologies) and 1% antibiotics. All the cells were maintained in a humidified incubator at 37 °C adjusted to 5% CO2. Methyl-β-cyclodextrin, cholesterol and filipin were purchased from Sigma-Aldrich (St. Louis, MO). Recombinant human VEGF-165 was purchased from R&D Systems (Minneapolis, MN).

Filipin staining

Filipin staining was performed as described with slight modifications [17]. HUVEC were cultured in a Nunc Lab-Tek II 8-Chamber Slide (Thermo Scientific, Rockford, IL) at 1 × 104 cells/well. Cells were treated with SERM with or without cholesterol and cyclodextrin complex for 24 h. Cells were then fixed with 4% paraformaldehyde for 20min at room temperature and stained with filipin at a final concentration of 50 μg/ml in the dark for 1 h at room temperature. Cells were washed with PBS, mounted with Immu-mount (Thermo Scientific), and observed under a Zeiss 510 Meta multiphoton confocal microscope (Carl Zeiss, Thornwood, NY).

Immunofluorescence imaging

For co-staining of proteins and cholesterol, HUVEC (1×10^4 cells/well) grown in a Nunc Lab-Tek II 8-Chamber Slide were treated with compounds for 24 h, fixed with 4% paraformaldehyde for 20 min at room temperature and stained with filipin (50 μg/ml) for 1 h at room temperature. Cells were then permeabilized with 0.2% saponin supplemented with 50 μg/ml filipin and 5% bovine serum albumin (BSA) in PBS for 30 min. Cells were incubated with primary antibodies in PBS together with 50 μg/ml filipin, 0.05% saponin and 5% BSA overnight at 4 °C. Cells were then incubated with secondary antibodies in PBS with 50 μg/ml filipin, 0.05% saponin and 5% BSA at room temperature for 1 h. Cells were washed with PBS, mounted with Immumount, and observed under a Zeiss 510 Meta multiphoton confocal microscope. For general immunofluorescence, cells were fixed with 4% paraformaldehyde for 10 min, permeabilized with 0.5% Triton X-100 for 10min and washed with PBS prior to blocking in 1% BSA in PBS containing 0.1% Tween 20 (PBST) for 1 h. Cells were then incubated with primary antibodies including anti-VEGFR2 (Cell Signaling Technology, Danvers, MA), anti-LAMP1 (Santa Cruz Biotechnology, Santa Cruz, CA), anti mTOR (Cell Signaling Technology) and anti-GM130 (BD Biosciences, San Jose, CA) in the blocking solution overnight at 4 °C, and then incubated with secondary antibodies conjugated with Alexa-Fluo488 or Alexa-Fluo594 for 1 h. The cellular nuclei were stained with 4',6-diamidino-2-phenylindole (DAPI) and actin cytoskeleton was stained with rhodamine-phalloidin (Life Technologies). The immunofluorescence images were obtained using the Zeiss 510 Meta multiphoton confocal microscope.

[^{3}H]-thymidine DNA incorporation assay

HUVEC, MCF-7 or MDA-MB-231were seeded at 3 × 10^3 cells/well in 96-well plates and allowed to adhere at 37 °C for 24 h. Cells were then treated with compounds for 24 h prior to being pulsed with 0.5 μCi [^{3}H]-thymidine (PerkinElmer, Waltham, MA) for 16 h and then trypsinized. The cells were harvested onto FilterMat A glass fiber filters (Wallac, Turku, Finland) using a Harvester 96 cell harvester (Tomtec, Hamden, CT), and the radioactivity of [3H]-thymidine incorporated into DNA was counted using a MicroBeta liquid scintillation plate reader (PerkinElmer). The IC_{50} values and 95% confidence intervals were calculated using the GraphPad Prism 5.0 software (GraphPad Software, San Diego, CA).

AlamarBlue cell viability assay

HUVEC, MCF-7 or MDA-MB-231were seeded at 3 × 10^3 cells/well in 96-well plates and allowed to adhere at 37 °C for 24 h. The cells were treated with compounds in the presence or absence of cholesterol or cyclodextrin, or both for 24 h. AlamarBlue reagent (Life Technologies) was added to the media at a final concentration of 10% and the incubation was continued for an additional 2 h. The fluorescence signal was read with an excitation wavelength of 570 nm and an emission wavelength of 590 nm using a SpectraMax M5 fluorescence microplate reader (Molecular Devices, Sunnyvale, CA).

Western blot analysis

HUVEC (2 × 10^5 cells/well) were seeded in 6-well plates and allowed to adhere overnight. Following drug treatment for 24 h, cells were lysed by adding 2× Laemmli

buffer containing 4% SDS, 20% glycerol, 10% 2-mercaptoethanol, 0.004% bromophenol blue, 0.125MTris–HCl, pH 6.8 and the lysateswere boiled for 10 min and vortexed. After SDS-PAGE, the proteins were transferred to nitrocellulose membranes (Bio-Rad, Hercules, CA). The blots were blocked with 5% non-fat dried milk at room temperature for 1 h, incubated with the primary antibodies including anti-VEGFR2 (Cell Signaling Technology), anti-phospho-VEGFR2 (Tyr1175, Cell Signaling Technology), anti-FGFR1 (Cell Signaling Technology), anti-mTOR (Cell Signaling Technology), anti-phospho mTOR (Ser2448, Cell Signaling Technology), anti-S6K (Cell Signaling Technology), anti-phospho-S6K (Thr389, Cell Signaling Technology), anti-PDGFRβ (Santa Cruz Biotechnologies), anti-actin (Santa Cruz Biotechnologies) or anti-α-tubulin (Santa Cruz Biotechnologies) antibodies overnight at 4 °C and then incubated with HRP-conjugated secondary antibodies at room temperature for 1 h. The immunecomplexes were detected using enhanced chemiluminescence (ECL) detection reagent (GE Healthcare, Pittsburgh, PA).

Endothelial cell tube formation assay

A 96-well plate was coated with 50 µl Matrigel (BD Biosciences) and was incubated at 37 °C for 1 h to allow for polymerization. HUVEC were mixed with appropriate compounds and seeded (2×10^4 cells/well) on the Matrigel-coated wells, followed by incubation in a CO_2 incubator for 16 h. Cells were washed carefully with PBS once and Calcein-AM (2 µM in PBS, Life Technologies) solution was added to the cells. After incubation at 37 °C for 30 minutes, the cells were washed gently with PBS and the fluorescence-labeled tubular structures were observed under a Nikon Eclipse

TS100 fluorescence microscope with an excitation wavelength of 485 nm and an emission wavelength of 520 nm at magnification ×100. The total tube lengths, sizes and number of junctions from the fluorescence images were quantified using the AngioQuant v1.33 software (The MathWorks, Natick, MA) and plotted using the GraphPad Prism 5.0 software.

Statistical analysis

Statistical significance of the data between control and test groups was determined by two-sided Student's t-test using the GraphPad Prism 5.0 software. The P values less than 0.05 were considered significant.

4.4 Results

Tamoxifen and SERM induce NPC-like phenotype in HUVEC

We tested four FDA-approved SERM including tamoxifen, toremifene, clomifene and raloxifene **(Figure 4.1)** for effects on cholesterol trafficking in HUVEC. Intracellular cholesterol was visualized by staining fixed cells with filipin (*20*). All four SERM induced accumulation of cholesterol in the perinuclear region of HUVEC, a phenotype similar to NPC and that induced by itraconazole **(Figure 4.2)**. The cell morphology was also changed from large flat morphology into a partially shrunken form. These effects, however, were reversed upon addition of exogenous cholesterol and its carrier methyl-β-cyclodextrin (CD) **(Figure 4.3)**, suggesting that they are mediated largely through inhibition of cholesterol trafficking.

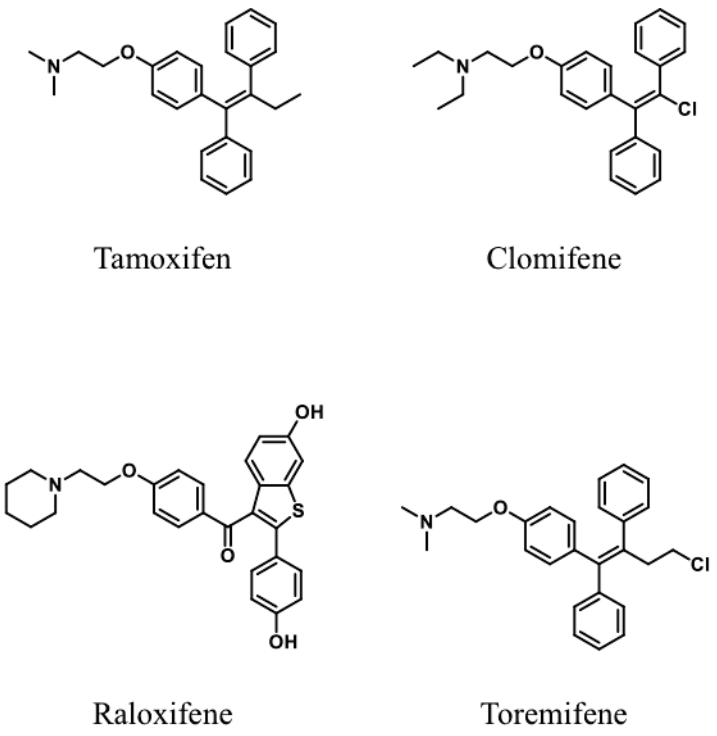

Figure 4.1: Chemical structures of SERM.

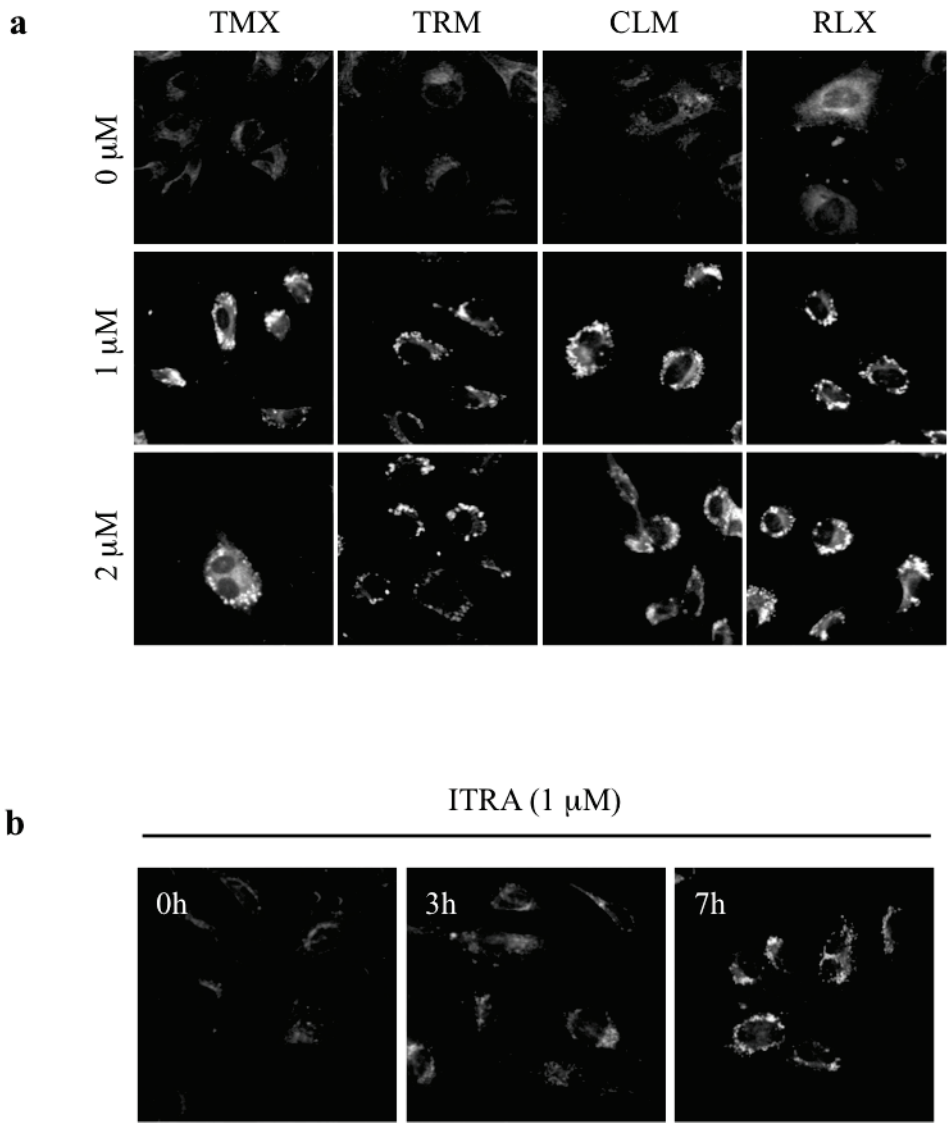

Figure 4.2: Effect of SERM on cholesterol trafficking in HUVEC.

(a) HUVEC were treated with tamoxifen (TMX), toremifene (TRM), clomifene (CLM) and raloxifene (RLX) for 24 h, and intracellular cholesterol was visualized by filipin. **(b)** HUVEC were treated with itraconazole (ITRA) for indicated time points, and intracellular cholesterol was visualized by filipin. Representative confocal images from four independent experiments are shown.

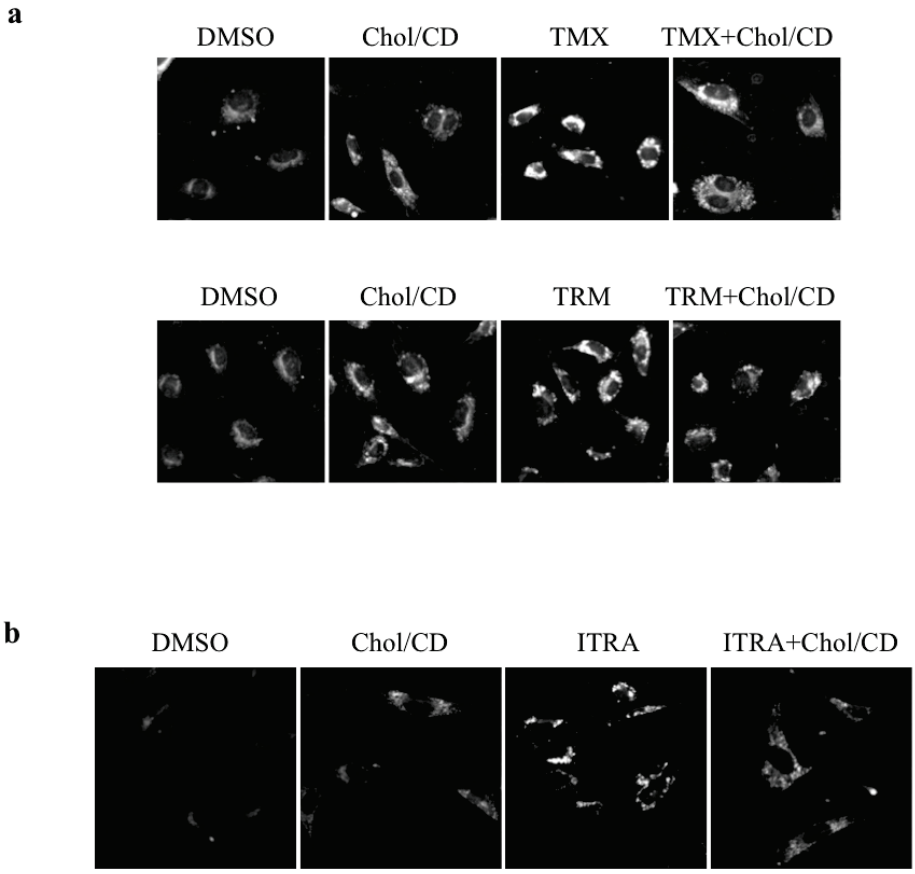

Figure 4.3: Rescue effect by addition of exogenous cholesterol.

(a) HUVEC were treated with 1 μM tamoxifen (TMX, upper panel) or 1 μM toremifene (TRM, lower panel) in the presence or absence of cholesterol (5 μg/ml)/cyclodextrin (0.1%) complex (Chol/CD) for 24 h, and intracellular cholesterol was visualized by filipin. **(b)** HUVEC were treated with 1 mM itraconazole (ITRA) in the presence or absence of cholesterol (5 mg/ml)/cyclodextrin (0.1%) complex (Chol/CD) for 24 h, and intracellular cholesterol was visualized by filipin. Representative confocal images from four independent experiments are shown.

Tamoxifen traps VEGFR2 in Golgi and induces perinuclear positioning of lysosomes in HUVEC

We have previously reported that a cholesterol trafficking inhibitor, itraconazole, inhibited the VEGFR2 and mTOR signaling pathways, both of which have been shown to be critical for angiogenesis (*17, 18*). To determine the effect of tamoxifen on VEGFR2 and mTOR signaling, we first analyzed the subcellular localization of those two proteins. Immunofluorescence labeling showed that VEGFR2 was localized largely in the plasma membrane and some in intracellular regions in control HUVEC **(Figure 4.4 a)**. Treatment of cells with tamoxifen caused an accumulation of a significant amount of VEGFR2 in the perinuclear region, which colocalized with the Golgi marker GM130 **(Figure 4.4 a and b)**. To determine if the abnormal subcellular distribution of VEGFR2 caused by tamoxifen is due to the inhibition of cholesterol trafficking, we added cholesterol/CD complex to the cell culture media. VEGFR2 mislocalization by tamoxifenwas clearly reversed by the cholesterol/CD complex **(Figure 4.4 b)**. On the other hand, mTOR was mainly located in the peripheral cytoplasm in control HUVEC and was well co-localized with the endolysosomal marker, LAMP1 **(Figure 4.4 c)**. Tamoxifen treatment caused cholesterol accumulation in the perinuclear region overlapping with the LAMP1-positive endolysosomes. Though tamoxifen did not alter mTOR association with LAMP1-positive endolysosomes, the localization of both mTOR and lysosomes was confined to the perinuclear region in the tamoxifen-treated HUVEC, whereas both proteins were more evenly distributed in the cytoplasm in control HUVEC. Staining of the actin cytoskeleton clearly showed that mTOR localization was confined to the perinuclear region by tamoxifen treatment **(Figure 4.4 d)**. This effect was reversed by cholesterol/CD complex

(Figure 4.4 d). These results indicated that tamoxifen caused subcellular redistribution of VEGFR2 and mTOR in endothelial cells in a cholesterol-dependent manner.

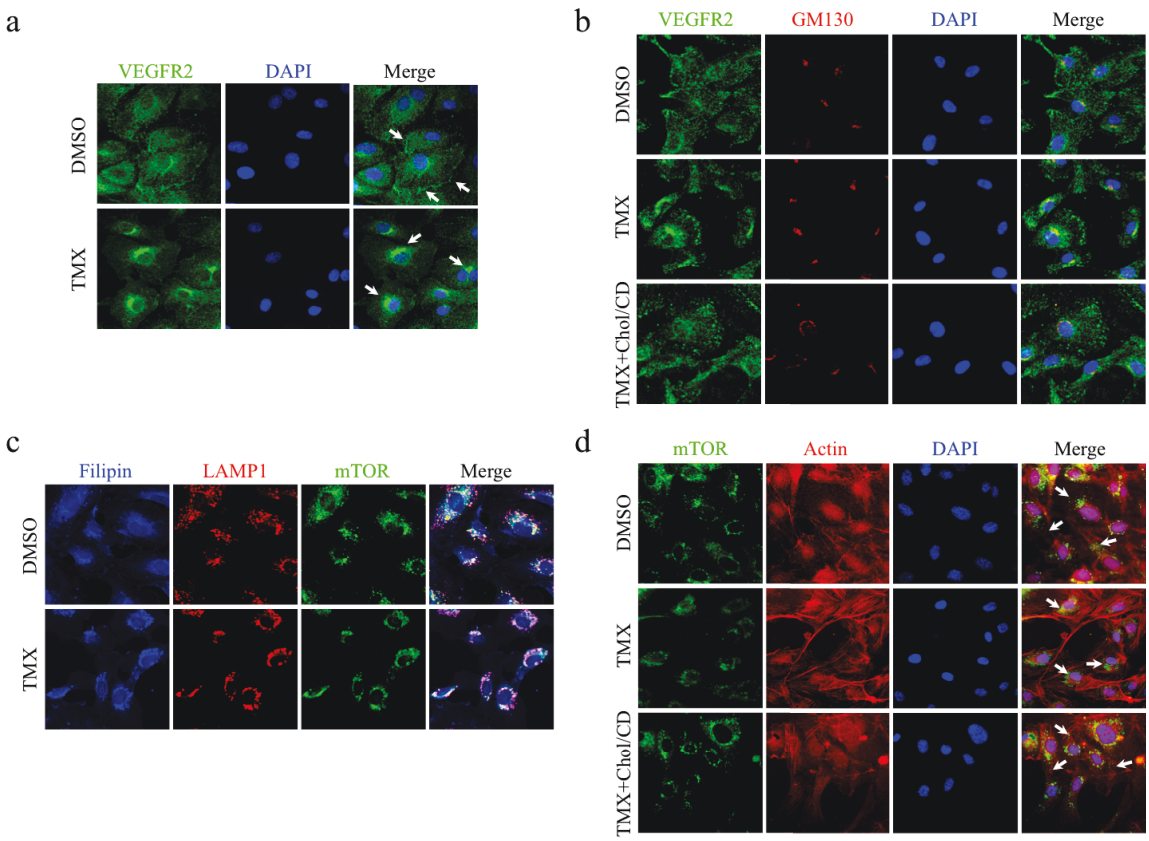

Figure 4.4: Effects of SERM and cholesterol on the subcellular localization of VEGFR2 and mTOR in HUVEC.

(a) HUVEC were treated with or without 1 μM tamoxifen (TMX) for 24 h and subcellular localization of VEGFR2 was assessed under a confocal microscope. Arrows indicate VEGFR2. **(b)** HUVEC were treated with or without 1 μM tamoxifen (TMX) in the presence or absence of cholesterol (5 μg/ml)/cyclodextrin (0.1%) complex (Chol/CD) for 24 h and subcellular localization of VEGFR2 and Golgi (GM130) was assessed. **(c)** HUVEC were treated with or without 1 μM tamoxifen (TMX) for 24 h and subcellular localization of cholesterol (Filipin), lysosomes (LAMP1), and mTOR was assessed. **(d)** HUVEC were treated with 1 μM tamoxifen (TMX) in the presence or absence of

cholesterol (5 μg/ml)/cyclodextrin (0.1%) complex (Chol/CD) for 24 h and subcellular localization of mTOR and actin was assessed. Arrows indicate that tamoxifen induced a change in mTOR localization from peripheral cytoplasm to the perinuclear region and this was reversed by cholesterol–cyclodextrin complex. Representative confocal images from four independent experiments are shown.

Tamoxifen inhibits VEGFR2 glycosylation and mTOR activity in HUVEC

Proper subcellular localization of proteins is critical for their proper function. Like other cell surface proteins, VEGFR2 is highly glycosylated and is expressed on the cell surface upon completion of glycosylation. Protein glycosylation occurs co-translationally in the endoplasmic reticulum and subsequently in the Golgi by a series of glycosidases and glycosyltransferases located in each organelle (*21*). Abnormal subcellular localization of glycoproteins will cause improper glycosylation and, therefore, affect their functions. As tamoxifen caused abnormal subcellular distribution of VEGFR2, we determined the effect of tamoxifen on the glycosylation pattern and the activity of VEGFR2. Control HUVEC showed two glycosylated forms of VEGFR2 (200 and 230 kD) **(Figure 4.5 a)**. The 230 kD (mature terminal glycosylated form) protein band was dominant over the 200 kD (intermediate glycosylated form) band. Tunicamycin is a glycosyltransferase inhibitor that acts in an initial step of glycosylation in the endoplasmic reticulum. It completely inhibited VEGFR2 glycosylation, reducing the protein's mass to 180 kD as expected. Deoxymannojirimycin (dMM), an inhibitor of α-mannosidases, and itraconazole are known to inhibit terminal glycosylation, thus shifting the VEGFR2 from 230 to 200 kD form. Similar to dMM and itraconazole, tamoxifen and other SERM caused a shift in the apparent molecular mass of VEGFR2 from 230 to 200 kD, suggesting that they inhibited terminal glycosylation which mainly occurs in the Golgi. Inhibition of terminal glycosylation of VEGFR2 by SERM occurred in a concentration-dependent manner **(Figure 4.5 b - d)**.

Subcellular localization of mTOR is also important for its activity. Recently, it was reported that nutrient starvation induced abnormal lysosomal positioning (increase in

perinuclear positioning) (*22*). This perinuclear lysosomal positioning was accompanied by mTOR Complex-1 (mTORC1) redistribution and inhibited the activity of mTOR. Tamoxifen and other SERM also caused perinuclear lysosomal positioning **(Figure 4.4 c and d)** and inhibited the phosphorylation of S6 kinase (S6K), a substrate of mTORC1, in HUVEC **(Figure 4.5 b - d)**. To further validate the inhibitory effect of tamoxifen on mTORC1 activity, the phosphorylation status of mTOR at Ser2448 was assessed. Like the direct mTOR inhibitor rapamycin, tamoxifen dose-dependently inhibited mTOR phosphorylation at Ser2448 in HUVEC **(Figure 4.6 a)**. The phosphorylation of S6K was also inhibited by tamoxifen in parallel with the inhibition of mTOR phosphorylation.

We next examined glycosylation patterns of other receptor tyrosine kinases related to angiogenesis, including fibroblast growth factor receptor 1 (FGFR1) and platelet-derived growth factor receptor β (PDGFRβ), to see if the tamoxifen effect was specific to VEGFR2. Similar to the effect observed on VEGFR2, tamoxifen caused a shift in the apparent molecular mass of PDGFRβ and FGFR1 **(Figure 4.6 b)**. Sorafenib, a kinase inhibitor, had no effect on the receptor molecular masses. However dMM caused a shift in the receptors' molecular masses in a manner similar to that of tamoxifen, suggesting that tamoxifen inhibited terminal glycosylation of the receptor tyrosine kinases. These results suggested that tamoxifen inhibits a common pathway in terminal glycosylation of receptor tyrosine kinases in endothelial cells.

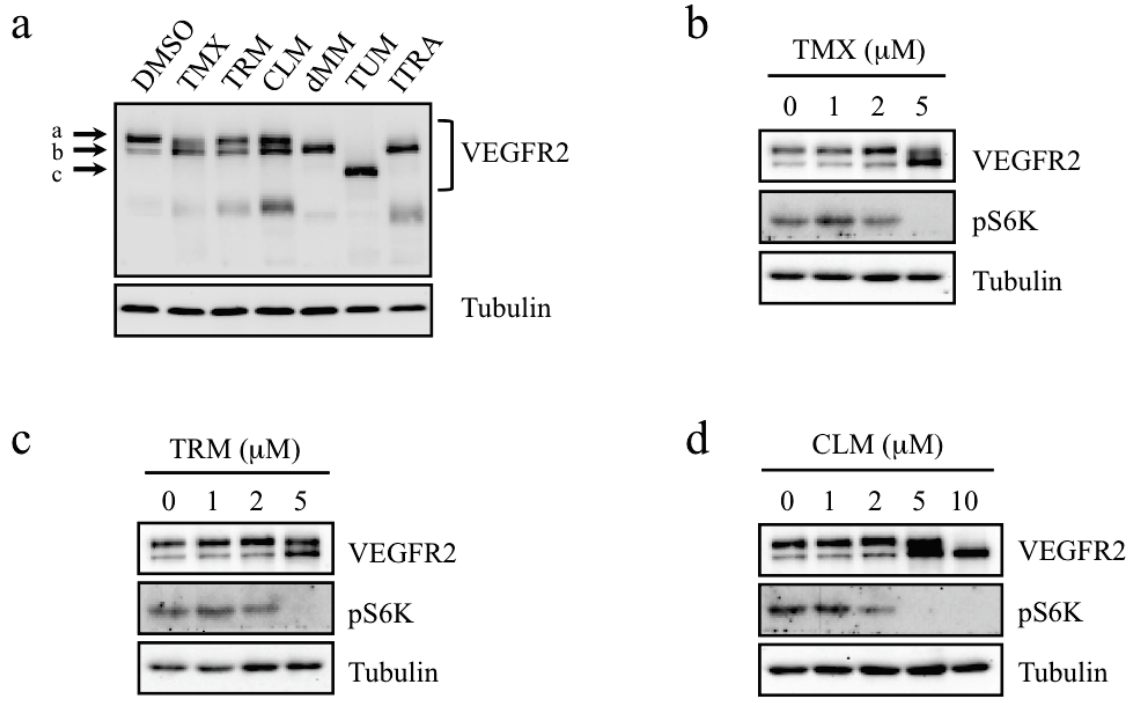

Figure 4.5: Effect of SERM on VEGFR2 glycosylation and mTORC1 pathway in HUVEC.

(a) HUVEC were treated with SERM including tamoxifen (TMX, 5 μM), toremifene (TRM, 5 μM) and clomifene (CLM, 5 μM) for 24 h and VEGFR2 glycosylation was assessed byWestern blotting. Glycosylation inhibitors including deoxymannojirimycin (dMM, 500 μM) and tunicamycin (TUM, 2 μg/ml), and a cholesterol trafficking inhibitor itraconazole (ITRA, 1 μM) were used as positive controls. Three different glycosylated forms of VEGFR2 (a: 230 kD hyper-glycosylated form, b: 200 kD intermediate glycosylated form and c: 180 kD unglycosylated form) are shown. **(b - d)** Effect of various concentrations of SERM on VEGFR2 glycosylation and mTORC1 pathway – indicated by the level of phosphorylated S6K (pS6K) – are shown. Representative Western blot images from three independent experiments are shown.

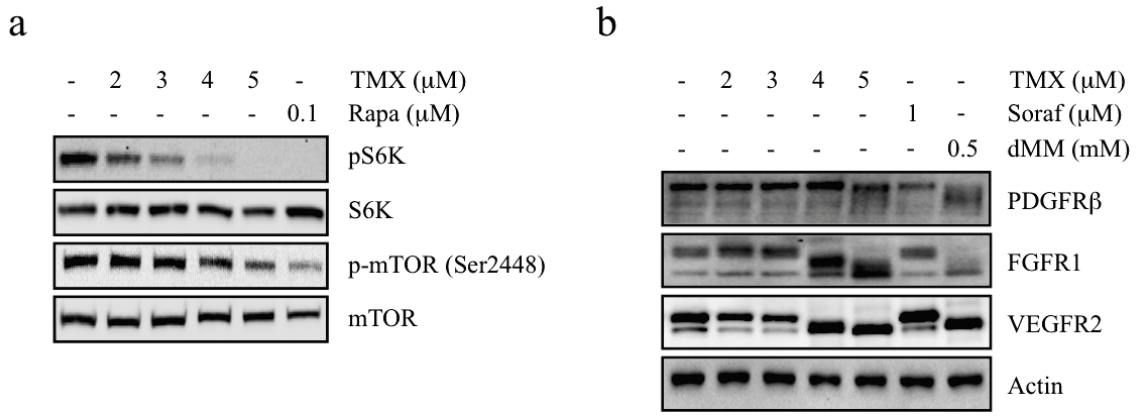

Figure 4.6: Effect of tamoxifen on the phosphorylation of mTOR and the glycosylation of receptor tyrosine kinases in HUVEC.

(a) HUVEC were treated with tamoxifen (TMX) or rapamycin (Rapa) at indicated concentrations for 24 h and the phosphorylation of mTOR at Ser2448 as well as phosphorylated S6K (pS6K) and total S6K was analyzed. **(b)** HUVEC were treated with tamoxifen (TMX), sorafenib (Soraf) or deoxymannojirimycin (dMM) at indicated concentrations for 24 h. The terminal glycosylation of the receptor tyrosine kinases was assessed by Western blotting using specific antibodies against each receptor tyrosine kinase in the presence of the known glycosylation inhibitor dMM. Representative Western blot images from three independent experiments are shown.

Cholesterol reverses the inhibitory effects of tamoxifen on VEGFR2 and mTOR signaling in HUVEC

We next determined the effect of cholesterol on the inhibition of VEGFR2 glycosylation by tamoxifen in HUVEC. Inhibition of terminal glycosylation by either tamoxifen or toremifene was completely reversed by the addition of cholesterol/CD complex **(Figure 4.7 a and b)**. To see if the inhibition of terminal glycosylation by tamoxifen affected VEGFR2 activity/signaling, tyrosine phosphorylation status of VEGFR2 was assessed. Inhibition of terminal glycosylation of VEGFR2 by tamoxifen led to the inhibition of VEGFR2 phosphorylation, which was completely reversed by cholesterol/CD complex **(Figure 4.7 c)**. A VEGFR2 tyrosine kinase inhibitor sunitinib also inhibited VEGFR2 phosphorylation. But this effect was not reversed by cholesterol/CD complex **(Figure 4.7 c)**. These data suggested that the effect of tamoxifen on VEGFR2 was mediated through inhibition of cholesterol trafficking in endothelial cells. We further investigated the effect of cholesterol on inhibition of mTOR signaling by tamoxifen in HUVEC. Inhibition of S6K phosphorylation by either tamoxifen or toremifene was completely reversed by cholesterol/CD complex **(Figure 4.7 d)**. CD alone could partially reverse tamoxifen activity. This was presumably due to the reversal effect of CD on NPC phenotype by releasing free cholesterol from endolysosomes (*23*). Inhibition of mTOR signaling by tamoxifen and its reversal by cholesterol were further confirmed by examining 4E-BP1 phosphorylation, which was also decreased **(Figure 4.8)**.

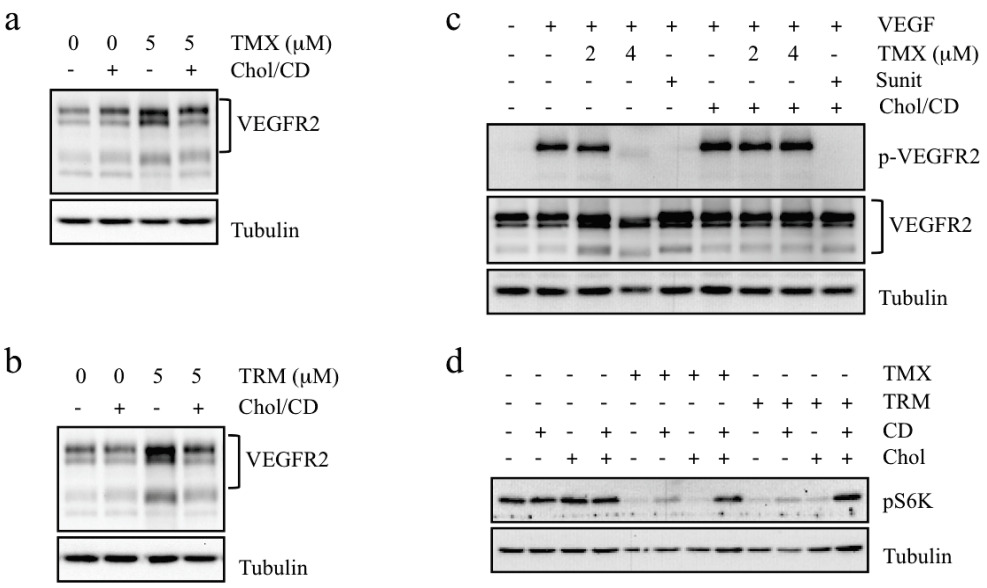

Figure 4.7: Reversal effect of cholesterol on the inhibition of VEGFR2 and mTOR activities by SERM.

(a and b) HUVEC were treated with tamoxifen (TMX) or toremifene (TRM) with or without cholesterol (5 μg/ml)/cyclodextrin (0.1%) complex (Chol/CD) for 24 h, and VEGFR2 glycosylation was assessed by Western blotting. **(c)** HUVEC were grown in low serum media (0.1% FBS without additional growth factor supplements) and treated with drugs including tamoxifen (TMX) and sunitinib (Sunit, 100 nM) for 24 h in the presence or absence of cholesterol (5 μg/ml)/cyclodextrin (0.1%) complex (Chol/CD). Cells were then stimulated with 50 ng/ml of VEGF-165 for 5 min and the levels of total and phosphorylated VEGFR2 were assessed by Western blotting. **(d)** HUVEC were treated with tamoxifen (TMX, 5 μM) or toremifene (TRM, 5 μM) with or without cholesterol (Chol, 5 μg/ml) and cyclodextrin (CD, 0.1%) for 24 h, and mTOR activity was assessed by Western blotting of phosphorylated S6-kinase (pS6K). Representative Western blot images from three independent experiments are shown.

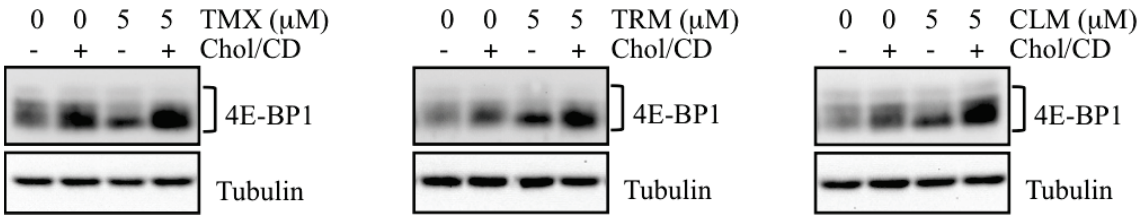

Figure 4.8: Reversal effect of cholesterol on inhibition of mTOR activity by SERM. HUVEC were treated with tamoxifen (TMX), toremifene (TRM) or clomifene (CLM) with or without cholesterol (Chol, 5 mg/ml)/cyclodextrin (CD, 0.1%) complex (Chol/CD) for 24 h, and mTOR activity was assessed by Western blotting of 4E-BP1. 4E-BP1 has multiple protein bands and lower molecular weight bands represent hypophosphorylated 4E-BP1. Note that SERM decreased the phosphorylation of 4E-BP1 as shown by decrease in the levels of higher molecular weight forms of 4E-BP1. Representative Western blot images from three independent experiments are shown.

Cholesterol reverses the inhibitory effects of tamoxifen on HUVEC proliferation

To assess the relationship between VEGFR2 phosphorylation, mTOR activity and cell proliferation, we examined the effect of SERM on HUVEC proliferation. Half maximal inhibitory concentrations (IC_{50}) of tamoxifen, toremifene and raloxifene for HUVEC proliferationwere determined to be 0.98, 1.2, and 1.42 μM, respectively **(Figure 4.9 a and Table 4.2)**.We then determined if cholesterol could reverse the inhibition of HUVEC proliferation by SERM. Tamoxifen and toremifene strongly inhibited the growth of HUVEC at 2 and 4 μM, respectively. The inhibitions were partially reversed by CD and were fully reversed by cholesterol/CD complex **(Figure 4.9 b)**. Cholesterol alone has no reversal effect on the cell growth inhibition by tamoxifen or toremifene. These data corroborated the effects of SERM on VEGFR2 and mTOR **(Figure 4.7 a - d)**.

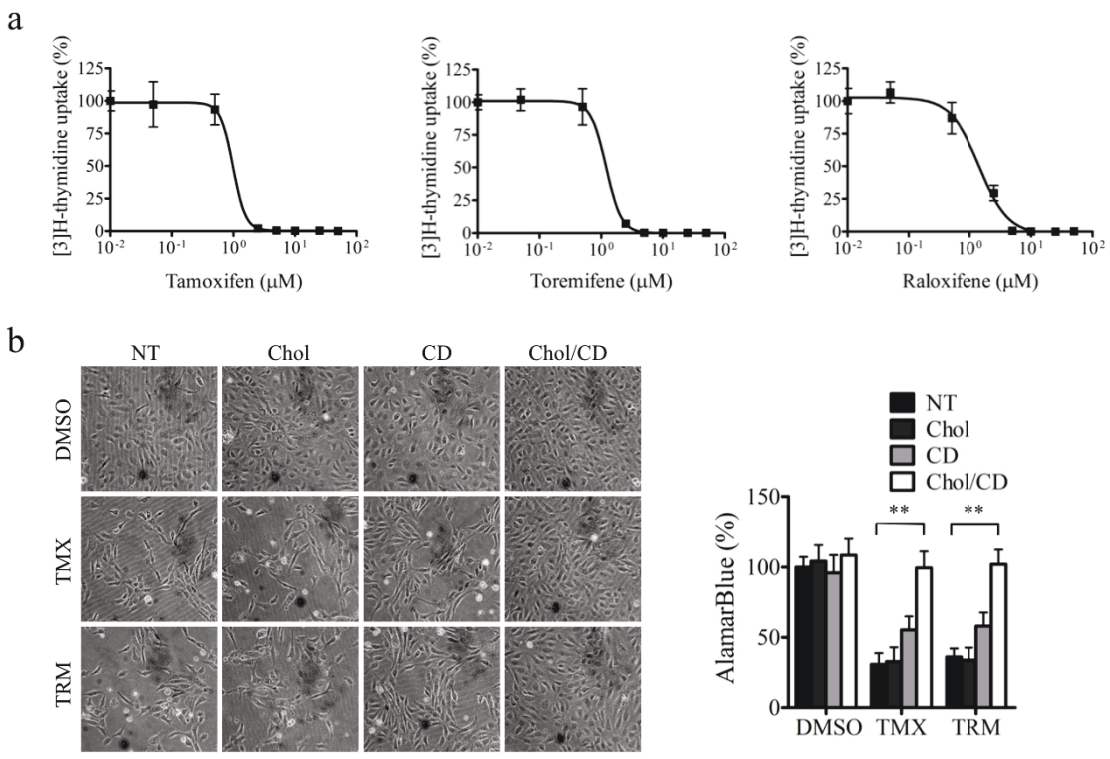

Figure 4.9: Effects of SERM and cholesterol on HUVEC proliferation.

(a) HUVEC were treated with various concentrations of tamoxifen, toremifene or raloxifene for 24 h and cell proliferation was assessed through the [3]H-thymidine uptake assay. **(b)** HUVEC were treated with tamoxifen (TMX, 2 μM) or toremifene (TRM, 4 μM) for 24 h and were observed under a phase contrast microscope. Cholesterol (Chol, 5 μg/ml) and cyclodextrin (CD, 0.1%) were added together to assess reversibility on the anti-proliferative effect of SERM. NT denotes not treated with Chol/CD. Representative phase-contrast images from four independent experiments are shown. The cell viability was quantified by AlamarBlue staining and was plotted using the GraphPad Prism 5.0 software (right panel). Data represent mean ± standard deviation (SD) from four independent experiments. **P < 0.01 between two indicated groups.

Table 4.2. Half-maximum inhibitory concentrations (IC50) of SERM on cell proliferation and 95% confidence intervals (CI) are shown.

Drugs	HUVEC		MCF-7 (ER+)		MDA-MB-231 (ER-)	
	IC_{50} (μM)	95% CI	IC_{50} (μM)	95% CI	IC_{50} (μM)	95% CI
Tamoxifen	0.98	0.57 to 1.68	3.03	2.20 to 4.15	5.49	5.05 to 5.97
Toremifene	1.20	0.92 to 1.57	4.86	3.37 to 7.01	9.42	8.39 to 10.59
Raloxifene	1.42	1.15 to 1.75	8.24	6.27 to 10.83	12.24	10.55 to 14.20

Inhibition of cholesterol trafficking by tamoxifen is independent of ER

SERM are potent antagonists of ER, with K_d values ranging from picomolar to single-digit nanomolar concentrations, hence showing anti-proliferative effects on ER-positive breast cancer cells (*24*). We thus tested whether SERM have different sensitivity on cell proliferation and cholesterol trafficking in cells with different ER expression statuses. In an ER-positive cell line (MCF-7), SERM showed a biphasic cell growth inhibition; marginal inhibition at lower concentrations (from nanomolar to single-digit micromolar, dotted arrows) and strong/complete inhibition at higher concentrations (from single- to double-digit micromolar, solid arrows) **(Figure 4.10 a)**. In an ER-negative cell line (MDA-MB-231), SERM showed a typical dose–response curve with growth inhibition at higher concentrations (from single- to double-digit micromolar) **(Figure 4.10 b)**. These data suggested that SERM have at least two independent targets for growth inhibition in MCF-7 cells. It could be postulated that the more sensitive target is ER while the less sensitive target is cholesterol trafficking in ER-positive MCF-7 cells.

We further tested the effect of a high concentration of tamoxifen (10 μM) on cholesterol trafficking in both MCF-7 and MDA-MB-231. Tamoxifen strongly inhibited cholesterol trafficking in both cells and the inhibition was reversed by cholesterol/CD complex **(Figure 4.11 a)**. A high concentration of tamoxifen strongly inhibited the cell growth of both MCF-7 and MDA-MB-231 and the inhibition was reversed by cholesterol/CD complex **(Figure 4.11 b)**. These data demonstrated that inhibition of cholesterol trafficking by tamoxifen is independent of its action on ER.

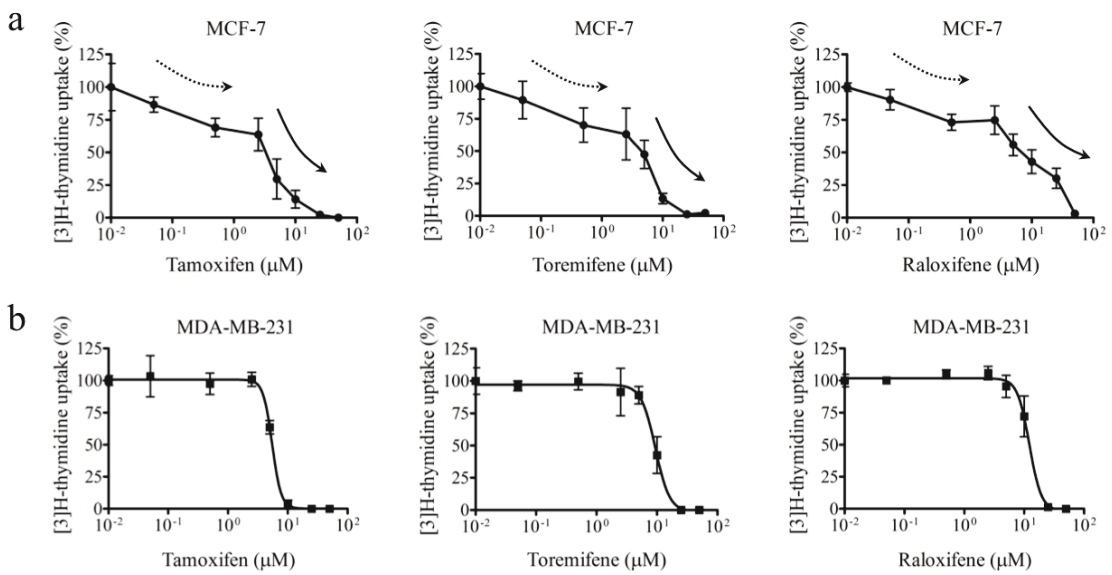

Figure 4.10: Effects of SERM and cholesterol on ER-positive or ER-negative breast cancer cell proliferation.

(a) MCF-7 (ER-positive) or **(b)** MDA-MB-231 (ER-negative) cells were treated with various concentrations of tamoxifen, toremifene or raloxifene for 24 h and cell proliferation was assessed through the [3]H-thymidine uptake assay. SERM showed a biphasic growth inhibition in MCF-7 cells. Dotted arrows indicate concentration ranges that show marginal cell growth inhibition, whereas solid arrows represent concentration ranges with strong cell growth inhibition. The cell viability was quantified by AlamarBlue staining and was plotted using the GraphPad Prism 5.0 software. Data represent mean ± standard deviation (SD) from four independent experiments.

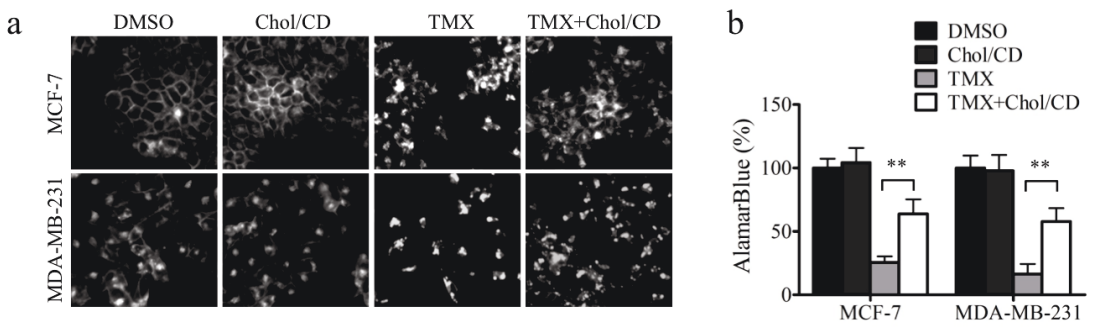

Figure 4.11: Tamoxifen strongly inhibited cholesterol trafficking in both cells and the inhibition was reversed by cholesterol/CD complex.

(a) MCF-7 or MDA-MB-231 cells were treated with 10 μM tamoxifen (TMX) in the presence or absence of cholesterol (5 μg/ml)/cyclodextrin (0.1%) complex (Chol/CD) for 24 h and intracellular cholesterol was labeled with filipin staining. Representative confocal images from four independent experiments are shown. **(b)** MCF-7 or MDA-MB-231 cells were treated with 10 μM tamoxifen (TMX) in the presence or absence of cholesterol (Chol, 5 μg/ml)/cyclodextrin (CD, 0.1%) complex (Chol/CD) for 24 h. The cell viability was quantified by AlamarBlue staining and was plotted using the GraphPad Prism 5.0 software. Data represent mean ± standard deviation (SD) from four independent experiments. **$P < 0.01$ between two indicated groups.

Cholesterol reverses the inhibitory effect of tamoxifen on HUVEC tube formation in Matrigel

We determined the effect of SERM on endothelial cell tube formation, a well-established in vitro assessment of angiogenesis. As expected from previous reports (*5, 7*), both tamoxifen and toremifene inhibited the tube formation of HUVEC on Matrigel **(Figure 4.12 a)**. The inhibition of tube formation by SERM, however, was significantly reversed by an addition of cholesterol/CD complex, while cholesterol/CD itself did not affect the tube structures **(Figure 4.12 a and b)**. Taken together, these results suggested that anti-angiogenic activity of tamoxifen is mainly mediated by its effect on cholesterol trafficking in endothelial cells.

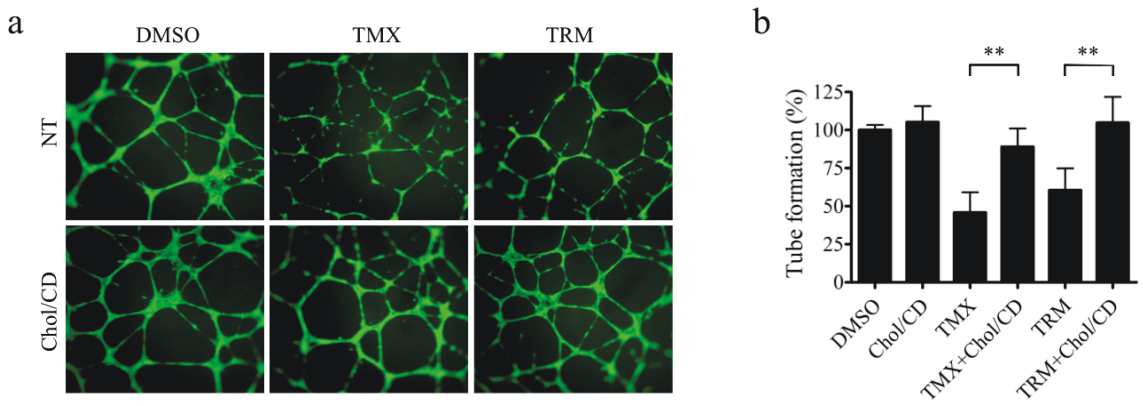

Figure 4.12: Effects of SERM and cholesterol on HUVEC tube formation.

(a) HUVEC were seeded onto a Matrigel-coated plate to promote tube formation. Cells were treated with 5 μM tamoxifen (TMX) or 5 μM toremifene (TRM) in the presence or absence (NT) of cholesterol (5 μg/ml)/cyclodextrin (0.1%) complex (Chol/CD) for 18 h. The tube formation was visualized by staining with Calcein-AM under a fluorescence microscope. Representative fluorescence images from six independent experiments are shown. **(b)** Total tube lengths, sizes and number of junctions from the fluorescence images from six experiments were quantified using the AngioQuant software. **$P < 0.01$ between two indicated groups.

4.5 Discussion

SERM are mixed agonists/antagonists of ER, which act differently depending on cell and tissue types. As they act as antagonists of ER in breast tissue, SERM, especially tamoxifen, have long been used to treat ER-positive breast cancer. However, it has been questioned whether the anticancer effect of SERM is solely due to the ER antagonism, since a number of reports have shown the therapeutic effects of tamoxifen on ER-negative breast cancer (*2-4*). The anti-angiogenic activity of SERM was first reported by Gagliardi and Collins in 1993 (*7*). SERM including clomiphene and tamoxifen significantly inhibited angiogenesis in the chorioallantoic membrane in growing chick embryos. Addition of excessive amount of 17β-estradiol did not alter the anti-angiogenic activity of SERM, suggesting that angiogenesis inhibition by SERM was independent of the blockade of ER. Subsequent studies have demonstrated that SERM are effective anti-angiogenic agents using several animal models, including ER-negative rat models (*5, 6*). Based on these observations, SERM are under review in several clinical studies as an antiangiogenic monotherapy or an adjuvant therapy with chemotherapy drugs in a broad range of cancer types (*8-10*). All the evidence strongly suggests that inhibition of angiogenesis is one of the major mechanisms underlying the anticancer activity of SERM in addition to ER. However, the mechanism underlying the anti-angiogenic activity of SERM has remained elusive.

In the present study, we showed that SERM inhibited cholesterol trafficking in endothelial cells, as evidenced by abnormal accumulation of free cholesterol in the endolysosomes. This effect was accompanied by aberrant subcellular localization of two major players in angiogenesis, VEGFR2 and mTOR, in endothelial cells. VEGFR2

undergoes glycosylation upon translation and the glycosylation is required for receptor auto-phosphorylation and activation (*25*). Tamoxifen treatment caused trapping of the VEGFR2 in the Golgi, inhibited the terminal glycosylation and depleted the receptor in the plasma membrane. Consequently, tamoxifen inhibited the VEGF-induced phosphorylation of VEGFR2 in endothelial cells. Tamoxifen also inhibited terminal glycosylation of other receptor tyrosine kinases related to angiogenesis such as FGFR1 and PDGFRβ in HUVEC. These data suggest that tamoxifen inhibits a common terminal glycosylation pathway in endothelial cells leading to the inhibition of maturation of the receptor tyrosine kinases. On the other hand, mTORC1 is recruited to the lysosome surface and regulates lysosomal functions when cells are in normal nutrient-rich state (*26*). Conversely, mTOR activity is also regulated by lysosomes by altering subcellular lysosomal positioning (*22*). The lysosomal positioning is critical for mTOR activity (*22, 27, 28*). Under starvation, intracellular pH (pHi) was increased and this pHi change in turn caused perinuclear clustering of lysosomes. The perinuclear clustering of lysosomes led to an inhibition of mTOR activity. Forced movement of lysosomes to the cell periphery by overexpressing kinesin family of proteins could restore mTOR activity, suggesting a critical role of lysosomal positioning in mTOR signaling pathway(*22*). In our study, we found that tamoxifen did not alter the association of mTOR with the LAMP1-positive endolysosomes. Instead, it switched lysosomal positioning from the cell periphery to the perinuclear region leading to the inhibition of mTOR activity. Although the mechanism by which lysosomal positioning influences mTOR activity remains to be elucidated, it has been proposed that lysosomes in the cell periphery would enable mTOR to access to its upstream signaling molecules such as activated Akt at the cell surface

membrane. Confining lysosomes to the perinuclear region would prevent mTOR from accessing its upstream signaling molecules at the cell membrane, leading to the blockade of its activation (*22*). Further studies are necessary to elucidate the causal relationship between SERM-induced lysosomal positioning and mTOR activity.

We further showed that addition of extracellular cholesterol could significantly reverse the abnormal localization of VEGFR2 and inhibition of terminal glycosylation and receptor phosphorylation caused by SERM. Cholesterol also could reverse SERM-induced perinuclear lysosomal positioning and inhibition of mTOR activity. These data strongly suggest that cholesterol trafficking lies upstream of VEGFR2 trafficking and glycosylation and lysosomal positioning by SERM. In addition, inhibition of endothelial cell proliferation and tube formation by SERM was markedly reversed by the addition of extracellular cholesterol, implying that inhibition of cholesterol trafficking led to the inhibition of twomajor signaling pathways, VEGFR2 and mTOR, which is likely the main mechanism mediating the antiangiogenic activity of SERM.

In this study,we have not identified the molecular target responsible for the inhibition of endothelial cell cholesterol trafficking by SERM. ER could be a candidate, but it was ruled out by testing two different breast cancer cell lines, MCF-7 (ER-positive) and MDA-MB-231 (ER-negative). SERM at high concentrations caused abnormal cholesterol accumulation in both cell lines regardless of the ER status and inhibited cell proliferation in a cholesterol-dependent manner. One possible mechanism of cholesterol trafficking inhibition by SERM could be that SERM, especially tamoxifen, act as a lipophilic weak base and increase the pH in acidic organelles such as lysosomes (*28*). Changes in organellar pH could inhibit enzyme activities in the organelles including NPC

proteins and glycosylation enzymes, which could potentially affect cholesterol and receptor tyrosine kinase trafficking in the cells. Ongoing studies are focused on lysosomal pH change in endothelial cells and the results will be presented in the near future.

The vascular endothelium is the first layer of cells that are in contact with the full circulating lipoproteins from blood plasma, and is responsible for the uptake of LDL-cholesterol from the plasma and efflux of cellular cholesterol to HDL in the plasma. Several recent reports showed that cholesterol uptake and efflux in endothelial cells are important regulators of angiogenesis (*19, 29, 30*). Usui et al. showed that LDL alone could activate VEGFR1 signaling in the absence of VEGF in macrophages (*30*). The activation of VEGFR1 signaling was mediated by recruitment of the LDL receptor to VEGFR1 by LDL during its uptake. Conversely, Fang et al. demonstrated that AIBP mediates cholesterol efflux from endothelial cells, and its overexpression suppresses angiogenesis in animal models through inhibition of VEGFR2 signaling (*19*). In our previous studies, itraconazole was found to inhibit cholesterol trafficking in endothelial cells (*17*). Itraconazole is undergoing multiple clinical studies as an anti-angiogenic agent. Several positive clinical results have been reported recently from Phase II studies for cancer treatment, including metastatic and castration-resistant prostate cancer, non-small cell lung cancer and basal cell carcinoma (*31-33*). These studies together with our current results suggest that endothelial cell cholesterol trafficking can serve as a novel therapeutic target for angiogenesis-related diseases including cancer.

4.6 References

1. L. J. Lerner, V. C. Jordan, Development of antiestrogens and their use in breast cancer: eighth Cain memorial award lecture. *Cancer research* **50**, 4177-4189 (1990)
2. C. Knabbe, G. Zugmaier, M. Schmahl, M. Dietel, M. E. Lippman, R. B. Dickson, Induction of transforming growth factor beta by the antiestrogens droloxifene, tamoxifen, and toremifene in MCF-7 cells. *American journal of clinical oncology* **14 Suppl 2**, S15-20 (1991).
3. V. C. Jordan, C. S. Murphy, Endocrine pharmacology of antiestrogens as antitumor agents. *Endocrine reviews* **11**, 578-610 (1990)
4. V. C. Jordan, Long-term adjuvant tamoxifen therapy for breast cancer. *Breast cancer research and treatment* **15**, 125-136 (1990)
5. K. L. Blackwell, Z. A. Haroon, S. Shan, W. Saito, G. Broadwater, C. S. Greenberg, M. W. Dewhirst, Tamoxifen inhibits angiogenesis in estrogen receptor-negative animal models. *Clinical cancer research : an official journal of the American Association for Cancer Research* **6**, 4359-4364 (2000)
6. E. F. Haran, A. F. Maretzek, I. Goldberg, A. Horowitz, H. Degani, Tamoxifen enhances cell death in implanted MCF7 breast cancer by inhibiting endothelium growth. *Cancer research* **54**, 5511-5514 (1994); published online EpubNov 1 (
7. A. Gagliardi, D. C. Collins, Inhibition of angiogenesis by antiestrogens. *Cancer research* **53**, 533-535 (1993)
8. T. Mele, D. Generali, S. Fox, M. P. Brizzi, A. Bersiga, M. Milani, G. Allevi, S. Bonardi, S. Aguggini, M. Volante, L. Dogliotti, A. Bottini, A. Harris, A. Berruti,

Anti-angiogenic effect of tamoxifen combined with epirubicin in breast cancer patients. *Breast cancer research and treatment* **123**, 795-804 (2010)

9. J. A. Hurteau, M. F. Brady, K. M. Darcy, W. P. McGuire, P. Edmonds, M. L. Pearl, I. Ivanov, K. S. Tewari, R. S. Mannel, K. Zanotti, D. M. Benbrook, Randomized phase III trial of tamoxifen versus thalidomide in women with biochemical-recurrent-only epithelial ovarian, fallopian tube or primary peritoneal carcinoma after a complete response to first-line platinum/taxane chemotherapy with an evaluation of serum vascular endothelial growth factor (VEGF): A Gynecologic Oncology Group Study. *Gynecologic oncology* **119**, 444-450 (2010)
10. J. Heidemann, H. Ogawa, M. F. Otterson, V. B. Shidham, D. G. Binion, Antiangiogenic treatment of mesenteric desmoid tumors with toremifene and interferon alfa-2b: report of two cases. *Diseases of the colon and rectum* **47**, 118-122 (2004)
11. F. R. Maxfield, I. Tabas, Role of cholesterol and lipid organization in disease. *Nature* **438**, 612-621 (2005); published online EpubDec 1 (10.1038/nature04399).
12. J. P. Incardona, S. Eaton, Cholesterol in signal transduction. *Current opinion in cell biology* **12**, 193-203 (2000)
13. L. Liscum, N. K. Dahl, Intracellular cholesterol transport. *Journal of lipid research* **33**, 1239-1254 (1992)
14. E. Ikonen, Cellular cholesterol trafficking and compartmentalization. *Nature reviews. Molecular cell biology* **9**, 125-138 (2008)

15. H. J. Kwon, L. Abi-Mosleh, M. L. Wang, J. Deisenhofer, J. L. Goldstein, M. S. Brown, R. E. Infante, Structure of N-terminal domain of NPC1 reveals distinct subdomains for binding and transfer of cholesterol. *Cell* **137**, 1213-1224 (2009)

16. K. B. Peake, J. E. Vance, Defective cholesterol trafficking in Niemann-Pick C-deficient cells. *FEBS letters* **584**, 2731-2739 (2010)

17. J. Xu, Y. Dang, Y. R. Ren, J. O. Liu, Cholesterol trafficking is required for mTOR activation in endothelial cells. *Proceedings of the National Academy of Sciences of the United States of America* **107**, 4764-4769 (2010)

18. B. A. Nacev, P. Grassi, A. Dell, S. M. Haslam, J. O. Liu, The antifungal drug itraconazole inhibits vascular endothelial growth factor receptor 2 (VEGFR2) glycosylation, trafficking, and signaling in endothelial cells. *The Journal of biological chemistry* **286**, 44045-44056 (2011)

19. L. Fang, S. H. Choi, J. S. Baek, C. Liu, F. Almazan, F. Ulrich, P. Wiesner, A. Taleb, E. Deer, J. Pattison, J. Torres-Vazquez, A. C. Li, Y. I. Miller, Control of angiogenesis by AIBP-mediated cholesterol efflux. *Nature* **498**, 118-122 (2013)

20. G. Gimpl, K. Gehrig-Burger, Cholesterol reporter molecules. *Bioscience reports* **27**, 335-358 (2007); published online EpubDec (10.1007/s10540-007-9060-1).

21. R. A. Dwek, T. D. Butters, F. M. Platt, N. Zitzmann, Targeting glycosylation as a therapeutic approach. *Nature reviews. Drug discovery* **1**, 65-75 (2002)

22. V. I. Korolchuk, S. Saiki, M. Lichtenberg, F. H. Siddiqi, E. A. Roberts, S. Imarisio, L. Jahreiss, S. Sarkar, M. Futter, F. M. Menzies, C. J. O'Kane, V. Deretic, D. C. Rubinsztein, Lysosomal positioning coordinates cellular nutrient responses. *Nature cell biology* **13**, 453-460 (2011)

23. J. E. Vance, K. B. Peake, Function of the Niemann-Pick type C proteins and their bypass by cyclodextrin. *Current opinion in lipidology* **22**, 204-209 (2011)

24. S. R. Goldstein, S. Siddhanti, A. V. Ciaccia, L. Plouffe, Jr., A pharmacological review of selective oestrogen receptor modulators. *Human reproduction update* **6**, 212-224 (2000)

25. T. Takahashi, M. Shibuya, The 230 kDa mature form of KDR/Flk-1 (VEGF receptor-2) activates the PLC-gamma pathway and partially induces mitotic signals in NIH3T3 fibroblasts. *Oncogene* **14**, 2079-2089 (1997)

26. Y. Sancak, L. Bar-Peled, R. Zoncu, A. L. Markhard, S. Nada, D. M. Sabatini, Ragulator-Rag complex targets mTORC1 to the lysosomal surface and is necessary for its activation by amino acids. *Cell* **141**, 290-303 (2010)

27. V. I. Korolchuk, D. C. Rubinsztein, Regulation of autophagy by lysosomal positioning. *Autophagy* **7**, 927-928 (2011)

28. Y. Chen, M. Schindler, S. M. Simon, A mechanism for tamoxifen-mediated inhibition of acidification. *The Journal of biological chemistry* **274**, 18364-18373 (1999)

29. F. Jin, N. Hagemann, U. Brockmeier, S. T. Schafer, A. Zechariah, D. M. Hermann, LDL attenuates VEGF-induced angiogenesis via mechanisms involving VEGFR2 internalization and degradation following endosome-trans-Golgi network trafficking. *Angiogenesis* **16**, 625-637 (2013)

30. R. Usui, M. Shibuya, S. Ishibashi, Y. Maru, Ligand-independent activation of vascular endothelial growth factor receptor 1 by low-density lipoprotein. *EMBO reports* **8**, 1155-1161 (2007)

31. D. J. Kim, J. Kim, K. Spaunhurst, J. Montoya, R. Khodosh, K. Chandra, T. Fu, A. Gilliam, M. Molgo, P. A. Beachy, J. Y. Tang, Open-label, exploratory phase II trial of oral itraconazole for the treatment of basal cell carcinoma. *Journal of clinical oncology : official journal of the American Society of Clinical Oncology* **32**, 745-751 (2014)

32. C. M. Rudin, J. R. Brahmer, R. A. Juergens, C. L. Hann, D. S. Ettinger, R. Sebree, R. Smith, B. T. Aftab, P. Huang, J. O. Liu, Phase 2 study of pemetrexed and itraconazole as second-line therapy for metastatic nonsquamous non-small-cell lung cancer. *Journal of thoracic oncology : official publication of the International Association for the Study of Lung Cancer* **8**, 619-623 (2013)

33. E. S. Antonarakis, E. I. Heath, D. C. Smith, D. Rathkopf, A. L. Blackford, D. C. Danila, S. King, A. Frost, A. S. Ajiboye, M. Zhao, J. Mendonca, S. K. Kachhap, M. A. Rudek, M. A. Carducci, Repurposing itraconazole as a treatment for advanced prostate cancer: a noncomparative randomized phase II trial in men with metastatic castration-resistant prostate cancer. *The oncologist* **18**, 163-173 (2013)

Curriculum Vitae

Ruojing Li

November 2016

Department of Pharmacology and Molecular Sciences
Johns Hopkins University School of Medicine

EDUCATION

- 2005-2009 B.S. in Pharmaceutical Sciences
  Peking University School of Pharmaceutical Sciences, Beijing, China
- 2009-2011 M.S. in Pharmaceutics
  Peking University School of Pharmaceutical Sciences, Beijing, China
  - Mentor: Dr. Wan-Liang Lu, Ph.D.
- 2011-2016 Ph.D. in Pharmacology and Molecular Sciences
  Johns Hopkins University School of Medicine, Baltimore, MD
  - Mentor: Dr. Jun Liu, Ph.D.

RESEARCH EXPERIENCE

- Feb 2007 – Jul 2011 Dr. Wan-Liang Lu (PKU) Beijing, China
  Volunteer undergrad student and Master student
  - All-trans retinoic acid stealth liposomes prevent the relapse of breast cancer arising from the cancer stem cells (First author paper).

- Aug 2011 – Dec 2011 Dr. Jin Zhang (JHMI) Baltimore, MD

  Ph.D. rotation student

  - Visualization of Compartmentalized Kinase Activity Dynamics Using Adaptable BimKARs (Co-author paper).

- Apr 2012 – Jun 2012 Dr. Robert F. Siliciano (JHMI) Baltimore, MD

  Ph.D. rotation student

  - Activation of latent HIV reservoir using small molecules

- Dec 2011 – Dec 2016 Dr. Jun Liu (JHMI) Baltimore, MD

  Ph.D. candidate

  - Regulation of mTORC1 by Lysosomal Calcium and Calmodulin (First author paper).

  - Divergence of Antiangiogenic Activity and Hepatotoxicity of Different Stereoisomers of Itraconazole (Co-first author paper).

  - Inhibition of angiogenesis by selective estrogen receptor modulators through blockade of cholesterol trafficking rather than estrogen receptor (Second author paper)

  - Identification of an old antibiotic clofoctol as a novel activator of unfolded protein response pathways and an inhibitor of prostate cancer (Co-first author paper)

- June 2016 – Sept 2016 Dr. Yaning Wang (FDA) Silver Spring, MD

  Summer intern

  - Exposure-Response Relationship of Metformin in Type 2 Diabetes in Pediatrics

WORK EXPERIENCE

	YEAR(s)	EMPLOYER	POSITION
•	07/2006-08/2006	AbMax Biotechnology Co.,LTD, Beijing, China	Research intern
•	03/2010-06/2010	Undergraduate courses of Pharmaceutics Experiment, Peking University School of Pharmaceutical Sciences, Beijing, China	Teaching assistant
•	06/2016-09/2016	Office of Clinical Pharmacology, Division of Pharmacometrics, U.S. Food and Drug Administration, Silver Spring, MD, U.S.A.	Summer intern

PUBLICATIONS (in chronological order)

1. Du J, Lu WL, Ying X, Liu Y, Du P, Tian W, Men Y, Guo J, Zhang Y, **Li RJ**, Zhou J, Lou JN, Wang JC, Zhang X, Zhang Q. Dual-Targeting Topotecan Liposomes Modified with Tamoxifen and Wheat Germ Agglutinin Significantly Improve Drug Transport across the Blood− Brain Barrier and Survival of Brain Tumor-Bearing Animals. *Molecular pharmaceutics.* 2009. 6 (3): 905-917.

2. Ying X, Wen H, Lu WL, Du J, Guo J, Tian W, Men Y, Zhang Y, **Li RJ**, Yang TY, Shang DW, Lou JN, Zhang LR, Zhang Q. Dual-targeting daunorubicin liposomes improve the therapeutic efficacy of brain glioma in animals. *Journal of Controlled Release.* 2010. 141 (2):183-92.

3. Tian W, Ying X, Du J, Guo J, Men Y, Zhang Y, **Li RJ**, Yao HJ, Lou JN, Zhang LR, Lu WL. Enhanced efficacy of functionalized epirubicin liposomes in treating

brain glioma-bearing rats. *European Journal of Pharmaceutical Sciences.* 2010. 41 (2): 232-43.

4. Guo J, Zhou J, Ying X, Men Y, **Li RJ**, Zhang Y, Du J, Tian W, Yao HJ, Wang XX, Ju RJ, Lu WL. Effects of stealth liposomal daunorubicin plus tamoxifen on the breast cancer and cancer stem cells. *Journal of Pharmacy & Pharmaceutical Sciences.* 2010. 13 (2):136-51.
5. Zhang Y, **Li RJ**, Ying X, Tian W, Yao HJ, Men Y, Yu Y, Zhang L, Ju RJ, Wang XX, Zhou J, Chen JX, Li N, Lu WL. Targeting therapy with mitosomal daunorubicin plus amlodipine has the potential to circumvent intrinsic resistant breast cancer. Mol Pharm. 2011 Feb 7;8(1):162-75.
6. Men Y, Wang XX, **Li RJ**, Zhang Y, Tian W, Yao HJ, Ju RJ, Ying X, Zhou J, Li N, Zhang L, Yu Y, Lu WL. The efficacy of mitochondrial targeting antiresistant epirubicin liposomes in treating resistant leukemia in animals. *International Journal of Nanomedicine.* 2011;6:3125-37.

7. **Li RJ**, Ying X, Zhang Y, Ju RJ, Wang XX, Yao HJ, Men Y, Tian W, Yu Y, Zhang L, Huang RJ, Lu WL. All-trans retinoic acid stealth liposomes prevent the relapse of breast cancer arising from the cancer stem cells. *Journal of Controlled Release.* 2011. 149 (3):281-91.

8. Yao HJ, Ju RJ, Wang XX, Zhang Y, **Li RJ**, Yu Y, Zhang L, Lu WL. The antitumor efficacy of functional paclitaxel nanomicelles in treating resistant breast cancers by oral delivery. *Biomaterials.* 2011. 32 (12): 3285-302.

9. Wang XX, Li YB, Yao HJ, Ju RJ, **Li RJ**, Yu Y, Zhang L, Lu WL. The use of mitochondrial targeting resveratrol liposomes modified with a dequalinium polyethylene glycol-distearoylphosphatidyl ethanolamine conjugate to induce apoptosis in resistant lung cancer cells. *Biomaterials.* 2011. 32 (24): 5673-87.

10. Zhang L, Yao HJ, Yu Y, **Li RJ**, Ju RJ, Wang XX, Sun MG, Shi JF, Lu WL. Mitochondrial targeting liposomes incorporating daunorubicin and quinacrine for treatment of relapsed breast cancer arising from cancer stem cells. *Biomaterials.* 2012. 33 (2): 565-82.

11. Yu Y, Wang ZH, Zhang L, Yao HJ, Zhang Y, **Li RJ**, Ju RJ, Wang XX, Zhou J, Li N, Lu WL. Mitochondrial targeting topotecan-loaded liposomes for treating drug-resistant breast cancer and inhibiting invasive metastases of melanoma. *Biomaterials.* 2012. 33 (6): 1808-20.

12. Ju RJ, Huang RJ, Zhou J, **Li RJ**, Zhou P, Zhang ZH, Xiang FJ, Xu DJ, Liu WX, Ma XT, Zhang Q, Lu WL. Separation of injectable salidroside by column chromatography of macroporous resins for treating myocardial ischemia. *Science China Chemistry* 55 (7), 1435-1444.

13. Wang M*, Shim JS*, **Li RJ***, Dang Y, He Q, Das M, Liu JO. Identification of an old antibiotic clofoctol as a novel activator of unfolded protein response pathways and an inhibitor of prostate cancer. *British journal of pharmacology*. 2014. 171 (19): 4478-89. *(Co-first author)*.

14. Zhang W, Wu J, Ward MD, Yang S, Chuang YA, Xiao M, **Li R**, Leahy DJ, Worley PF. Structural Basis of Arc Binding to Synaptic Proteins: Implications for Cognitive Disease. Neuron. 2015 Apr 22; 86 (2): 490-500.

15. Shim JS, **Li RJ**, Lv J, Head SA, Yang EJ, Liu JO. Inhibition of angiogenesis by selective estrogen receptor modulators through blockade of cholesterol trafficking rather than estrogen receptor antagonism. *Cancer letters* 362 (1), 106-115.

16. Fu C, Xu J, **Li RJ**, Crawford JA, Khan AB, Ma TM, Cha JY, Snowman AM, Pletnikov MV, Snyder SH. Inositol Hexakisphosphate Kinase-3 Regulates the Morphology and Synapse Formation of Cerebellar Purkinje Cells via Spectrin/Adducin. *The Journal of Neuroscience* 35 (31), 11056-11067.

17. Wang G, Rajpurohit SK, Delaspre F, Walker SL, White DT, Ceasrine A, Kuruvilla R, **Li RJ**, Shim JS, Liu JO, Parsons MJ, Mumm JS. First quantitative high-throughput screen in zebrafish identifies novel pathways for increasing pancreatic β-cell mass. *Elife*. 2015 Jul 28; 4.

18. Depry C, Mehta S, **Li R**, Zhang J. Visualization of Compartmentalized Kinase Activity Dynamics Using Adaptable BimKARs. *Chemistry & Biology*. 2015 Nov 19;22(11):1470-9.

19. Head SA, Shi W, Zhao L, Gorshkov K, Pasunooti K, Chen Y, Deng Z, **Li RJ**, Shim JS, Tan W, Hartung T, Zhang J, Zhao Y, Colombini M, Liu JO. Antifungal drug itraconazole targets VDAC1 to modulate the AMPK/mTOR signaling axis in endothelial cells. *Proc Natl Acad Sci U S A*. 2015 Dec 29;112(52):E7276-85.

20. Shim JS*, **Li RJ***, Bumpus N, Head S, Kumar K, Shi W, Liu JO. Divergence of Anti-angiogenic Activity and Hepatotoxicity of Different Stereoisomers of Itraconazole. Accepted by *Clinical Cancer Research* (*Co-first author*)

TECHNICAL SKILLS

- ***Data analysis:*** data statistical analysis and display using R and GraphPad Prism.
- ***Molecular Biology****:* PCR; plasmid construction (conventional, Infusion and Gateway); site-directed mutagenesis; DNA/RNA purification; quantitative RT-PCR; DNA electrophoresis
- ***Biochemistry****:* expression of recombinant proteins in bacteria and mammalian cells; affinity purification; affinity and size-exclusion chromatography;

immunoprecipitation; tandem affinity pull-down; biotin pull-down; differential centrifugation; SDS-PAGE; immunoblotting; Coomassie blue staining; silver staining; *in vitro* kinase assay

- ***Cell Biology****:* bacteria and mammalian cell culture; human primary cell culture; electroporation; plasmid transfection; production and harvest of lentivirus; lentiviral transduction; gene silencing (siRNA and shRNA); generation of stable cell lines; soft agar colony formation assay; 3D spheroid invasion assay; endothelial tube formation assay on Matrigel; cell cycle analysis using flow cytometry; immunofluorescent staining; sorting and identification of breast cancer stem cells
- ***Microscopy****:* confocal microscopy
- ***Pharmaceutics****:* preparation of lysosomes using a film dispersion method; characterization of the liposomes (encapsulation efficiencies, particle sizes, *in vitro* release, stability)
- ***High-throughput Assays****:* determination of IC_{50}, EC_{50}, k_{cat}, K_m and K_i values; cell proliferation and viability assays ([^{3}H]-thymidine incorporation, alamarBlue and Calcein AM assays)
- ***Animal experiments***: *in vivo* Matrigel plug angiogenesis assay; *in vivo* tumor xenograft assay; mouse gavage; mice intraperitoneal injection
- ***Population PK/PD modeling****:* population PK/PD data analysis and modeling using NONMEM.
- ***Other experimental skills****:* HPLC, structure–activity relationship studies
- ***Computer Softwares****:* R, NONMEM, Pirana, GraphPad Prism; ImageJ; CLC Sequence Viewer; Microsoft Office (Word, Excel & PowerPoint); Adobe Illustrator

OTHER ACADEMIC ACTIVITIES

- ***Poster presentations:*** 06/2016 Gordon Research Seminar and Gordon Research Conferences (Phosphorylation & G-Protein Mediated Signaling Networks);
- ***Discussion leader:*** Gordon Research Seminar 2016 (Phosphorylation & G-Protein Mediated Signaling Networks)

HONORS AND AWARDS

- Spring 2016 Scheinberg Travel Award, Johns Hopkins University
- 2009 – 2010 National Scholarship for Outstanding Graduate Students in Pharmaceutical Sciences
- 2007 – 2008 The Third Prize of Peking University Scholarship for Outstanding Biomedical Students
- 2006 – 2007 The Second Prize of Peking University Scholarship for Outstanding Biomedical Students
- 2005 – 2006 The Third Prize of Peking University Scholarship for Outstanding Biomedical Students

ADDITIONAL INFO

Language: English (fluent); Mandarin Chinese (native)